1-1-2013

Numerical Study Of The Targeted Energy Transfer Between The Euler-Bernoulli Beam And A Nonlinear Energy Sink

Mohi U. Rahamat Ullah
Ryerson University

NUMERICAL STUDY OF THE TARGETED ENERGY TRANSFER BETWEEN THE EULER-BERNOULLI BEAM AND A NONLINEAR ENERGY SINK

by

Mohi Uddin Rahamat Ullah,

B.Eng., Mechanical Engineering

Ryerson University, Toronto, Ontario, Canada, 2011

A Thesis

Presented to Ryerson University

In partial fulfilment of the

requirements for the degree of

Master of Applied Science

in the program of

Mechanical and Industrial Engineering

Tortonto, Ontario, Canada, 2013

Author’s Declaration

I hereby declare that I am the sole author of this thesis. This is a true copy of the thesis, including any required final revisions, as accepted by my examiners.

I authorize Ryerson University to lend this to other institutions or individuals for the purpose of scholarly research.

I further authorize Ryerson University to reproduce this thesis by photocopying or by other means, in total or in part, at the request of other institutions or individuals for the purpose of scholarly research.

I understand that my thesis may be electronically available to the public.

ABSTRACT

NUMERICAL STUDY OF THE TARGETED ENERGY TRANSFER BETWEEN THE EULER-BERNOULLI BEAM AND A NONLINEAR ENERGY SINK

© Mohi Uddin Rahamat Ullah, 2013

Master of Applied Science

In the program of

Mechanical Engineering

Ryerson University

Targeted energy transfer (TET) refers to the spatial transfer of energy between a primary structure of interest and isolated oscillators called the energy sink (ES). In this work, the primary structure of interest is a slender beam modeled by the Euler-Bernoulli theory, and the ES is a single-degree-of-freedom oscillator with either linear or cubic nonlinear stiffness property. The objective of this study is to characterize the TET and the effectiveness of ES under impact and periodic excitations. By using the scientific computation package, MATLAB, numerical simulations are carried out based on excitations of various strength and locations. Both time and frequency domain characterizations are used. For the impact excitation, the ES with the cubic nonlinear stiffness property is more superior to the linear oscillator in that larger percentage of the impact energy can be dissipated there. The main energy transfer was found to be due to a 3-to-1 frequency coupling between the first bending mode and the ES. For the periodic excitation, however, both linear and nonlinear ES exhibit generally poorer performance than the case with the impact excitation. Future works should focus on the frequency-energy relationship of the periodic solution of the underlying Hamiltonian, as well as using finite element model to verify the simulation results.

Acknowledgments

I would like to convey sincere gratitude to my supervisors Dr. Der Chyan Lin and Dr. Donatus Oguamanam for their guidance, motivation, and continuous support during my graduate studies. This thesis could not have been written without their sound advice and immense guidance.

I am very thankful to my wife Sharmin, for her immense patience and emotional support. Without her encouragement and understanding, it would have been impossible for me to finish this work.

I would like to thank my parents in law for their love and support throughout my studies. Their encouragement convinced and motivated me to pursue graduate studies.

I am very appreciative of the financial assistance from the National Science and Engineering Research Council Canada (NSERC) throughout my research.

Dedication

To my wife Sharmin Islam and our sons Sameen and Sayhan

Table of Contents

Author's Declaration ii

Abstract iii

Acknowledgements iv

Dedication v

Table of Contents vi

List of Figures viii

Nomenclature xii

1. Introduction and Literature Review 1

1.1. Background 1

1.2. Literature Review 2

1.3. Research Objectives 4

1.4. Thesis Overview 4

2. Mathematical Model of Beam and Energy Sink 5

2.1. Modeling of the Beam and Energy Sink 5

2.1.1. Equation of Motion of the Beam 5

2.1.2. Equations of Motion for the Energy Sink 7

2.2. Dimensionless Equations of Motion 8

2.3. Modal Characterizations of the Beam Vibration 8

2.4. Kinetic and Potential Energy of the Beam 9

2.4.1. Initial Conditions of the Beam due to an Impulsive Force 9

2.4.2. Kinetic Energy 10

2.4.3. Potential Energy 11

2.5. Energy Variables for ES and TET Analysis 12

3. Targeted Energy Transfer Under Impact Excitation 14

3.1. Targeted Energy Transfer by the NES at D_1=0.5 14

3.2. Targeted Energy Transfer by the Linear Energy Sink 18

3.2.1. Simulation Results 18

3.3. Dominant Frequency Components in TET 21

3.3.1. Dominant Frequency Components in TET for Impact Location $D_1 = 0.5$ 21
3.3.2. Dominant Frequency Components in TET for Different Impact Locations 28
4. Targeted Energy Transfer Under Periodic Excitation 40
5. Discussions, Conclusion and Future Works 45
5.1. Discussions and Conclusion 45
5.2. Recommendations for Future Work 47
Appendix A 48
A.1 Clamped-clamped boundary configuration for the slender beam 48
Appendix B 49
B.1 MATLAB Codes 49
Appendix C 57
C.1 Energy dissipation by the LES due to impulsive force **57**
References 60

List of Figures

Figure 2.1: Clamped-clamped beam. 5

Figure 2.2: Free body diagram (FBD) of a small element of the beam. 6

Figure 2.3: ES attached to the actual model. 7

Figure 2.4: FBD for NES. 7

Figure 2.5: FBD for LES. 7

Figure 3.1: Energy dissipation by the NES and LES as a function of impact intensity. 15

Figure 3.2: Transient response of the system when $F_I = 10.5$: (a) Beam and NES response; (b) Close-up of the Beam and NES response. 16

Figure 3.3: Transient dynamics of the system when $F_I = 10.5$: (a) Instantaneous total energy in the 1st mode; (b) 2nd mode and (c) 3rd mode; (d) Instantaneous energy in the NES; (e) energy dissipation by the NES and (f) Power Spectral Density of system response. 16

Figure 3.4: Transient response of the system when $F_I = 14.5$: (a) Beam and NES response; (b) Close-up of the Beam and NES response. 17

Figure 3.5: Transient dynamics of the system when $F_I = 14.5$: (a) Instantaneous total energy in the 1st mode; (b) 2nd mode and (c) 3rd mode; (d) Instantaneous energy in the NES; (e) energy dissipation by the NES and (f) Power Spectral Density of system response. 17

Figure 3.6: Transient response of the system when $F_I = 18$: (a) Beam and NES response; (b) Close-up of the Beam and NES response. 19

Figure 3.7: Transient dynamics of the system when $F_I = 18$: (a) Instantaneous total energy in the 1st mode; (b) 2nd mode and (c) 3rd mode; (d) Instantaneous energy in the NES; (e) energy dissipation by the NES and (f) Power Spectral Density of system response. 19

Figure 3.8: Transient response of the system when $F_I = 23.5$: (a) Beam and NES response; (b) Close-up of the Beam and NES response. 20

Figure 3.9: Transient dynamics of the system when $F_I = 23.5$: (a) Instantaneous total energy in the 1st mode; (b) 2nd mode and (c) 3rd mode; (d) Instantaneous energy in the NES; (e) energy dissipation by the NES and (f) Power Spectral Density of system response. 20

Figure 3.10: Transient response of the system when $F_I = 10.5$:(a) Beam and LES response; (b) Close-up of the Beam and LES response. 22

Figure 3.11: Transient dynamics of the system when $F_I = 10.5$: (a) Instantaneous total energy in the 1st mode; (b) 2nd mode and (c) 3rd mode; (d) Instantaneous energy in the LES; (e) energy dissipation by the LES and (f) Power Spectral Density of system response. 22

Figure 3.12: Transient response of the system when $F_I = 14.5$:(a) Beam and LES response; (b) Close-up of the Beam and LES response. 23

Figure 3.13: Transient dynamics of the system when $F_I = 14.5$: (a) Instantaneous total energy in the 1st mode; (b) 2nd mode and (c) 3rd mode; (d) Instantaneous energy in the LES; (e) energy dissipation by the LES and (f) Power Spectral Density of system response. 23

Figure 3.14: Transient response of the system when $F_I = 18$:(a) Beam and LES response; (b) Close-up of the Beam and LES response. 24

Figure 3.15: Transient dynamics of the system when $F_I = 18$: (a) Instantaneous total energy in the 1st mode; (b) 2nd mode and (c) 3rd mode; (d) Instantaneous energy in the LES; (e) energy dissipation by the LES and (f) Power Spectral Density of system response. 24

Figure 3.16: Transient response of the system when $F_I = 23.5$:(a) Beam and LES response; (b) Close-up of the Beam and LES response. 25

Figure 3.17: Transient dynamics of the system when $F_I = 23.5$: (a) Instantaneous total energy in the 1st mode; (b) 2nd mode and (c) 3rd mode; (d) Instantaneous energy in the LES; (e) energy dissipation by the LES and (f) Power Spectral Density of system response. 25

Figure 3.18: Required time for dissipating a certain amount of energy as a function of F_I: (a) 5% energy dissipation; (b) 15% energy dissipation; (c) 30% energy dissipation; (d) 45% energy dissipation. 26

Figure 3.19: Dominant frequency as a function of F_I at $D_1 = 0.5$ for NES. 27

Figure 3.20: Dominant frequency as a function of F_I at $D_1 = 0.5$ for LES. 27

Figure 3.21: Frequency ratio as a function of F_I for NES: (a) $D_1 = 0.3$; (b) $D_1 = 0.4$; (c) $D_1 = 0.5$; (d) $D_1 = 0.6$, and (e) $D_1 = 0.7$. 29

Figure 3.22: Energy dissipation as a function of F_I for various locations :(a) $D_1 = 0.3$; (b) $D_1 = 0.4$; (c) $D_1 = 0.6$ and (d) $D_1 = 0.7$. 30

Figure 3.23: Dominant frequency as a function of F_I at $D_1 = 0.3$ for NES. 30

Figure 3.24: Dominant frequency as a function of F_I at $D_1 = 0.4$ for NES. 31
Figure 3.25: Dominant frequency as a function of F_I at $D_1 = 0.6$ for NES. 31
Figure 3.26: Dominant frequency as a function of F_I at $D_1 = 0.7$ for NES. 32
Figure 3.27: Dominant frequency as a function of F_I at $D_1 = 0.3$ for LES. 32
Figure 3.28: Dominant frequency as a function of F_I at $D_1 = 0.4$ for LES. 33
Figure 3.29: Dominant frequency as a function of F_I at $D_1 = 0.6$ for LES. 33
Figure 3.30: Dominant frequency as a function of F_I at $D_1 = 0.7$ for LES. 34
Figure 3.31: Frequency ratio as a function of F_I for LES: (a) $D_1 = 0.3$; (b) $D_1 = 0.4$; (c) $D_1 = 0.5$; (d) $D_1 = 0.6$ and (e) $D_1 = 0.7$. 34
Figure 3.32: Time response for the 1st mode and NES when F_I applied at $D_1 = 0.3$: (a) $F_I = 10.5$; (b) $F_I = 14.5$; (c) $F_I = 18$, and (d) $F_I = 23.5$; —— 1st mode, ▬▬ NES. 35
Figure 3.33: Time response for the 1st mode and NES when F_I applied at $D_1 = 0.4$: (a) $F_I = 10.5$; (b) $F_I = 14.5$; (c) $F_I = 18$, and (d) $F_I = 23.5$; —— 1st mode, ▬▬ NES. 35
Figure 3.34: Time response for the 1st mode and NES when F_I applied at $D_1 = 0.5$: (a) $F_I = 10.5$; (b) $F_I = 14.5$; (c) $F_I = 18$, and (d) $F_I = 23.5$; —— 1st mode, ▬▬ NES. 36
Figure 3.35: Time response for the 1st mode and NES when F_I applied at $D_1 = 0.6$: (a) $F_I = 10.5$; (b) $F_I = 14.5$; (c) $F_I = 18$, and (d) $F_I = 23.5$; —— 1st mode, ▬▬ NES. 36
Figure 3.36: Time response for the 1st mode and NES when F_I applied at $D_1 = 0.7$: (a) $F_I = 10.5$; (b) $F_I = 14.5$; (c) $F_I = 18$, and (d) $F_I = 23.5$; —— 1st mode, ▬▬ NES. 37
Figure 3.37: Time response for the 1st mode and LES when F_I applied at $D_1 = 0.3$: (a) $F_I = 10.5$; (b) $F_I = 14.5$; (c) $F_I = 18$, and (d) $F_I = 23.5$; —— 1st mode, ▬▬ LES. 37
Figure 3.38: Time response for the 1st mode and LES when F_I applied at $D_1 = 0.4$: (a) $F_I = 10.5$; (b) $F_I = 14.5$; (c) $F_I = 18$, and (d) $F_I = 23.5$; —— 1st mode, ▬▬ LES. 38
Figure 3.39: Time response for the 1st mode and LES when F_I applied at $D_1 = 0.5$: (a) $F_I = 10.5$; (b) $F_I = 14.5$; (c) $F_I = 18$, and (d) $F_I = 23.5$; —— 1st mode, ▬▬ LES. 38
Figure 3.40: Time response for the 1st mode and LES when F_I applied at $D_1 = 0.6$: (a) $F_I = 10.5$; (b) $F_I = 14.5$; (c) $F_I = 18$, and (d) $F_I = 23.5$; —— 1st mode, ▬▬ LES. 39
Figure 3.41: Time response for the 1st mode and LES when F_I applied at $D_1 = 0.7$: (a) $F_I = 10.5$; (b) $F_I = 14.5$; (c) $F_I = 18$, and (d) $F_I = 23.5$; —— 1st mode, ▬▬ LES. 39
Figure 4.1: Energy characterization of the beam with the forcing frequency at $D_1 = 0.3$: (a) total energy in the beam and each vibration mode; (b) stored and dissipated energy of the ES and (c)

the ratio of the energy dissipation by the ES and the total energy in the beam (solid lines refer to NES and symbols refer to LES). 42
Figure 4.2: Energy characterization of the beam with the forcing frequency at D_1 = 0.4: (a) total energy in the beam and each vibration mode; (b) stored and dissipated energy of the ES and (c) the ratio of the energy dissipation by the ES and the total energy in the beam (solid lines refer to NES and symbols refer to LES). 42
Figure 4.3: Energy characterization of the beam with the forcing frequency at D_1 = 0.5: (a) total energy in the beam and each vibration mode; (b) stored and dissipated energy of the ES and (c) the ratio of the energy dissipation by the ES and the total energy in the beam (solid lines refer to NES and symbols refer to LES). 43
Figure 4.4: Energy characterization of the beam with the forcing frequency at D_1 = 0.6: (a) total energy in the beam and each vibration mode; (b) stored and dissipated energy of the ES and (c) the ratio of the energy dissipation by the ES and the total energy in the beam (solid lines refer to NES and symbols refer to LES). 43
Figure 4.5: Energy characterization of the beam with the forcing frequency at D_1 = 0.7: (a) total energy in the beam and each vibration mode; (b) stored and dissipated energy of the ES and (c) the ratio of the energy dissipation by the ES and the total energy in the beam (solid lines refer to NES and symbols refer to LES). 44

Nomenclature

A	Beam cross-section area
$a_n(X)$	Mode shape
b_1	Dimensionless viscous damping coefficient
b_2	Dimensionless linear stiffness coefficient
b_3	Dimensionless nonlinear stiffness coefficient
c	Dimensional damping coefficient of the energy sink
C_c	Dimensionless damping coefficient of the beam
C_k	Dimensionless stiffness coefficient of the beam
C_f	Dimensionless coefficient of the damping force
d	Dimensional location of the energy sink
D	Dimensionless location of the energy sink
D_1	Dimensionless location for the applied impulse / periodic force
E	Young's modulus
EI	Flexural rigidity
F	Dimensional force exerted by the energy sink
F_D	Dimensionless damping force
F_{ES}	Dimensionless force exerted by the energy sink
F_I	Dimensionless impulsive force
F_p	Dimensionless forcing amplitude
$f(x,t)$	Transverse load per unit length
f_c	Damping force per unit length
$g_n(\tau)$	Modal response
$g_{k,\tau}$	Modal velocity
I	Moment of inertia
k	Stiffness coefficient of the spring

L	Dimensional length of the beam
L_1	Dimensionless length of the beam
m	Mass of the energy sink
$M(x, t)$	Bending moment
T	Simulation time
T_1	Forcing period
U	Strain energy
$V(x, t)$	Shear force
$w(x, t)$	Dimensional displacement of the beam
$W(X,\tau)$	Dimensionless displacement of the beam
x, y, z	Cartesian coordinates
$y(t)$	Dimensional displacement of the damper mass
Y	Dimensionless displacement of the damper mass
τ	Dimensionless time
$\alpha_1 = \frac{\rho A L^4}{EIT^2}$	Dimensionless modal mass of the beam
$\alpha_2 = \frac{\gamma L^4}{EIT}$	Dimensionless modal damping coefficient of the beam
$\beta_n L$	Weighted natural frequency
γ	Damping coefficient of the beam
δ	Kronecker delta
ΔE	Energy dissipation
ρ	Density of the beam material
σ_n	Mode shape coefficient
ω	Forcing frequency
ω_n	Natural frequency
$_{,X}$	Spatial derivative with X, $\left(\frac{\partial}{\partial X}\right)$
$_{,\tau}$	Temporal derivative with τ, $\left(\frac{\partial}{\partial \tau}\right)$

Chapter 1
Introduction and Literature Review

Vibration analysis of structure is of critical importance in applications: from the structural integrity of the skyscraper, stability of the offshore oil platform, to the comfort of a running vehicle, and the motion of the satellite. The central theme of such analysis has been to discover innovative ways to channel and to dissipate unwanted vibration energy in a timely and effective fashion. Classical tuned mass damper based on the notion of vibration absorption of linear oscillator provides the prime example of how the vibration of a main system of interest can be completely annihilated by attaching a secondary oscillatory system [1]. Indeed, such concepts have been successfully put into use in well known slender structures all over the world, such as the Dublin Spire in Ireland, the Bloomberg building in New York City, and the Taipei 101 building in Taiwan.

While the idea of vibration absorption can be successfully implemented, improving the effectiveness and efficiency of the vibration energy transfer and achieving better robustness against environmental variation remain as major challenges facing the field. In recent decades, the idea of using nonlinear oscillators as the secondary system attached to a primary system has been considered, and shown to be capable of meeting these challenges.

1.1. Background

This thesis describes the investigation on the Targeted Energy Transfer (TET) from a multimodal beam vibration to the Energy Sink (ES). The beam can experience various external disturbances such as impact loading, periodic or random excitation. The purpose of the ES is to absorb or dissipate the unwanted vibration of the beam due to the disturbance. An ES is normally modelled with a nonlinear or linear stiffness term and a linear viscous damping term. It can therefore be categorized as nonlinear energy sink (NES) or linear energy sink (LES). The main energy transfer mechanism is contributed by “mode locking” of specific frequency of vibration of the beam and the ES. For the beam, or more generally, other structural members, this frequency is mostly the natural frequency. For the ES, it is related to the frequency of the limit cycle. Hence, the energy is channeled through a kind of resonance mechanism or resonant modal

interaction to ES [2, 3]. The attachment of the ES can be grounded or ungrounded and it can be single-degree-of-freedom (SDOF) or multi-degree-of-freedom (MDOF) system depending on the design and use.

In this work, an ungrounded and light-weight ES is chosen. In addition, the so-called "essentially" nonlinear ES is considered. For the NES this is when the nonlinear restoring force does not contain a linear stiffness term and only cubic nonlinearity is included (Chapter 2). As a result, NES does not have any resonance frequency in the sense of linear oscillator.

1.2. Literature Review

This section contains the survey of pertinent literature of TET. In the context of vibration theory, TET can in general be regarded as the method of energy control. Vakakis [4] suggested that the NES can be considered as a generalization of the concept of the classical linear vibration absorber. Nayfeh and Mook [5] showed that in a vibration system with coupled nonlinear oscillators, energy interactions can occur via the mechanism of internal resonance where the vibration of the coupled oscillators "locked" into a specific frequency ratio. In connection to TET, Vakakis [4] coined the term resonance capture to describe TET. The analysis of internal resonance is a technically challenging task, and requires basic concepts, methodologies and computational techniques from the dynamical systems and applied mathematics, such as bifurcation theory, asymptotic approximations, and numerical signal processing [6].

In the works by Gendelman et al. [8] and Vakakis et al. [7] a grounded and relatively heavy nonlinear attachment is investigated. To obtain a better understanding of the energy transfer, the authors analyzed the dynamics of the underlying Hamiltonian system. Lee et al. [9] examined the energy exchange between the oscillators in the damped vibration of a 2-DOF system and identified at least three different energy transfer mechanisms. They are either fundamental and subharmonic resonance captures or nonlinear beat phenomena.

Malatkar and Nayfeh [10] experimentally analyzed the nonlinear energy transfer between widely spaced modes in harmonically forced system. The authors showed that passive energy transfer is caused by the resonance interaction at the Hopf bifurcation frequency of the NES and the natural frequency of the first mode of the linear oscillator.

Lee et al. [2] studied the multimodal vibration of the primary structure and demonstrated resonance interaction between NES and the vibration modes of the primary structure. By

facilitating these energy transfers, through the excitation of periodic and quasi-periodic motions, significant input energy dissipation via the oscillation of NES was shown.

Glendelman et al. [11] investigated the dynamics of a linear oscillator coupled to an essentially nonlinear attachment of substantially lower mass. It is demonstrated that efficient energy transfer can be obtained for a small attachment mass with properly chosen damping and coupling terms of the system. Two mechanisms of energy transfer in the system were revealed; one is the resonance capture and the second is related to the non-resonant excitation of the attachment at the high frequency.

Dynamics of a linear oscillator with strongly nonlinear attachment having small mass and multiple states of equilibrium has been investigated by Gendelman and Lamarque [12]. Three types of dynamical regimes during the energy transfer were revealed in their works. First, *energy pumping* where the energy is efficiently transferred to the nonlinear attachment, second, *smooth damping* where the system loses its energy smoothly without essential pumping to the attachment, and third, *transient chaos* between the primary mass and the attachment.

Gendelman et al. [13] considered MDOF NES and demonstrated the TET can be significantly enhanced. They showed that, if the primary structure is excited by the shock energy above a certain critical threshold, the NES can effectively absorb the vibration energy from the primary structure in an irreversible manner. In addition, they showed that the efficiency of vibration protection and shock mitigation using NES exceeds those of the linear tuned mass damper. Besides, due to their essential stiffness nonlinearities, the NESs can operate over broad frequency ranges. But these authors found that high TET efficiency of the SDOF NES is only achieved in the relatively narrow range of the external forcing amplitudes.

In the works by Gendelman et al. [8] the use of a combination of coupled, linear and nonlinear ES to achieve energy transfer was considered. It was shown that 1:1 stable subharmonic motion of the underlying Hamiltonian system was mainly responsible for the energy transfer between the ES and the primary system. Kerschen et al. [14] studied energy transfer from a damped linear oscillator to an ungrounded light-weight nonlinear oscillator. It is shown that energy transfer is caused by either fundamental or subharmonic resonance capture and in some cases it is initiated by nonlinear beat phenomena.

Jiang et al. [15] demonstrated application of NESs to shock isolation. Essentially non-linear stiffness elements were used for robust energy transfer at a sufficiently fast timescale,

because fast energy transfer at the early stage is crucial for shock isolation purposes. By adding two symmetrically placed NESs these authors showed that it is possible to achieve dual mode shock isolation to reduce unwanted disturbances generated at different ends of the primary system.

1.3. Research Objectives

The external disturbance of impact or periodic excitation is considered in this investigation. The objective of this study is to conduct numerical simulation to analyze TET and the beam. Of particular interest is the energy transfer pattern in terms of how it varies with the parameters of the input excitation, such as impact strength, periodic forcing amplitude, frequency as well as the location of the disturbance. Numerical analysis is also focused on the estimation of frequency modes involved in the energy transfer and how such coupling varies with the input parameters.

1.4. Thesis Overview

This research is arranged in five chapters. Chapter two presents the mathematical model of the beam and ES. The equations of motion for both beam and ES are derived using Newton's second law of motion. In Chapter three, numerical analysis of the TET due to impact intensity is presented based on the free vibration analysis and periodic excitation is discussed in Chapter four. Finally Chapter five contains a summary of the contributions of this research and suggestion for future work.

Chapter 2

Mathematical Model of Beam and Energy Sink

In this chapter the mathematical modeling of a beam structure with an energy sink component is described. This base model is used to investigate the targeted energy transfer. In section 2.1 the beam and energy sink models are presented. In section 2.2, dimensionless equations of motion are derived. In section 2.3, modal characterizations of the beam vibration are described. In section 2.4, the kinetic and potential energies of the beam are derived and in section 2.5, other energy terms that are used to characterize TET in both the beam and ES are defined.

2.1. Modeling of the Beam and Energy Sink

2.1.1. Equation of Motion of the Beam

The beam model considered in this research has a clamped-clamped boundary condition with a cross-sectional area A, density ρ and length L. A standard Cartesian coordinates system is used to describe the beam transverse displacement $w(x,t)$; see Figure 2.1. Let the transverse external load per unit length be $f(x,t)$, a damping force per unit length $f_c = \gamma \dfrac{\partial w}{\partial t}$, flexural rigidity of the beam EI, where E is the Young's elastic modulus for the beam and I is the cross-sectional area moment of inertia about the z-axis.

In this study, Euler-Bernoulli beam is assumed. Hence, the beam is a slender beam (large width-to-depth ratio) and only small amplitude oscillation is considered.

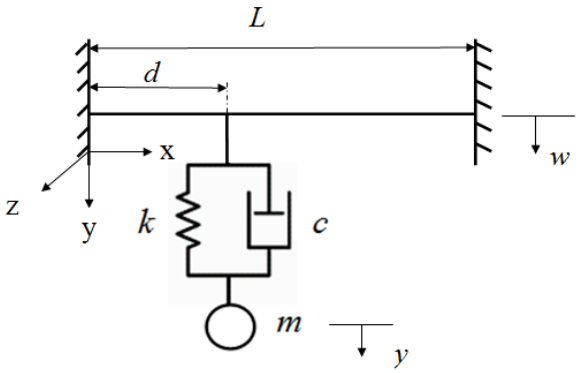

Figure 2.1: Clamped-clamped beam.

The energy sink is assumed to consist of a spring and viscous damper element. Both linear and nonlinear springs (cubic nonlinearity) will be considered. In addition, the following simplifications are made.

- Uniform mass per unit length.
- Linear, homogeneous, isotropic and elastic material.
- Constant *E, I* and *A.*

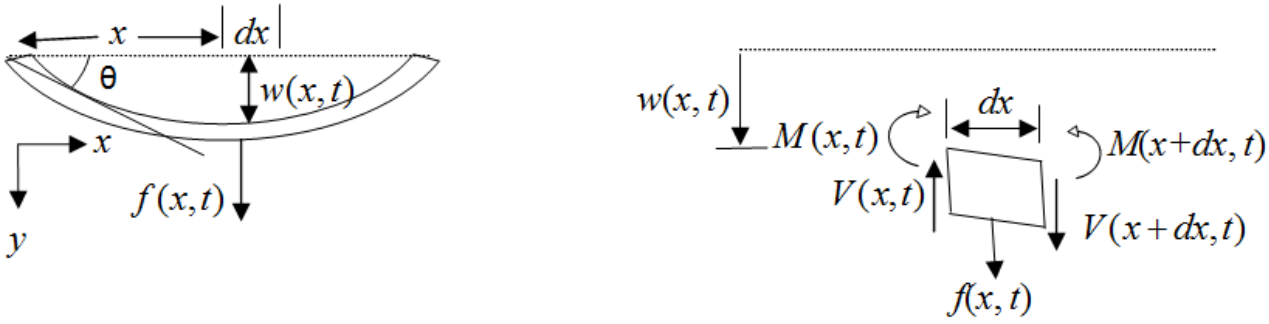

Figure 2.2: Free body diagram (FBD) of a small element of the beam.

Figure 2.2 shows the free body diagram of a small beam element as it is deformed by the external force $f(x,t)$, where $w(x,t)$ denotes transverse deflection of the beam. Here, $M(x,t)$, $V(x,t)$ and $M(x+dx,t), V(x+dx,t)$ represent the bending moment, and the shear force at the left and right ends of the beam element, respectively. The shear force and bending moment relationships are given as

$$V(x,t) = -\frac{\partial M(x,t)}{\partial x},\ M(x,t) = EI\frac{\partial^2 w(x,t)}{\partial x^2}. \tag{2.1}$$

By the Newton's law of motion the following equation of motion for the Euler-Bernoulli beam can be obtained:

$$EI\frac{\partial^4 w}{\partial x^4} + \rho A\frac{\partial^2 w}{\partial t^2} + \gamma\frac{\partial w}{\partial t} = f(x,t). \tag{2.2}$$

Note that the term $f(x,t)$ from the above denotes the external force applied to the beam. The reaction force from the energy sink at the point of attachment will be the primary source of this load (see section 2.1.2). The case of the beam subjected to an external impulsive or a harmonic

force excitation will also be considered. In that case, $f(x, t)$ will be given by the sum of two terms: one from the reaction force of the energy sink and the other from the external forcing.

2.1.2. Equations of Motion for the Energy Sink

The energy sink (ES) attached to the beam is modeled as a lumped mass-spring-damper system of mass m, damping coefficient c and stiffness constant k. A linear and nonlinear ES denoted as LES and NES, respectively, are considered. A LES is given by the standard linear mass-spring-damper system. A NES is characterized by a strongly nonlinear spring element of cubic nonlinearity without a linear stiffness term. Let $y(t), w_d(t)$ and $F(t)$ be the vertical absolute displacement of the damper mass, beam and damping force at the location $x = d$, respectively; (see Figures 2.1). Applying Newton's 2nd law of motion (see Figure 2.3) yields

$$m\ddot{y} = -F \tag{2.3}$$

where

$$F = c(\dot{y} - \dot{w}_d) + k(y - w_d)^3$$

for the NES (Figure 2.4), and

$$F = c(\dot{y} - \dot{w}_d) + k(y - w_d)$$

for the LES (Figure 2.5). Together, the coupled equations (2.2) and (2.3) represent the model used in the investigation of this study.

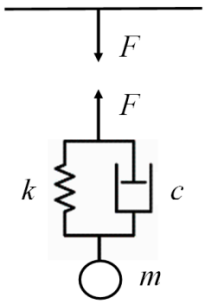

Figure 2.3: ES attached to the actual model.

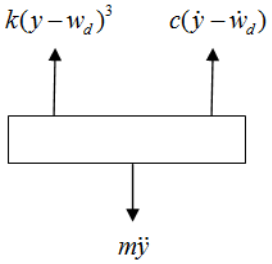

Figure 2.4: FBD for NES.

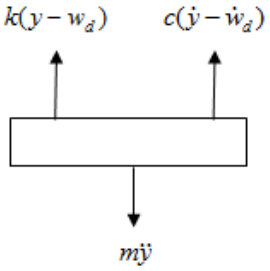

Figure 2.5: FBD for LES.

2.2. Dimensionless Equations of Motion

The analysis of the system equations of motion (2.2) and (2.3) will be conducted based on their dimensionless forms. This is achieved by introducing the following dimensionless variables,

$$X = \frac{x}{L},\ Y = \frac{y}{L},\ W = \frac{w}{L},\ \tau = \frac{t}{T},\ D = \frac{d}{L}. \tag{2.4}$$

Substituting these variables into the equations of motion yields

$$\frac{\partial^4 W}{\partial X^4} + \frac{\rho A L^4}{EIT^2}\frac{\partial^2 W}{\partial \tau^2} + \frac{\gamma L^4}{EIT}\frac{\partial W}{\partial \tau} = \frac{L^3}{EI} f(x,t) = F_{ES}\,\delta(X - D) \tag{2.5}$$

where F_{ES} represents the dimensionless force that exerted by the ES and is defined in equation (2.8) and (2.9) below. To be specific $f(x,t) = F(t)\delta(x-d)$ is used to complete the derivation of the equation of the beam where $F(t)$ is given in equation (2.3).

Let $\alpha_1 = \frac{\rho A L^4}{EIT^2}$, $\alpha_2 = \frac{\gamma L^4}{EIT}$, equation (2.5) now reads

$$W_{XXXX} + \alpha_1 W_{\tau\tau} + \alpha_2 W_{\tau} = F_{ES}\,\delta(X - D) \tag{2.6}$$

where the subscript X and τ denote the derivative with the dimensionless X and τ, respectively.

For the ES, repeating the same procedure on equation (2.3) yields

$$Y_{\tau\tau} = -F_{ES} \tag{2.7a}$$

where

$$F_{ES} = \frac{cT}{m}\left(Y_{\tau} - W_{D,\tau}\right) + \frac{kL^2T^2}{m}\left(Y - W_D\right)^3 \tag{2.7b}$$

for the NES, and

$$F_{ES} = \frac{cT}{m}\left(Y_{\tau} - W_{D,\tau}\right) + \frac{kT^2}{m}\left(Y - W_D\right) \tag{2.7c}$$

for the LES. Letting $b_1 = \frac{cT}{m}$, $b_2 = \frac{kT^2}{m}$, $b_3 = \frac{kL^2T^2}{m}$ and with (2.7b), (2.7c), (2.7a) becomes

$$Y_{\tau\tau} + b_1\left(Y_{\tau} - W_{D,\tau}\right) + b_3\left(Y - W_D\right)^3 = 0 \tag{2.8}$$

for the NES, and

$$Y_{\tau\tau} + b_1\left(Y_{\tau} - W_{D,\tau}\right) + b_2\left(Y - W_D\right) = 0 \tag{2.9}$$

for the LES. Equations (2.8) and (2.9) describe the equations of motion for the ES with the viscous damping coefficient b_1, linear and nonlinear stiffness coefficients b_2 and b_3, respectively.

2.3. Modal Characterizations of the Beam Vibration

In this research, TET will first be characterized based on the impact excitation. The objective of this section is to show the response and derive the energy measures to characterize the energy transfer. The Euler-Bernoulli beam displacement $W(X,\tau)$ can in general be solved using separation of variables technique

$$W(X,\tau)=\sum_{n=1}^{N} a_n(X)g_n(\tau) \tag{2.10}$$

where a_n denotes the *n* th mode shape (see Appendix A)

$$a_n(X)=(\cosh\beta_n X-\cos\beta_n X)-\sigma_n(\sinh\beta_n X-\sin\beta_n X) \tag{2.11}$$

and $g_n(\tau)$ is the modal response function. Substituting the above into equation (2.6) and by orthogonal condition $\int_0^1 a_k(X)a_n(X)dX=\delta_{kn}$, where δ_{kn} is the Kronecker delta, the modal equation of motion can be written as

$$g_{k,\tau\tau}+C_c g_{k,\tau}+C_k g_k=C_f F_{ES} \tag{2.12}$$

where

$$C_c=\frac{\alpha_2}{\alpha_1},C_k=\frac{\beta_k^4}{\alpha_1},C_f=\frac{a_k(D)}{\alpha_1\int_0^1 a_k^2 dX}.$$

2.4. Kinetic and Potential Energy of the Beam

To assess the energy transfer between the beam and the ES, it is necessary to excite the beam and estimate the energy dissipation in the ES. Both impact and periodic excitations are considered in this work. By the basic impulse momentum principle, the impact can be characterized by giving an initial velocity for the beam element. The purpose of this section is to derive the initial conditions due to the impact and the energy terms that are necessary to characterize the energy transfer between the beam and the ES.

2.4.1. Initial Conditions of the Beam due to an Impulsive Force

Assume a dimensionless impulsive force F_I applied at the location $X=D_1$. The equation of motion for the beam is now described by

$$W_{XXXX} + \alpha_1 W_{\tau\tau} + \alpha_2 W_{\tau} = F_{ES}\delta(X - D) + F_I \delta(X - D_1)\delta(\tau). \tag{2.13}$$

Substituting the equation (2.10) into (2.13) and applying orthogonality condition, the above becomes

$$\int_0^1 a_k^2(X)dX\left[\beta_k^4 g_k(\tau) + \alpha_1 g_{k,\tau\tau}(\tau) + \alpha_2 g_{k,\tau}(\tau)\right] = F_{ES}a_k(D) + F_I a_k(D_1)\delta(\tau). \tag{2.14}$$

Integrating equation (2.14) from 0^- to 0^+ yields

$$\begin{aligned}\int_0^1 a_k^2(X)dX\left[\int_{0^-}^{0^+}\beta_k^4 g_k(\tau)d\tau + \alpha_1\int_{0^-}^{0^+} g_{k,\tau\tau}(\tau)d\tau + \alpha_2\int_{0^-}^{0^+} g_{k,\tau}(\tau)d\tau\right] \\ = \int_{0^-}^{0^+} F_{ES}\, a_k(D)d\tau + \int_{0^-}^{0^+} F_I a_k(D_1)\delta(\tau)d\tau.\end{aligned} \tag{2.15}$$

Assume the beam is in static equilibrium before the impact. That means, due to the nature of the impulsive force, the impulse by the F_{ES} will be insignificant during the short timespan of the impact and, thus,

$$\int_{0^-}^{0^+} F_{ES}a_k(D)d\tau = 0.$$

Dropping this term from equation (2.15) and rearranging terms, yields

$$\beta_k^4\left[g_k(\tau)\right]_{0^-}^{0^+} + \alpha_1\left[g_{k,\tau}(\tau)\right]_{0^-}^{0^+} + \alpha_2\left[g_k(\tau)\right]_{0^-}^{0^+} = \frac{F_I a_k(D_1)}{\int_0^1 a_k^2(X)dX}. \tag{2.16}$$

The assumption of the beam in static equilibrium means

$$g_k(0^-) = g_k(0^+) = g_{k,\tau}(0^-) = 0.$$

Substituting the above into equation (2.16) gives the initial velocity of the *k*th mode

$$g_{k,\tau}(0^+) = \frac{F_I a_k(D_1)}{\alpha_1\int_0^1 a_k^2(X)dX} = \frac{F_I a_k(D_1)}{\alpha_1}. \tag{2.17}$$

2.4.2. Kinetic Energy

The kinetic energy of the beam can be expressed as

$$KE = \frac{1}{2}\rho A\int_0^L \dot{w}^2 dx$$

By using dimensionless variables the above can be written as

$$KE = \frac{1}{2}\frac{EI\alpha_1}{L}\int_0^1 W_\tau^2 dX. \tag{2.18}$$

By the orthogonal condition, equation (2.18) can be written as the sum of kinetic energy of the modes, $T_n = \frac{1}{2}\frac{EI\alpha_1}{L} g_{n,\tau}^2$, n = 1, 2, …, N,

$$KE = \sum_{n=1}^{N} T_n . \tag{2.19}$$

2.4.3. Potential Energy

The potential energy (PE) of a beam element is derived from the strain energy. For the Euler-Bernoulli beam, only the strain energy from the flexural bending is considered. The strain energy U of the beam is the same as the work done in deforming the beam. If the beam deforms through an angle $d\theta$ then work done by a bending moment M is $Md\theta$. Therefore, the total strain energy stored in the beam over the length 0 to L is

$$U = PE = \frac{1}{2}\int_0^L M d\theta \tag{2.20}$$

where M is given by the equation (2.1) and $\theta = \frac{\partial w}{\partial x}$ is the slope of the deformed beam element [16]. Thus, the above equation can be written as

$$PE = \frac{1}{2} EI \int_0^L \left(\frac{\partial^2 w}{\partial x^2} \right)^2 dx.$$

By using dimensionless variables the above can be expressed as

$$PE = \frac{1}{2}\frac{EI}{L}\int_0^1 \left(\frac{\partial^2 W}{\partial X^2} \right)^2 dX. \tag{2.21}$$

Expressed in modal sum, the equation (2.21) becomes

$$PE = \frac{1}{2}\frac{EI}{L}\sum_{n=1}^{N}\sum_{m=1}^{M} g_n g_m \int_0^1 a_{n,XX}\, a_{m,XX} dX = \frac{1}{2}\sum_{n=1}^{N}\sum_{m=1}^{M} k_{nm} g_n g_m \tag{2.22}$$

where

$$k_{nm} = \frac{EI}{L}\int_0^1 a_{n,XX}\, a_{m,XX}\, dX. \tag{2.23}$$

By orthogonality, integration by parts and boundary conditions, the above is simplified to

$$k_{nn} = \frac{EI}{L}\int_0^1 \left(a_{n,XX}\right)^2 dX \tag{2.24}$$

So that

$$PE = \frac{1}{2}\sum_{n=1}^{N} k_{nn} g_n^2. \tag{2.25}$$

Substituting equation (2.23) into (2.24) yields the final *PE* form used in the analysis

$$PE = \frac{1}{2}\frac{EI\beta_n^{\,4}}{L}\sum_{n=1}^{N} g_n^2. \tag{2.26}$$

2.5. Energy Variables for ES and TET Analysis

In this section, the energy variables that are used to characterize the TET between the beam and ES are defined. Both the energy remaining in the beam and the ES as well as the energy dissipated by the ES are of main importance in the characterization. When the excitation is by the impulsive force, the total instantaneous energy of the beam, ET_{beam}, is calculated by adding kinetic energy and potential energy of all the vibration modes (E_{mn}). The total instantaneous energy of the ES, ET_{ES}, is calculated from the Hamiltonian of the undamped ES.

Let $P_n = \frac{1}{2}\frac{EI\beta_n^{\,4}}{L} g_n^2$ and recall $T_n = \frac{1}{2}\frac{EI\alpha_1}{L} g_{n,\tau}^2$. The following energy terms are defined:

$$E_{mn} = T_n + P_n,$$

$$ET_{beam} = \sum_{n=1}^{N} E_{mn}, \tag{2.27}$$

$$ET_{NES} = \frac{1}{2}Y_\tau^2 + \frac{1}{4}b_3(Y - W_D)^4, \tag{2.28}$$

and

$$ET_{LES} = \frac{1}{2}Y_\tau^2 + \frac{1}{2}b_2(Y - W_D)^2. \tag{2.29}$$

The instantaneous energy in the ES and bending modes can be examined by computing the non-dimensional energy ratio E_d and E_{bn}, respectively. Here E_d denotes the portion of instantaneous total energy stored in the ES, and E_{bn} denotes the ratio of the amount of energy in each mode to the total amount of energy in the beam and sink, where

$$E_{d,NES,LES} = \frac{ET_{NES,LES}}{ET_{beam} + ET_{NES,LES}} \tag{2.30}$$

and

$$E_{bn} = \frac{E_{mn}}{ET_{beam} + ET_{NES,LES}}. \quad n = 1,2,...N \tag{2.31}$$

Energy dissipated ΔE in a viscously damped system in equation (2.8) and (2.9) with damping force F_D and viscous damping coefficient b_1 is given by

$$\Delta E = \int_0^\tau F_D d(Y - W_D) = \int_0^\tau b_1 (Y_\tau - W_{D,\tau}) \frac{d(Y - W_D)}{d\tau} d\tau = b_1 \int_0^\tau (Y_\tau - W_{D,\tau})^2 d\tau.$$

The energy dissipation measure E_{ES} represents the percentage of impulsive energy dissipated by the end of damped motion. A quantitative measure of the capacity of the ES to dissipate impulsive energy from the beam can be obtained by the ratio of the energy dissipation by the ES to the total input impulsive energy in the beam, where

$$E_{NES,LES} = \frac{\Delta E}{Input\ energy} = \frac{b_1 \int_0^\tau (Y_\tau - W_{D,\tau})^2 d\tau}{\frac{1}{2} \frac{EI\alpha_1}{L} \left(\sum_{n=1}^{N} g_{n,\tau}^2 (0^+) \right)}. \tag{2.32}$$

Chapter 3

Targeted Energy Transfer Under Impact Excitation

In this chapter numerical analysis of the TET of the clamp-clamp Euler Bernoulli beam subjected to impact will be given. The system equations (2.8), (2.9) and (2.12) will be simulated for different impulse strength applied at various locations along the beam. Both time and frequency domain characterizations will be used to analyze the TET between the beam and the ES. They include the long-time energy dissipation in the ES, total energy in the beam and the ES, and the power spectral density (PSD) of the beam and ES. The main objective of the numerical experiment is to examine the effectiveness of the ES in achieving the TET. The results from the LES will be given to provide the contrast with the NES. All simulations are conducted using the scientific package MATLAB [18] and the numeric codes are listed in Appendix B.

For the numerical simulations, the beam of dimensionless length L_1 = 1, the mass per unit length $\alpha_1 = 1$, damping coefficient $\alpha_2 = 0.02$, and flexural rigidity EI =1 is considered. For both LES and NES, $b_1 = 0.2$, $b_2 = 20$ and $b_3 = 20$ are used for the damping, linear and nonlinear stiffness coefficients, respectively. The dimensionless impulsive force is varied over the range F_I =10.5 to 40 in 0.5 increment. A sampling frequency of 1,000 Hz is used in all numerical simulations and 200,000 data points are collected to calculate various energy terms defined in section 2.5. The primary mode of energy transfer is estimated from the PSD of the response. This is calculated using the periodogram and with a Hanning windowing to eliminate aliasing.

To demonstrate energy transfer and its basic characteristics, results from NES based on an impact delivered at the mid-span of the beam D_1 = 0.5 will first be discussed in section 3.1. Its linear counterpart given by the LES is presented in section 3.2. These sections show mainly time-domain characterization. In section 3.3, the frequency-domain method is used to provide further details of the underlying dynamics of the energy transfer process for different impact locations.

3.1. Targeted Energy Transfer by the NES at D_1 = 0.5

Figure 3.1 reveals the relationship between the energy dissipation by the LES and NES as a function of F_I. It is seen that 35% to 75% energy dissipation is achievable by the NES. NES

appears more advantageous than the LES for larger F_I whereas LES is more beneficial of the system for low F_I. To examine the dynamics that carry the energy transfer, the time history and PSD of the response from four cases are studied in detail. These cases are identified in Figure 3.1 as *A*, *B*, *C* and *D*. They correspond to F_I = 10.5, 14.5, 18 and 23.5, respectively.

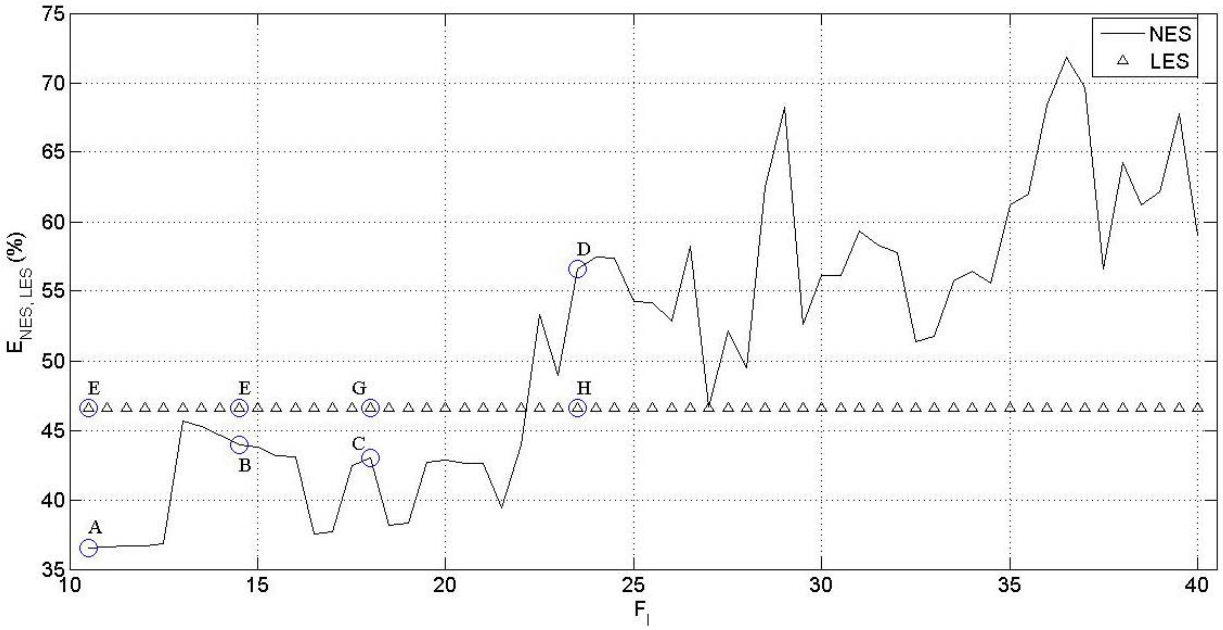

Figure 3.1: Energy dissipation by the NES and LES as a function of impact intensity.

Figures 3.2 and 3.3 show the response at $F_I = 10.5$ (point A in Figure 3.1). Figure 3.2b shows that the oscillation is concentrated initially in the first mode (Figure 3.2). But, after the transient period elapsed, most of the energy flowed into the 3rd mode (Figure 3.3c). Overall, it took $\tau = 60$ of dimensionless time for the NES to dissipate the energy (Figure 3.3d). In this case, only 36.5% input energy is dissipated by the NES (Figure 3.3e).

When F_I increases from 10.5 to 14.5 (point B in Figure 3.1), different dynamical behaviour is realized (Figures 3.4 and 3.5). At the beginning, NES is oscillating with small amplitude. The main difference is noticed in the NES response. In particular, NES exhibits faster oscillation as F_I increases. Qualitatively, the energy flows among the modes and NES are similar to the F_I =10.5 case. The residual energy is seen to remain mainly in the 3rd mode with a rather drastic transition compared to F_I =10.5 case. Most energy transfer is seen to be completed after $\tau = 65$ and it dissipates around 42% of input energy (Figures 3.5d and 3.5e).

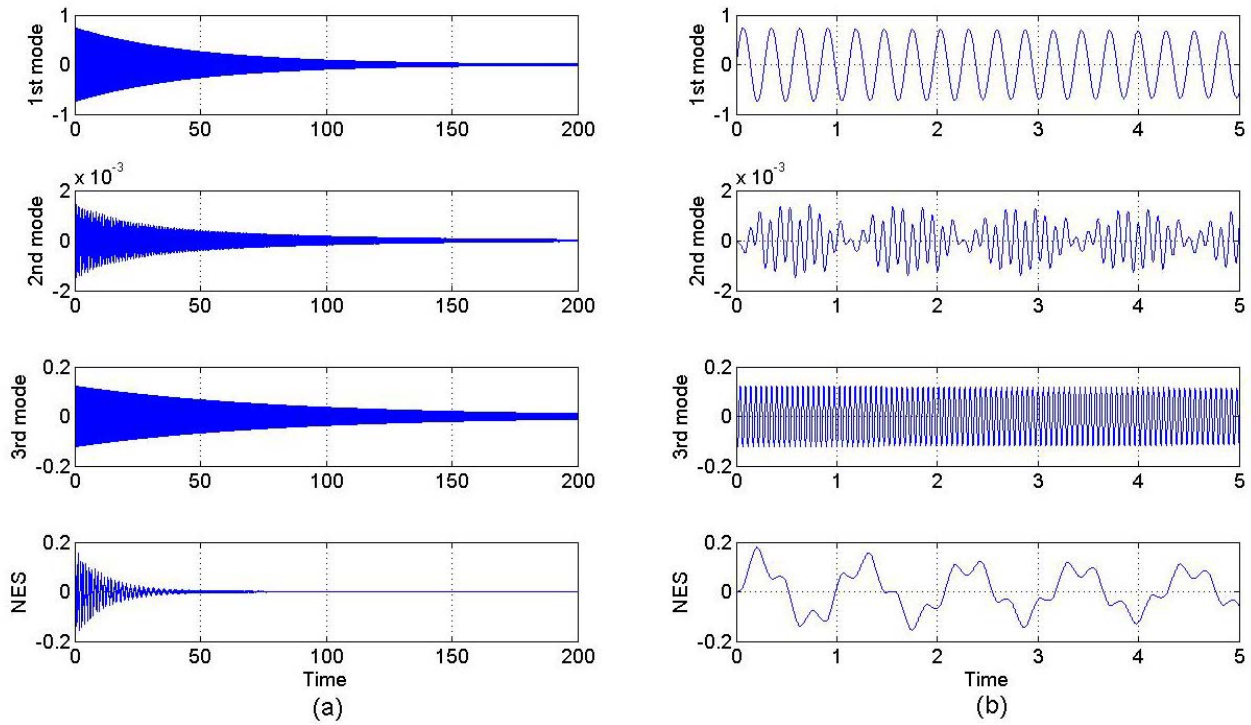

Figure 3.2: Transient response of the system when $F_1 = 10.5$: (a) Beam and NES response; (b) Close-up of the Beam and NES response.

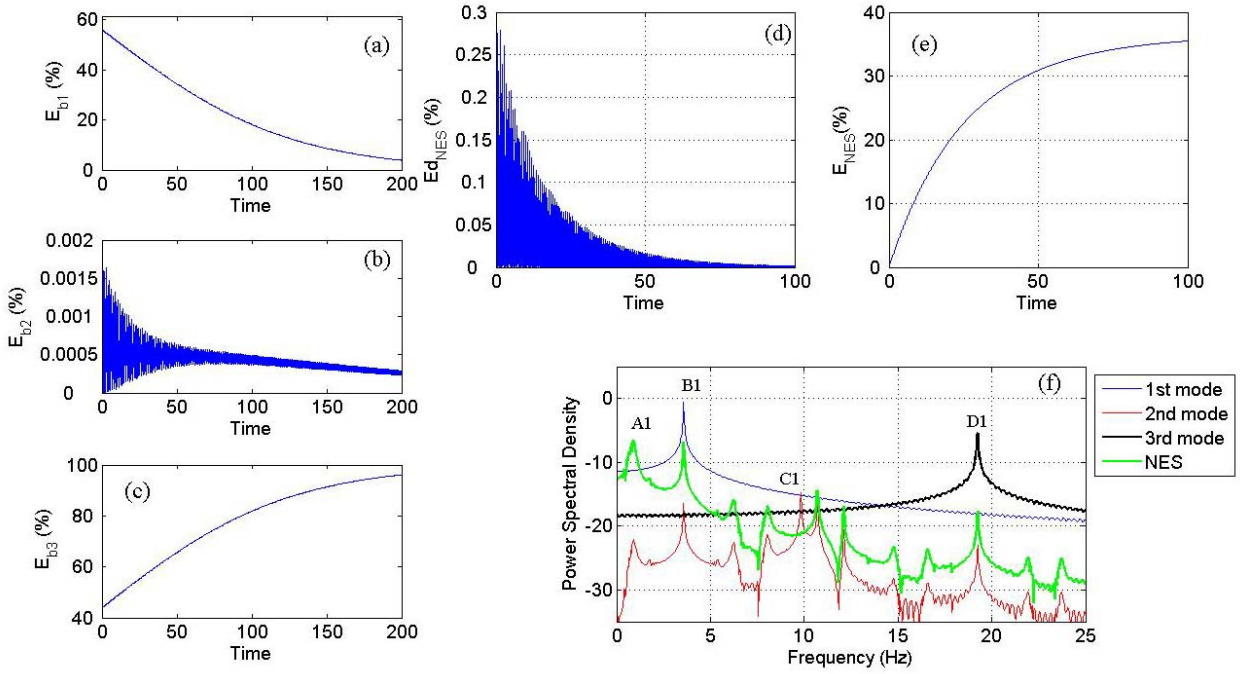

Figure 3.3: Transient dynamics of the system when $F_1 = 10.5$: (a) Instantaneous total energy in the 1st mode; (b) 2nd mode and (c) 3rd mode; (d) Instantaneous energy in the NES; (e) energy dissipation by the NES and (f) Power Spectral Density of system response.

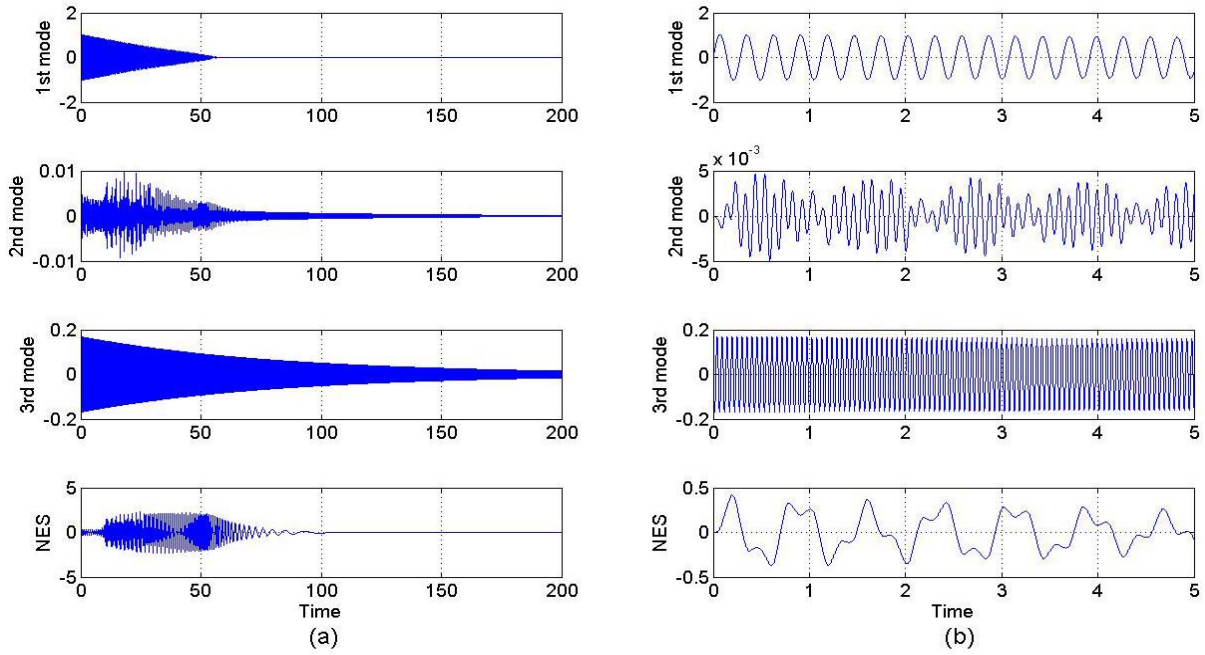

Figure 3.4: Transient response of the system when $F_I = 14.5$: (a) Beam and NES response; (b) Close-up of the Beam and NES response.

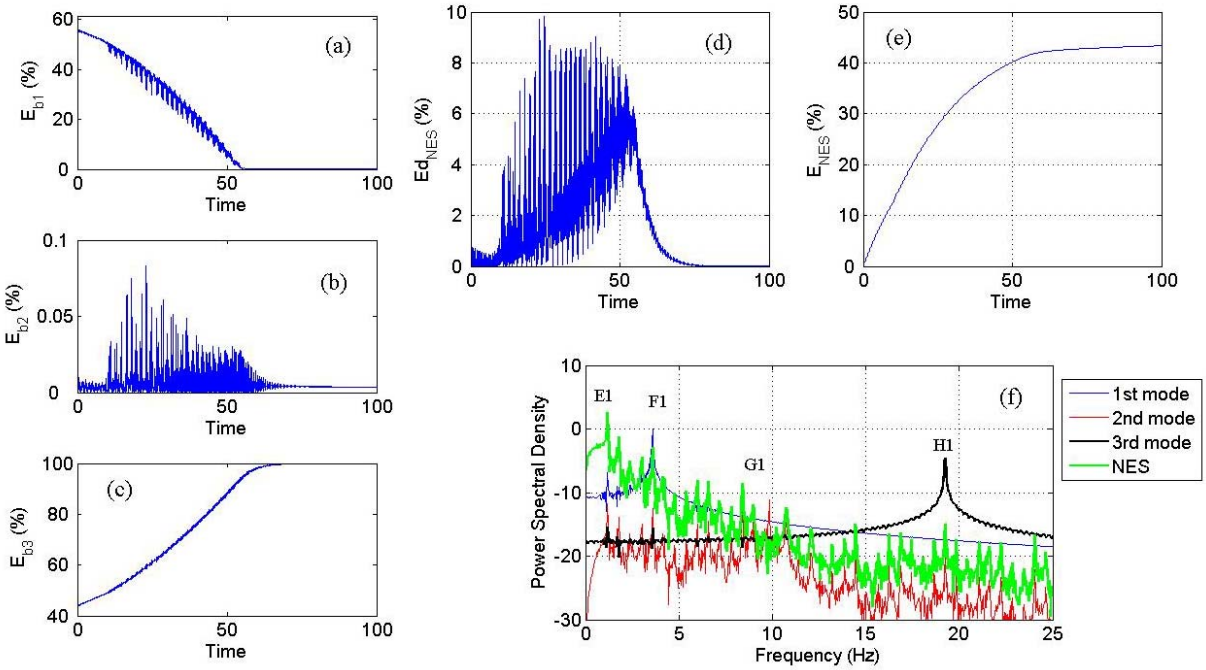

Figure 3.5: Transient dynamics of the system when $F_I = 14.5$: (a) Instantaneous total energy in the 1st mode; (b) 2nd mode and (c) 3rd mode; (d) Instantaneous energy in the NES; (e) energy dissipation by the NES and (f) Power Spectral Density of system response.

Moving towards the higher $F_I = 18$ (point C in Figure 3.1), qualitatively, similar dynamics is observed (Figure 3.6 and 3.7). NES continues the trend of moving towards the higher frequency oscillation. The energy transfer follows the same pattern as the previous case. Initially all the input impulse energy is in the beam then it flows back and forth between the beam and NES. Figure 3.7d shows that for $\tau \geq 60$, 5% of the total energy still remains in the NES, but, after a while (τ >80), this number starts to drop down to near 0%. In fact, this energy flows back to the beam where the third mode is capturing most of the energy (Figure 3.7c). For this case, around 42% of the input energy is dissipated by the NES (Figure 3.7e).

Moving to the even higher energy $F_I = 23.5$ (see Figures 3.8, 3.9 and point D in Figure 3.1), the pattern of oscillations of the modes and NES, and the energy transfer contains the trend indicated in previous cases. Namely, NES oscillates at higher frequency and most residual energy remains primarily in the third mode.

To gain better understanding of the underlying dynamics of the energy transfer, dominant Fourier mode in the PSD of the beam modes and NES are identified and compared. The PSD results from the cases discussed above have been shown in Figures 3.3f, 3.5f, 3.7f, and 3.9f. Here for each F_I value, the frequency ratio (FR) between the dominant Fourier modes of the mode and NES recalculated and displayed in a FR Vs. F_I diagram.

3.2. Targeted Energy Transfer by Linear Energy Sink

In this section, results from the LES are given. They are to provide the contrast with the performance of NES with the same parameter setting (section 3.1).

3.2.1. Simulation Results

To demonstrate, results used in section 3.1 from the same F_I values are shown. Similar to NES, the dominant mode of energy transfer continues to be the first bending mode as it has the largest vibration amplitude. Compared to the NES, there is a more specific frequency ratio between the LES and the first bending mode. For example, there is clear 5:1 frequency ratio seen here compared to that in Figure 3.2b. In addition, all bending modes oscillate in their own resonance frequency whereas those of the NES case show more complicated pattern.

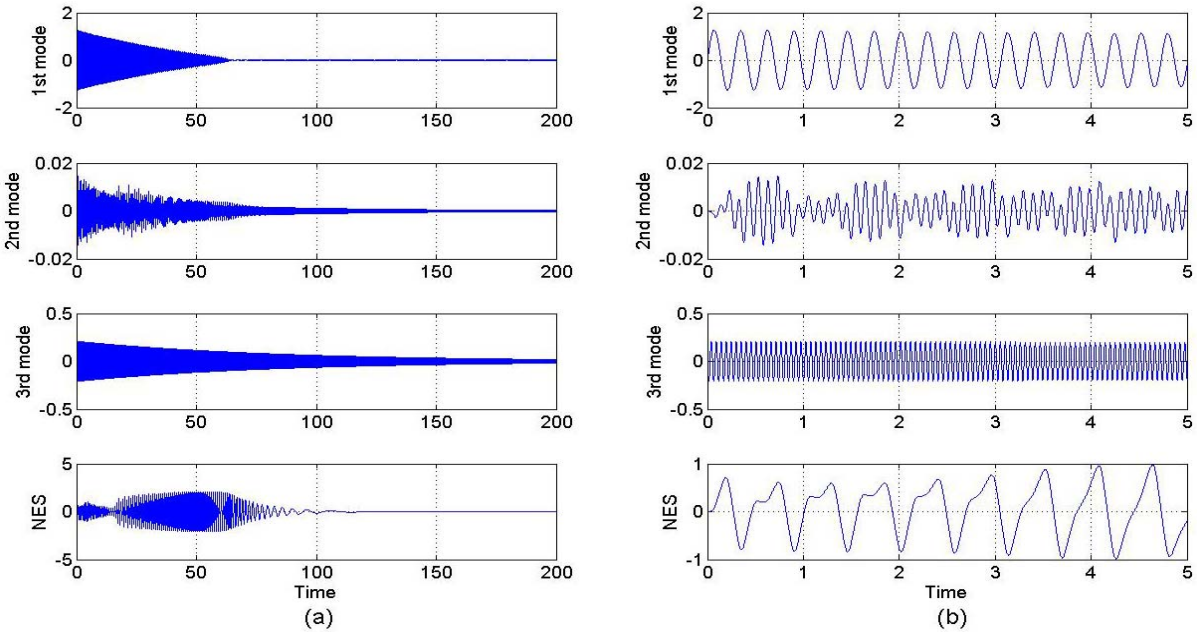

Figure 3.6: Transient response of the system when $F_1 = 18$: (a) Beam and NES response; (b) Close-up of the Beam and NES response.

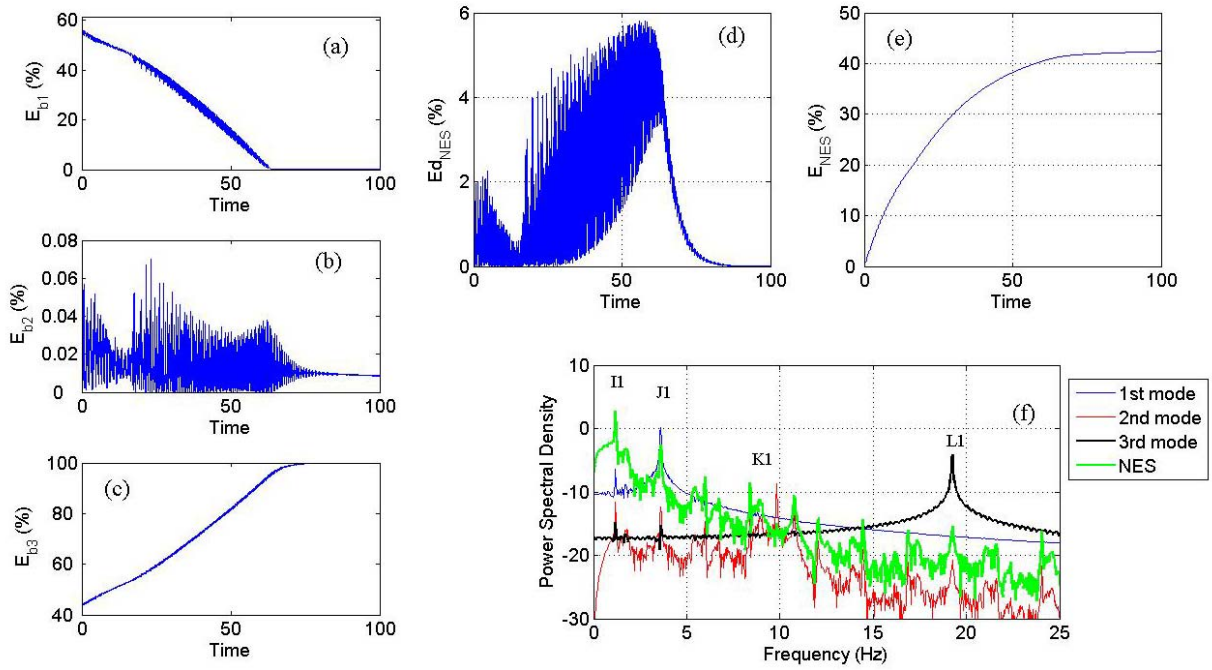

Figure 3.7: Transient dynamics of the system when $F_1 = 18$: (a) Instantaneous total energy in the 1st mode; (b) 2nd mode and (c) 3rd mode; (d) Instantaneous energy in the NES; (e) energy dissipation by the NES and (f) Power Spectral Density of system response.

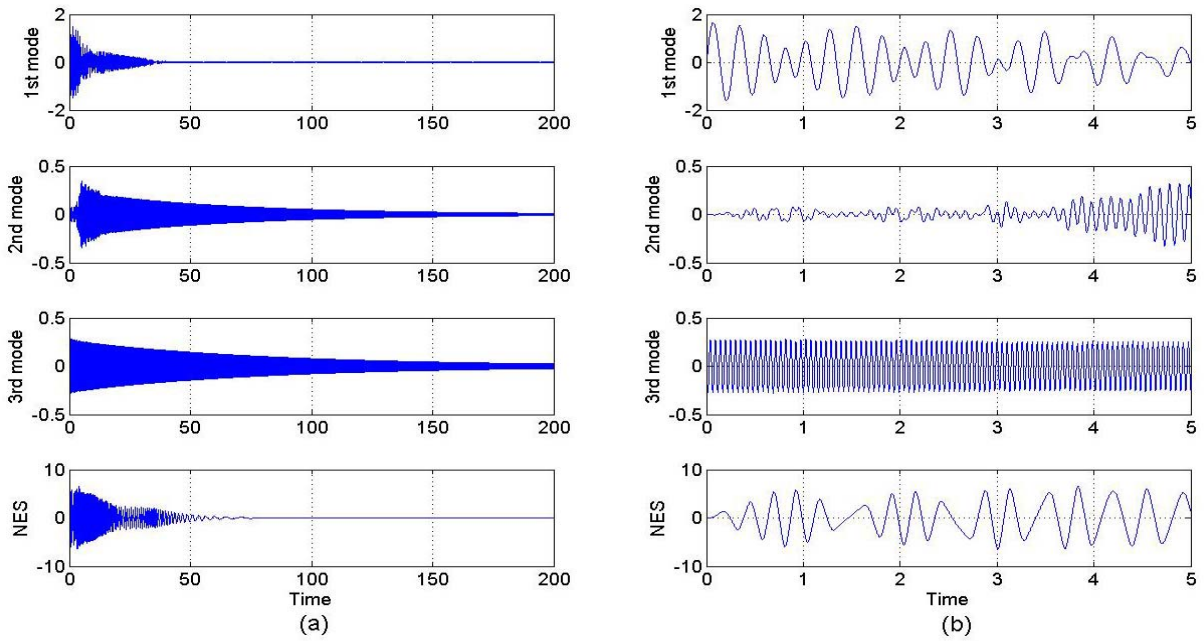

Figure 3.8: Transient response of the system when $F_I = 23.5$: (a) Beam and NES response; (b) Close-up of the Beam and NES response.

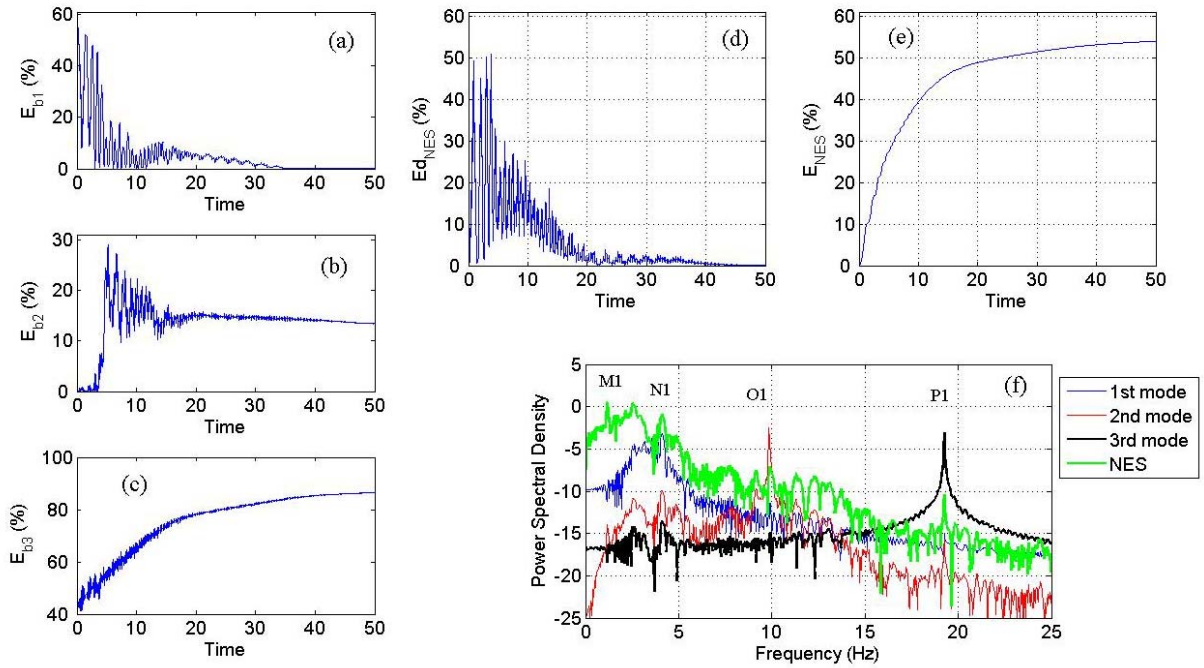

Figure 3.9: Transient dynamics of the system when $F_I = 23.5$: (a) Instantaneous total energy in the 1st mode; (b) 2nd mode and (c) 3rd mode; (d) Instantaneous energy in the NES; (e) energy dissipation by the NES and (f) Power Spectral Density of system response.

In particular, the second mode exhibits beating characteristics in the NES case (Figure 3.2b), but not in LES case (Figure 3.10b). This implies more significant energy transfer in and out of the second mode in the NES case, albeit it is a very small proportion compared to that in the first mode. These characteristics are also reflected in the results from various energy measures. For example, residual energy portion in second mode is higher in NES than in LES.

The PSDs confirm the more complicated dynamics in the NES than the LES case. However, for F_I=10.5, more energy is dissipated by the LES (47% versus 36% in the NES). In addition, E_{LES} (Figure 3.11e) rises faster than E_{NES} (Figure 3.3e), suggesting a more efficient energy transfer for LES in the low F_I range. Similar observations are made for other F_I=14.5 (Figures 3.12, 3.13), 18 (Figures 3.14, 3.15) and 23.5 (Figures 3.16, 3.17). Namely, as expected the dynamics of the LES is much simpler compared to the NES. With regard to energy transfer pattern, the $E_{LES}(\tau)$ in most cases rises faster than $E_{NES}(\tau)$ for $F_I \le 23$, NES is able to dissipate energy much faster. This can be shown more clearly by the $\tau_p^{(NES)}$, $\tau_p^{(LES)}$ versus F_I plot, where $\tau_p^{(NES,LES)}$ is determined from $E_{NES,LES}(\tau_p^{(NES,LES)}) = p$ (Figure 3.18).

3.3. Dominant Frequency Components in TET

To gain better understanding of the underlying dynamics of the energy transfer, dominant Fourier modes of the beam and NES are identified from the PSD and compared. The PSD results from the cases discussed above have been shown in Figures 3.3f, 3.5f, 3.7f, and 3.9f. For each F_I value the frequency ratio (FR) between the dominant Fourier modes of the beam and NES, LES are calculated. The results are displayed in a FR Vs. F_I diagram.

3.3.1. Dominant Frequency Components in TET for Impact Location D_1 = 0.5

To gain further understanding of the energy transfer between the beam and the ES, a frequency domain characterization is adopted. In particular, the frequency of the dominant Fourier modes of the beam and ES are first located and, then, compared to identify potential coupling. Such coupling can contain valuable information as it implies the dominant motion that carries the energy transfer between the beam and ES.

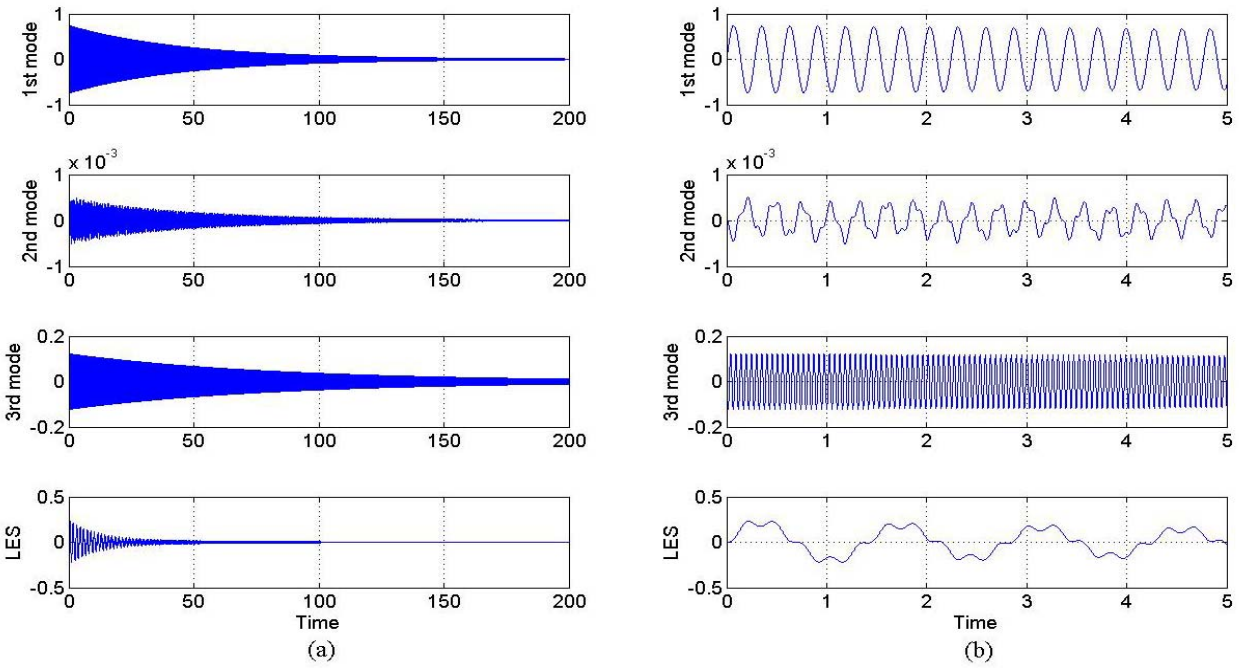

Figure 3.10: Transient response of the system when $F_1 = 10.5$:(a) Beam and LES response; (b) Close-up of the Beam and LES response.

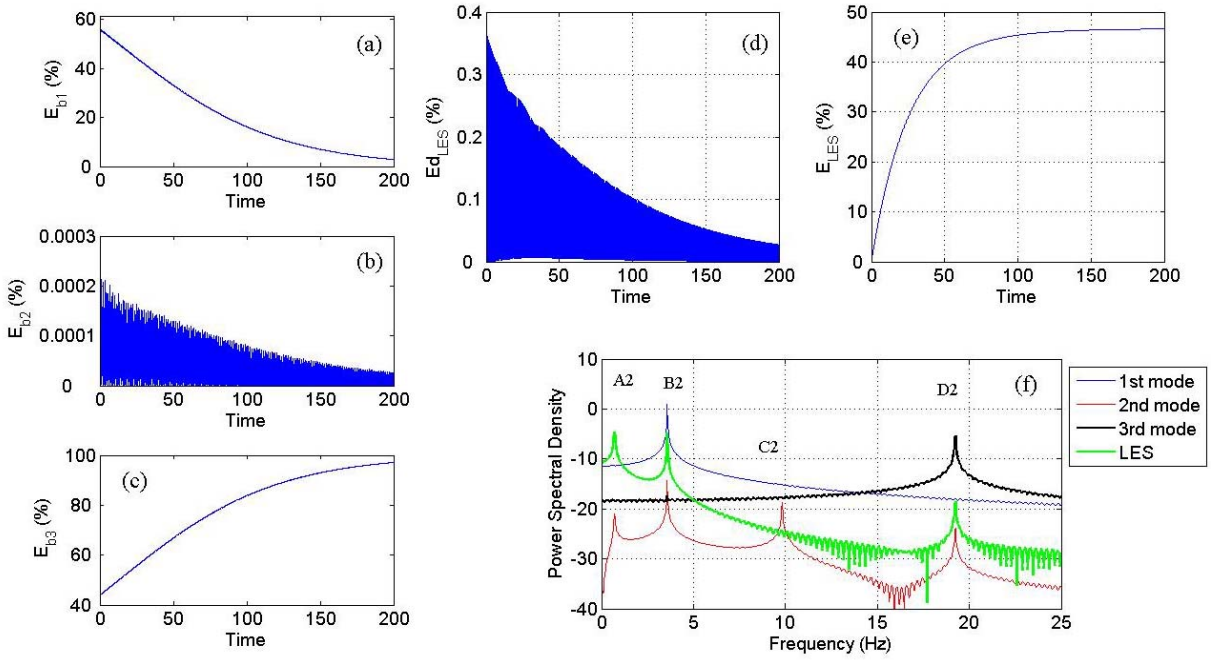

Figure 3.11: Transient dynamics of the system when $F_1 = 10.5$: (a) Instantaneous total energy in the 1st mode; (b) 2nd mode and (c) 3rd mode; (d) Instantaneous energy in the LES; (e) energy dissipation by the LES and (f) Power Spectral Density of system response.

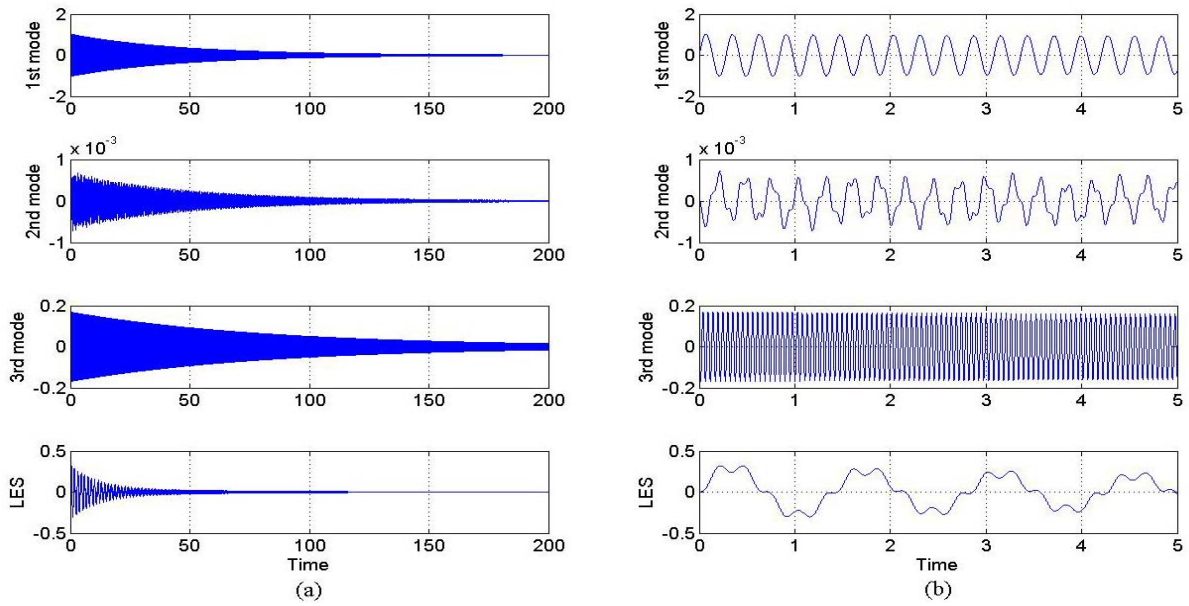

Figure 3.12: Transient response of the system when $F_1 = 14.5$:(a) Beam and LES response; (b) Close-up of the Beam and LES response.

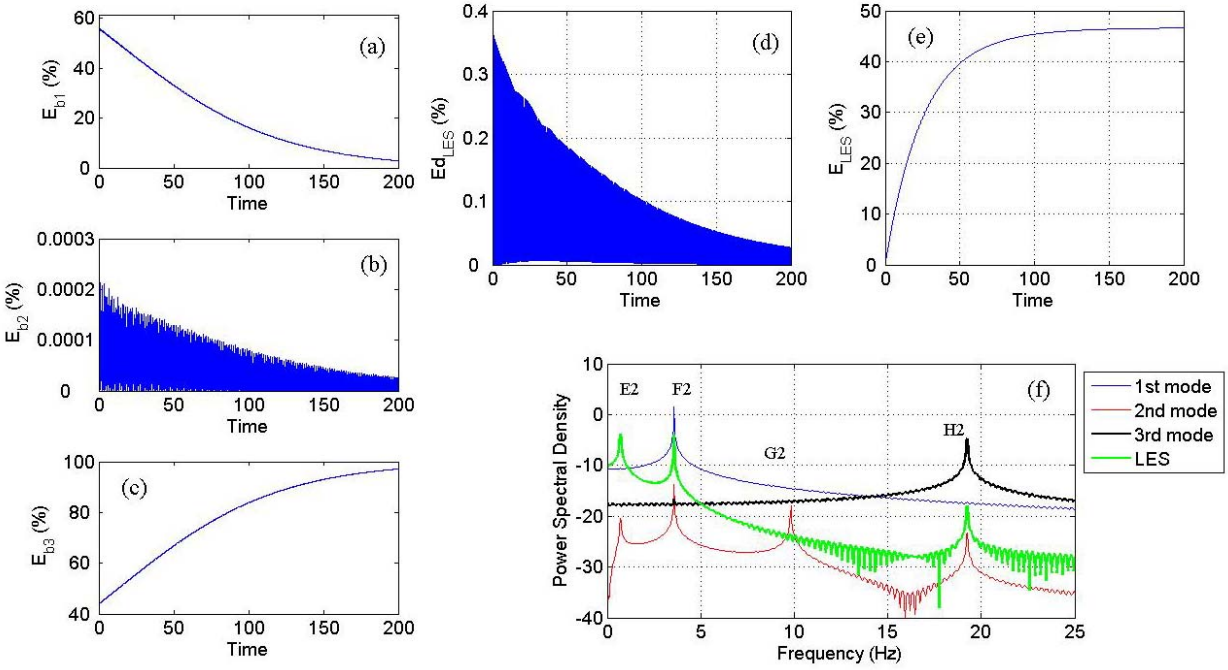

Figure 3.13: Transient dynamics of the system when $F_1 = 14.5$: (a) Instantaneous total energy in the 1st mode; (b) 2nd mode and (c) 3rd mode; (d) Instantaneous energy in the LES; (e) energy dissipation by the LES and (f) Power Spectral Density of system response.

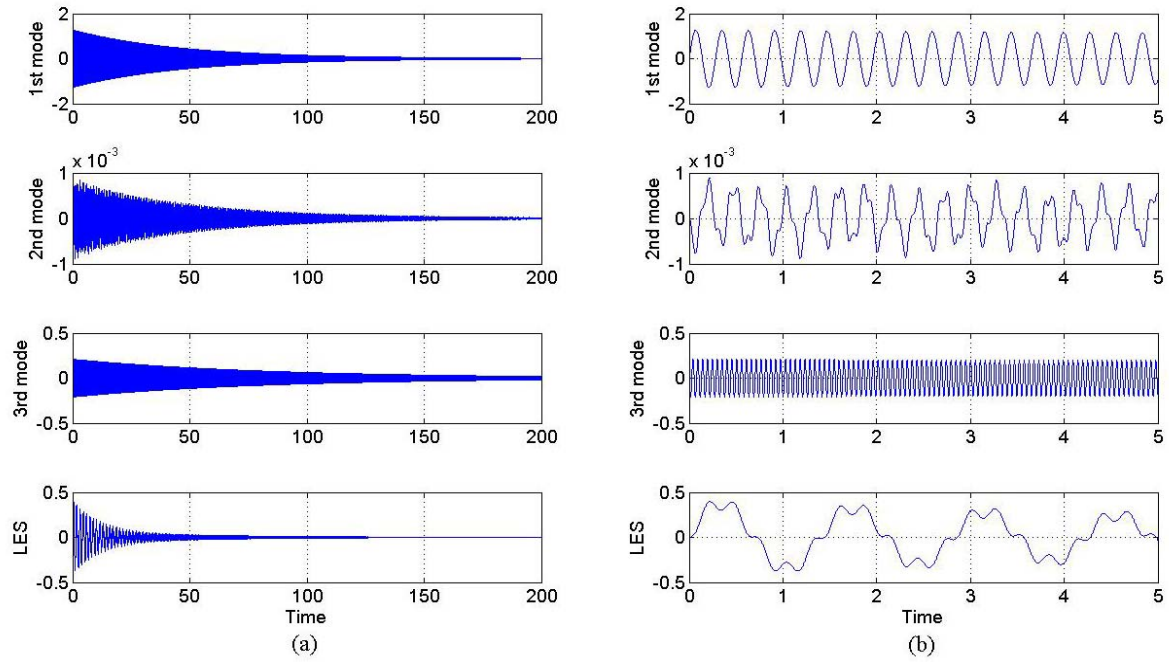

Figure 3.14: Transient response of the system when $F_1 = 18$: (a) Beam and LES response; (b) Close-up of the Beam and LES response.

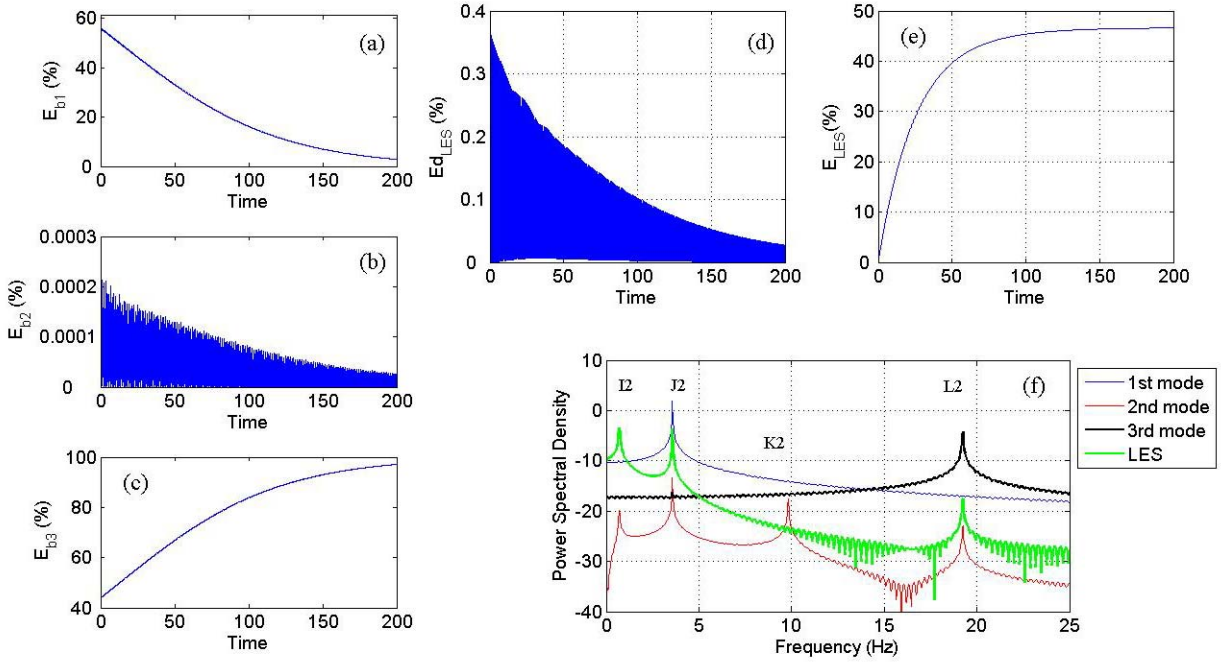

Figure 3.15: Transient dynamics of the system when $F_1 = 18$: (a) Instantaneous total energy in the 1st mode; (b) 2nd mode and (c) 3rd mode; (d) Instantaneous energy in the LES; (e) energy dissipation by the LES and (f) Power Spectral Density of system response.

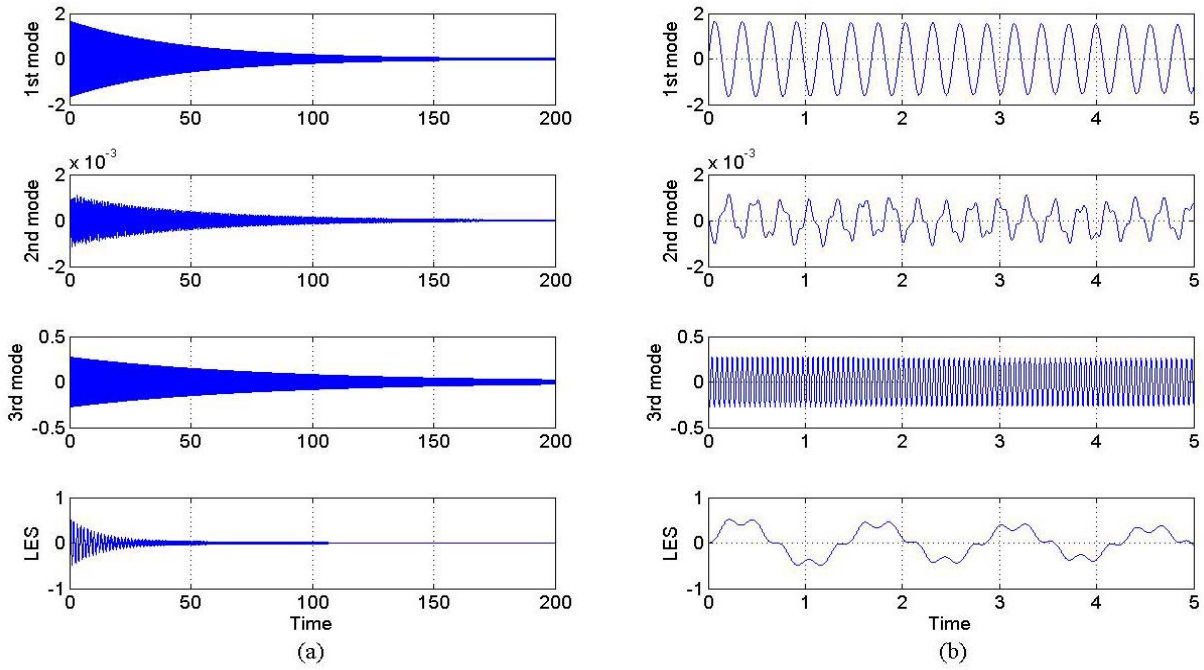

Figure 3.16: Transient response of the system when $F_1 = 23.5$: (a) Beam and LES response; (b) Close-up of the Beam and LES response.

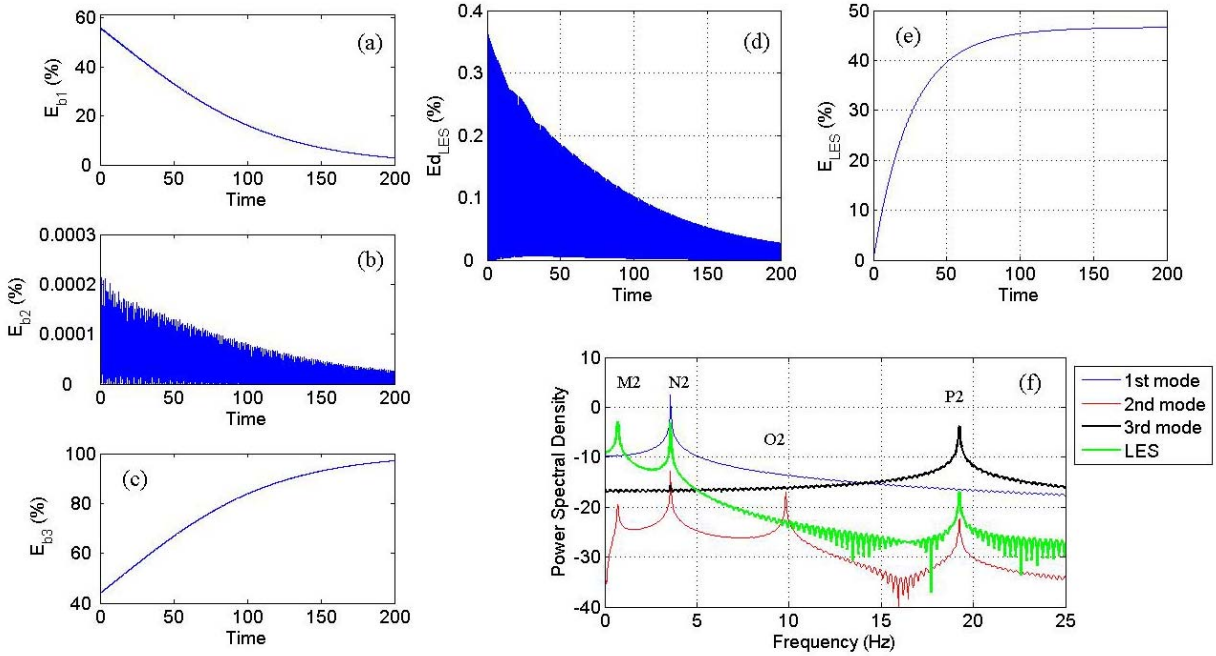

Figure 3.17: Transient dynamics of the system when $F_1 = 23.5$: (a) Instantaneous total energy in the 1st mode; (b) 2nd mode and (c) 3rd mode; (d) Instantaneous energy in the LES; (e) energy dissipation by the LES and (f) Power Spectral Density of system response.

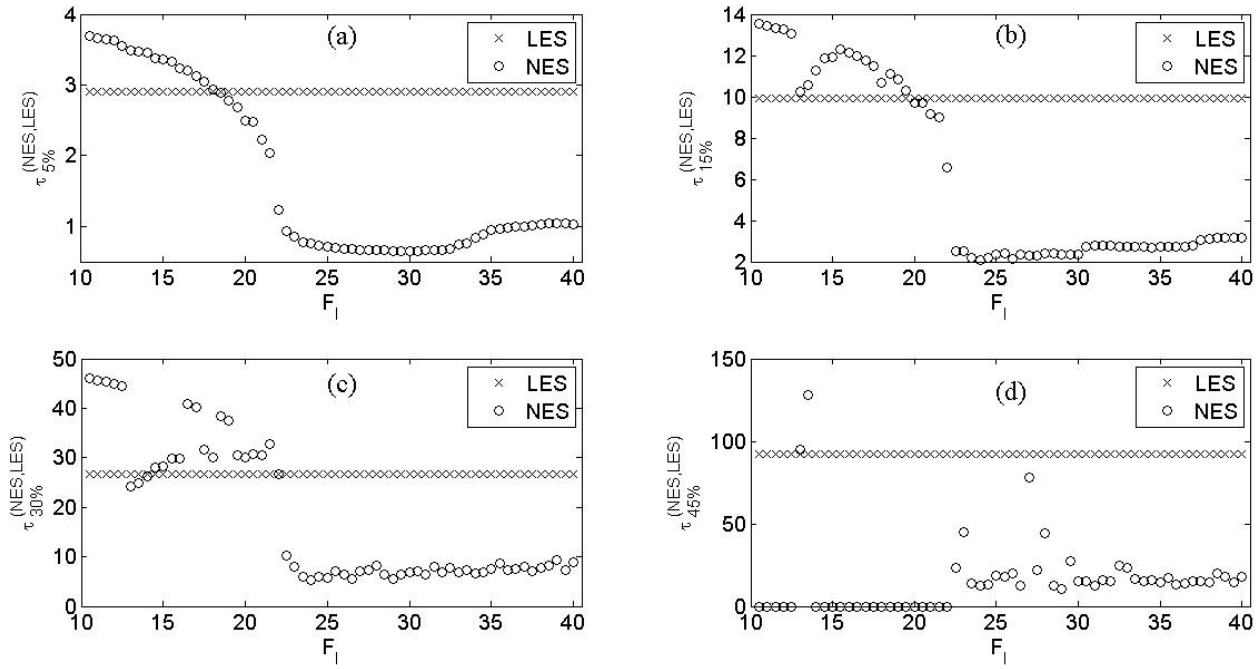

Figure 3.18: Required time for dissipating a certain amount of energy as a function of F_I: (a) 5% energy dissipation; (b) 15% energy dissipation; (c) 30% energy dissipation; (d) 45% energy dissipation.

Figures 3.19 and 3.20 show the dominant frequencies as a function of F_I for the case of NES and LES. Of particular importance is the dominant frequency of the NES f_D^{NES} in TET and its relationship with the dominant frequencies of the bending modes, f_D^{Beam}. For example, in Figure 3.3f, two dominant frequencies $f_{D1}^{NES} \sim 0.89$ (point A1) and $f_{D2}^{NES} \sim 3.57$ (point B1) are identified. The Fourier amplitudes at these two frequencies are very close. It is seen that f_{D2}^{NES} matches well with the dominant frequency of the first bending modes, $f_{D1}^{Beam} \sim 3.57$. This result may follow intuitively in that most of the impact energy is captured by the first bending mode, which exhibits the largest amplitude of vibration (see, e.g., Figures 3.2a, 3.4a, 3.6a, and 3.8a). It is plausible that the main energy transfer should involve the first bending mode. This frequency coupling is found to persist in general for all the F_I value. But for $F_I > 23.5$ (Figure 3.9f), a bifurcation pattern emerges where a third f_{D3}^{NES} appears between f_{D1}^{NES} and f_{D2}^{NES}.

The results of Figure 3.19 can be summarized in Figure 3.21(c) where the dominant frequency ratio of the first bending mode and NES $f_{D1}^{Beam} / f_{D1,D2}^{NES}$ are shown. Frequency ratio

between NES and other bending modes is not considered since their Fourier amplitudes are generally orders of magnitude smaller, albeit they are physically coupled in the model.

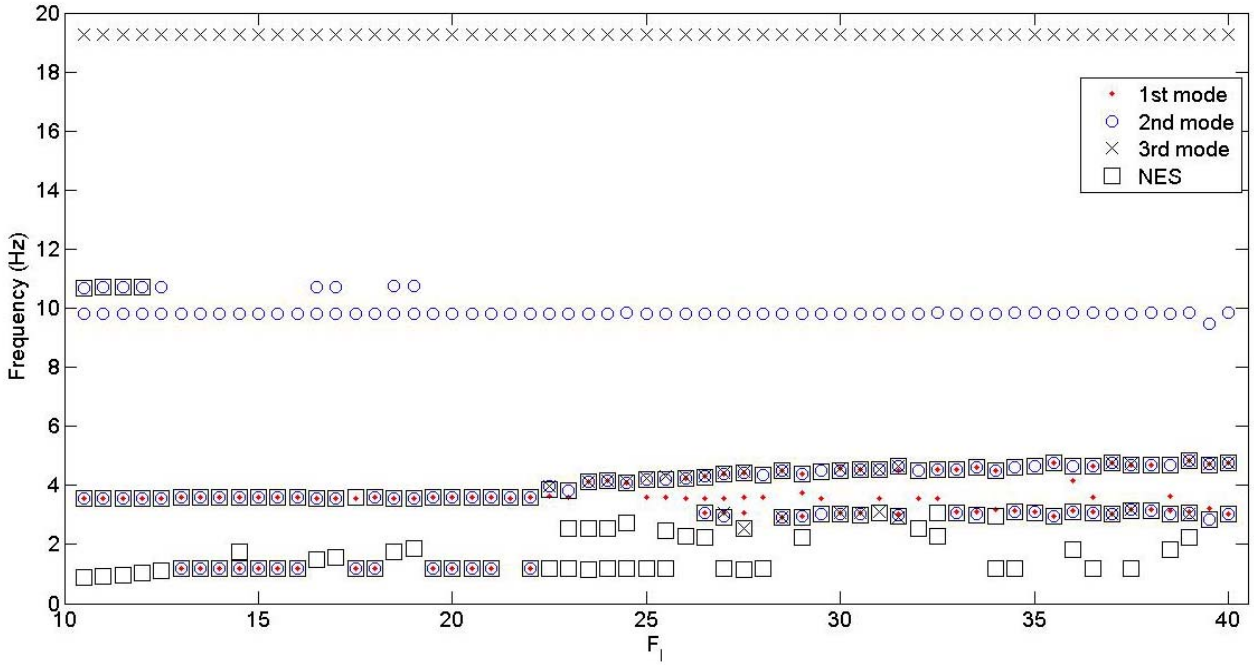

Figure 3.19: Dominant frequency as a function of F_I at $D_1 = 0.5$ for NES.

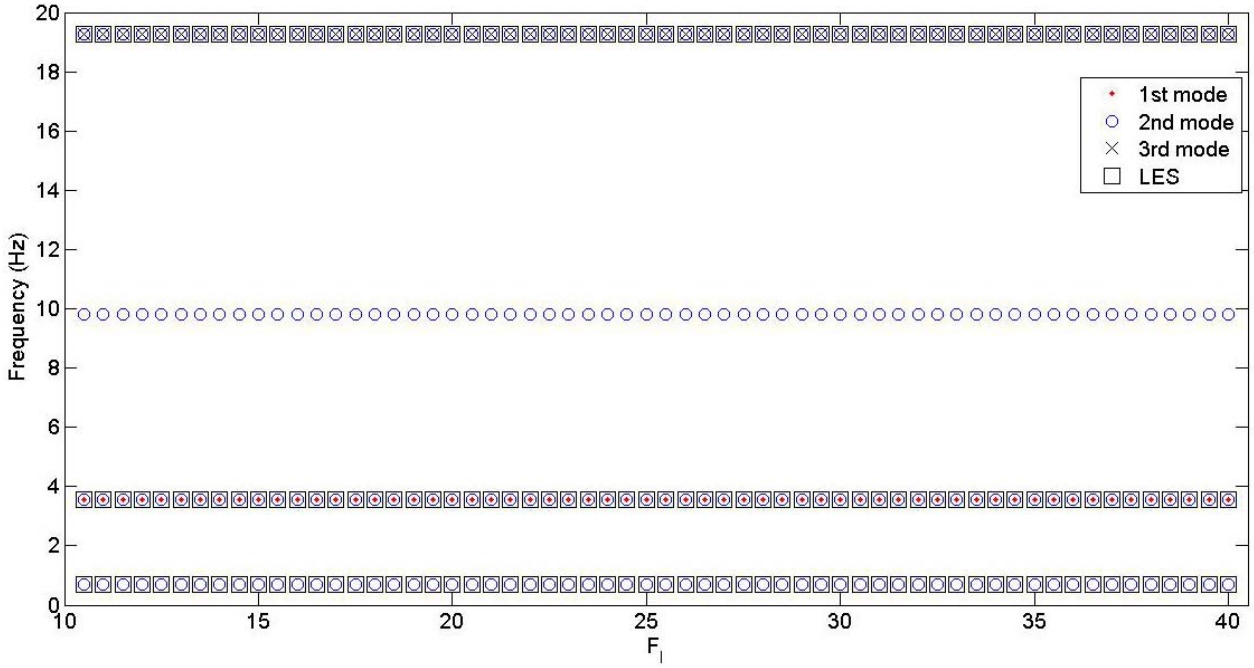

Figure 3.20: Dominant frequency as a function of F_I at $D_1 = 0.5$ for LES.

3.3.2. Dominant Frequency Components in TET for Different Impact Locations

Detailed energy dissipation pattern of E_{NES}, E_{LES}, according to the impact locations are shown in Figure 3.22. The percent dissipation captured by these variables varies depending on how close the impact is delivered relative to the ES location (D = 0.4): higher percentage of dissipation is obtained when the impact is delivered closer to the ES location. A unique F_I level appears to exist where $E_{NES,\ LES}$ begins to rise. Such a transition appears particularly sharp when the impact is applied at exactly the location of the ES (D = 0.4). In addition, E_{LES} is independent of F_I. This particular property can be shown using the linear system theory [17]. Briefly, both the energy dissipation by ES in the numerator and the input energy from the impact in the denominator of E_{LES}, equation (2.32), can be expressed as linear functions of F_I. The dependence of F_I in LES is therefore cancelled out; see Appendix C for details.

Similar to the case at D_1 = 0.5 (sections 3.1, 3.2), the frequency-domain analysis at different impact locations continues to show the first bending mode being the dominant degree-of-freedom involving in the energy transfer with the ES. In contrast, the dominant Fourier modes of the other bending modes exhibit much smaller amplitudes of vibration. These results are summarized in Figures 3.21, and 3.23 through 3.26 for NES and Figures 3.27 through 3.30 for LES at D_1 = 0.3, 0.4, 0.6 and 0.7, respectively. It is also observed that the underlying dynamics is more complex when the impact is applied away from the boundaries. In particular, more Fourier modes are excited when the impact is delivered around the mid-span area of the beam. The estimated FR in different impact locations has been summarized in Figure 3.21 for the NES and Figure 3.31 for the LES. Here, two FRs are provided based on the first two dominant Fourier modes of the ES: FR1 = $f_{D1}^{Beam} / f_{D1}^{NES,LES}$ and FR2 = $f_{D1}^{Beam} / f_{D2}^{NES,LES}$. For the NES, FR1 and FR2 exhibit an initial drop for small F_I before they appear to approach the "asymptotic" values FR1 ~ 3, FR2 ~ 1 for large F_I; see also Figure 3.21. For the LES, the FR is constant: FR1 = 5, FR2 = 1 for all F_I values. Note that energy transfer is more effective for larger F_I values since E_{NES}, E_{LES} are larger. The corresponding FR1, FR2 values in this parameter range may therefore be significant.

The estimated frequency ratios reported above may be observable from the oscillation of the first bending mode and the ES, granted it can be less obvious when it comes to the nonlinear response of NES. For example, shown in Figures 3.32 through 3.36 are samples of $g_1(\tau)$ and $Y(\tau)$ for NES and Figures 3.37 through 3.41 for the LES with F_I = 10.5, 14.5, 18, 23.5 and D_1 =

0.3, 0.4, 0.5, 0.6, and 0.7, respectively. A decreasing FR can be observed in Figures 3.32 through 3.36 over the same 5-sec period, there are roughly 3 cycles of $Y(\tau)$ for F_I = 10.5 and this number increases to approximately 8 cycles for F_I = 18. When examined closely, it is also seen at a high frequency component that appears to oscillate in 1:1 synchronization with $g_1(\tau)$. For LES, there is a very clear 5:1 frequency ratio between $g_1(\tau)$ and $Y(\tau)$: over the same 5-sec period, there is roughly 17.5 cycles of $g_1(\tau)$ and 3.5 cycles of $Y(\tau)$. Similar to the NES case, the high frequency component in $Y(\tau)$ that exhibits 1:1 synchronization with $g_1(\tau)$ is also discernable. These counts verify the FR1 = 5 and FR2 = 1 estimates from Figures 3.27 through 3.30.

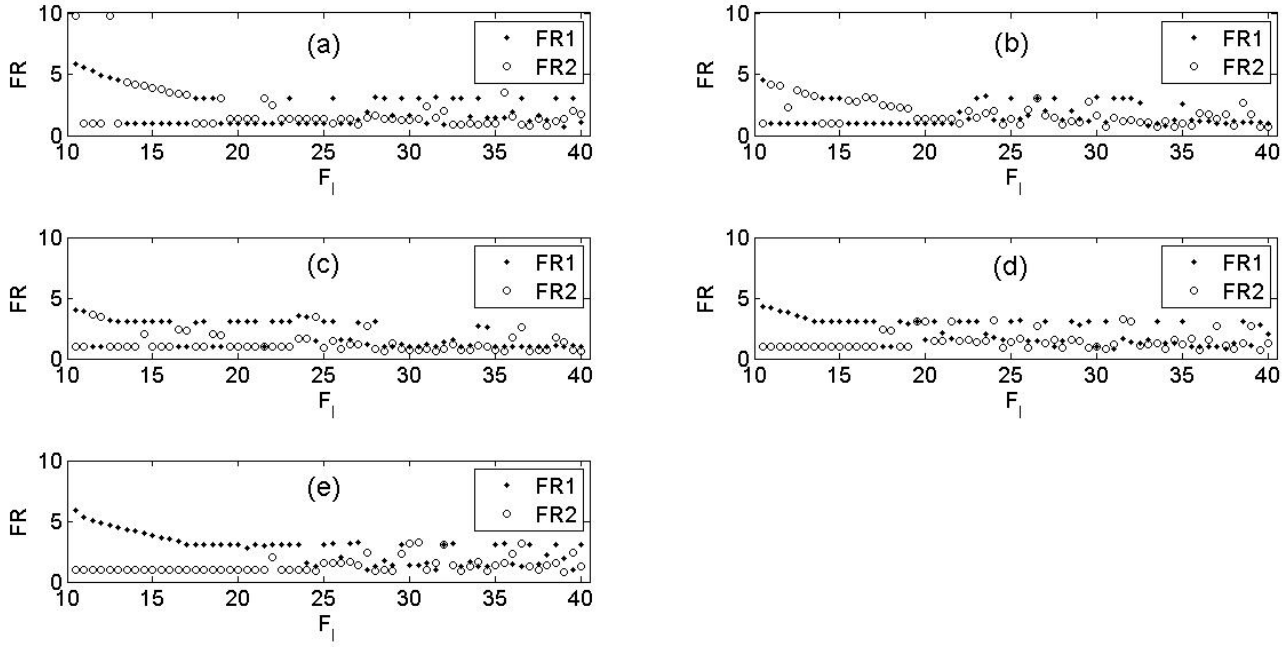

Figure 3.21: Frequency ratio as a function of F_I for NES: (a) D_I = 0.3; (b) D_I = 0.4; (c) D_I = 0.5; (d) D_I = 0.6, and (e) D_I = 0.7.

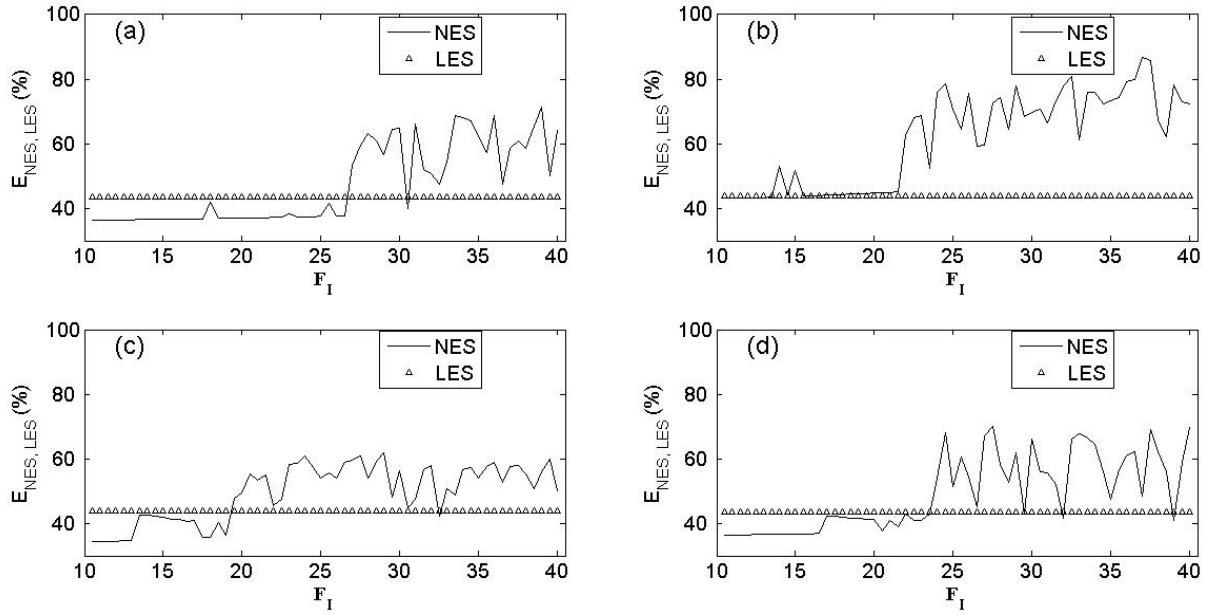

Figure 3.22: Energy dissipation as a function of F_I for various locations: (a) D_I = 0.3; (b) D_I = 0.4; (c) D_I = 0.6 and (d) D_I = 0.7.

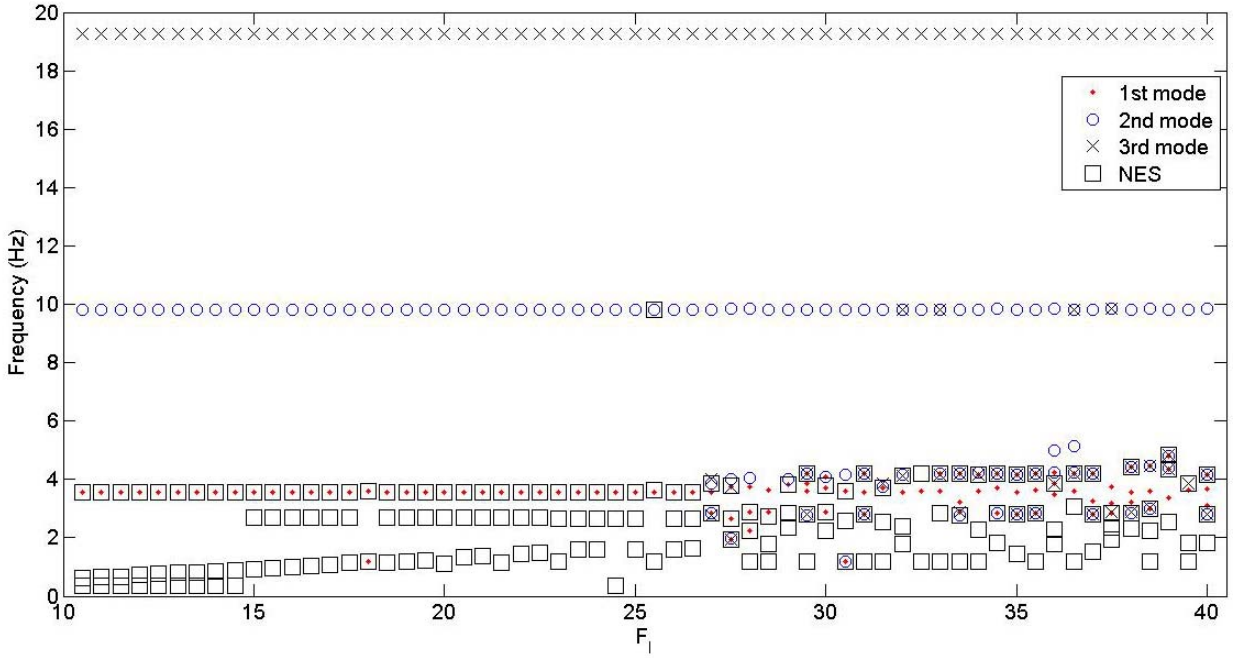

Figure 3.23: Dominant frequency as a function of F_I at D_1 = 0.3 for NES.

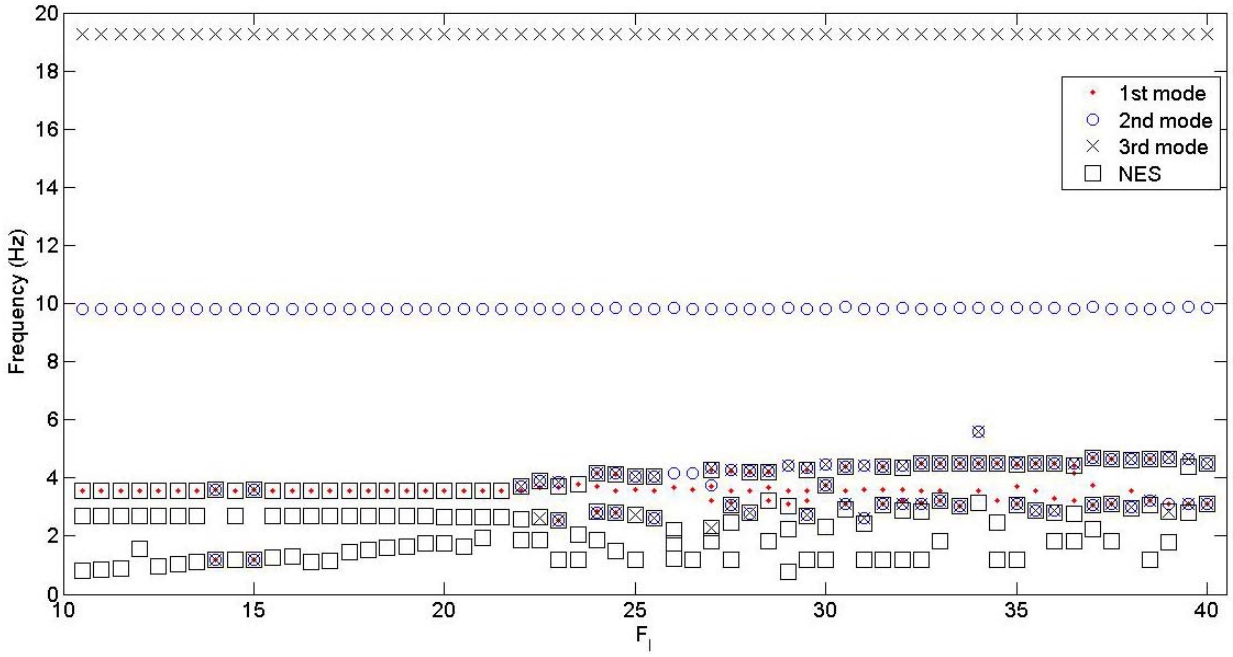

Figure 3.24: Dominant frequency as a function of F_I at $D_1 = 0.4$ for NES.

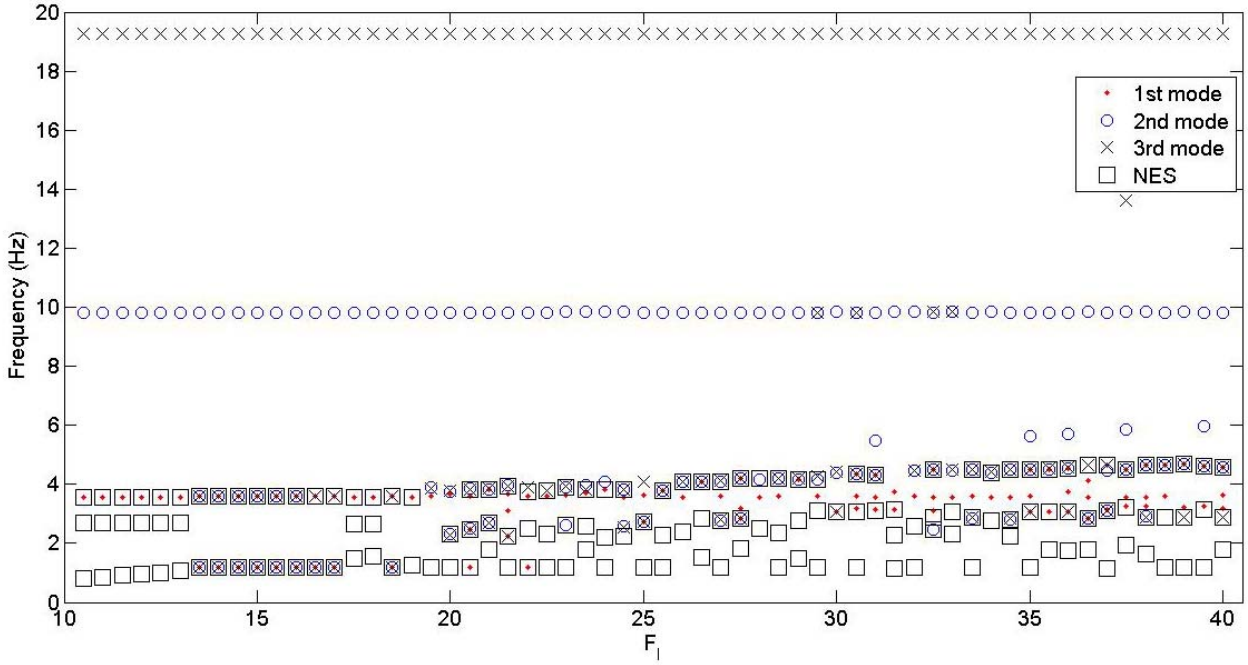

Figure 3.25: Dominant frequency as a function of F_I at $D_1 = 0.6$ for NES.

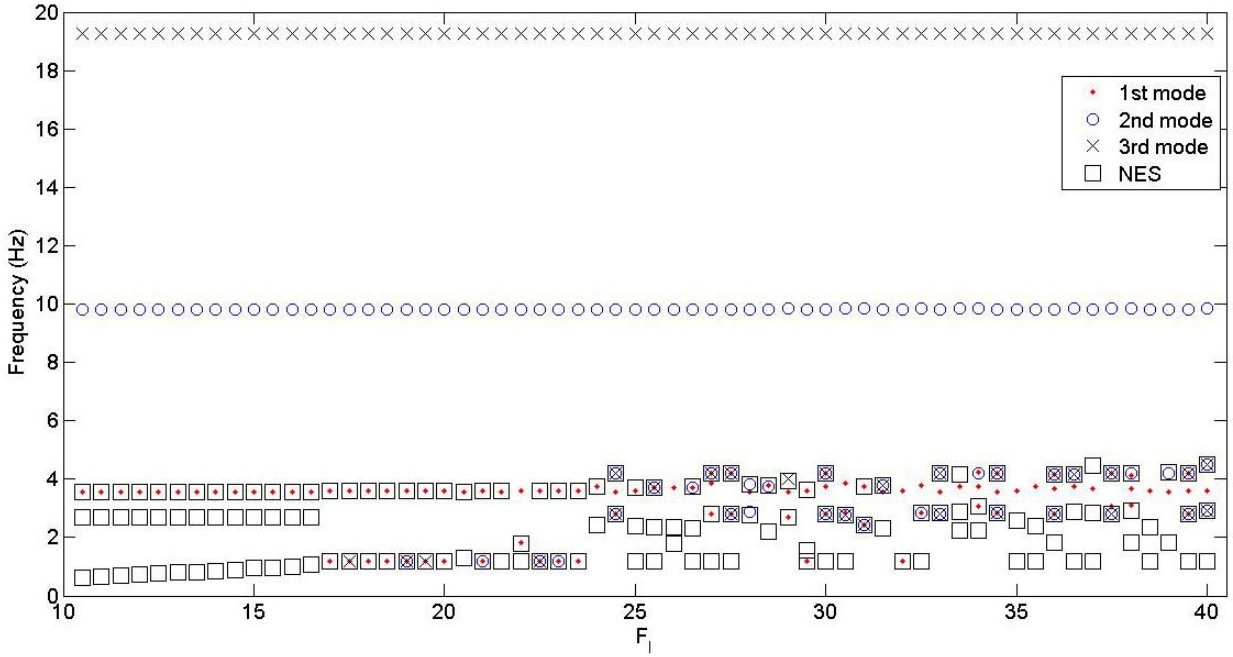

Figure 3.26: Dominant frequency as a function of F_l at $D_1 = 0.7$ for NES.

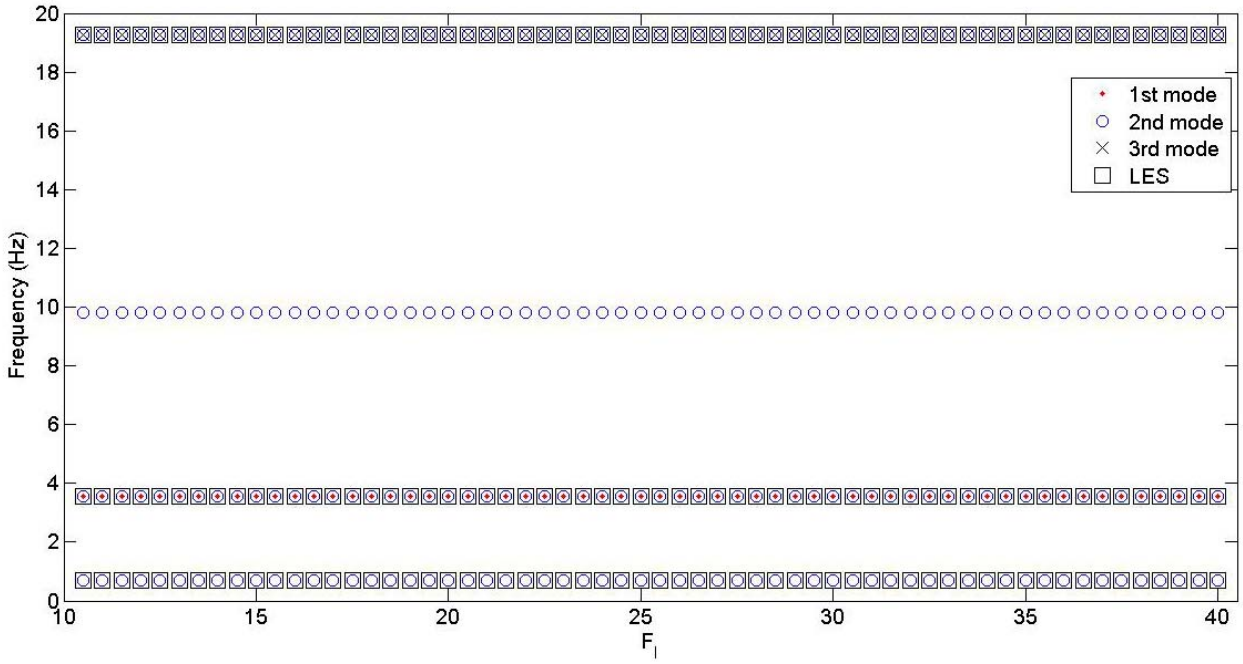

Figure 3.27: Dominant frequency as a function of F_l at $D_1 = 0.3$ for LES.

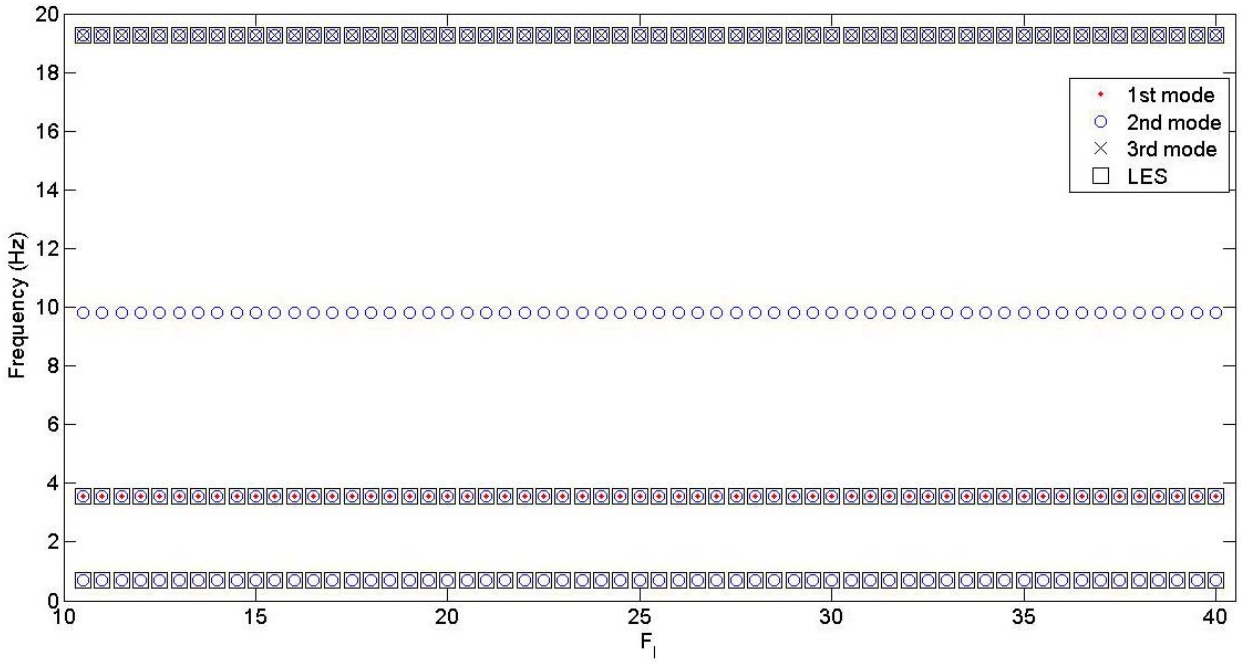

Figure 3.28: Dominant frequency as a function of F_I at $D_1 = 0.4$ for LES.

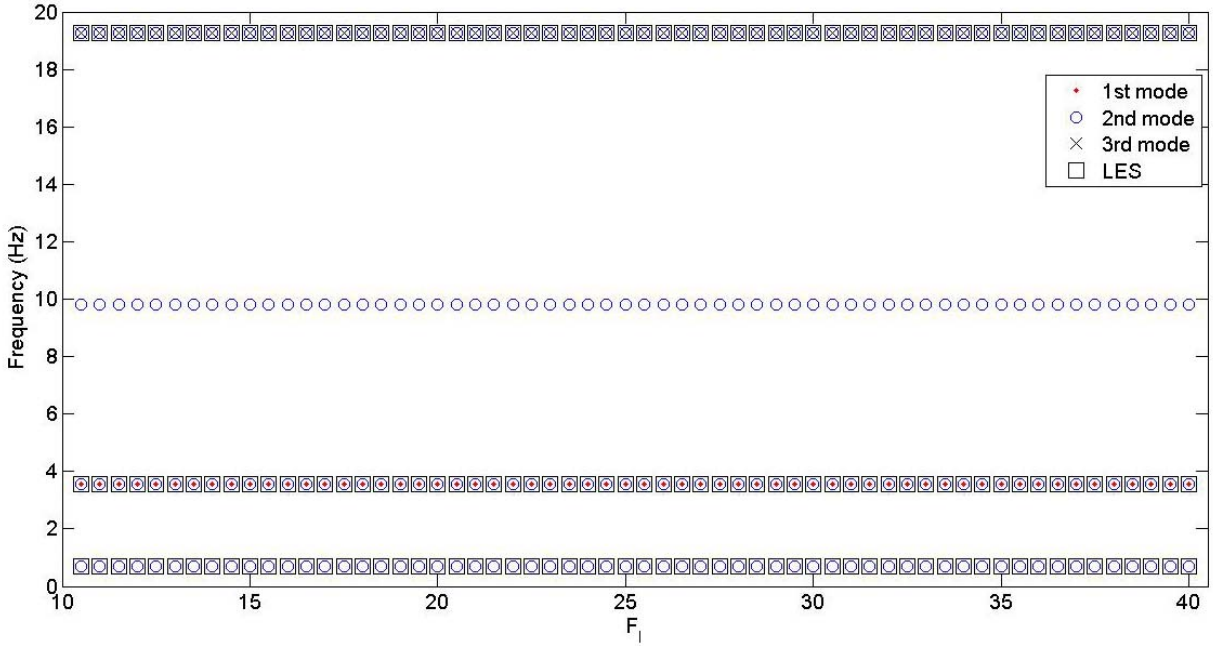

Figure 3.29: Dominant frequency as a function of F_I at $D_1 = 0.6$ for LES.

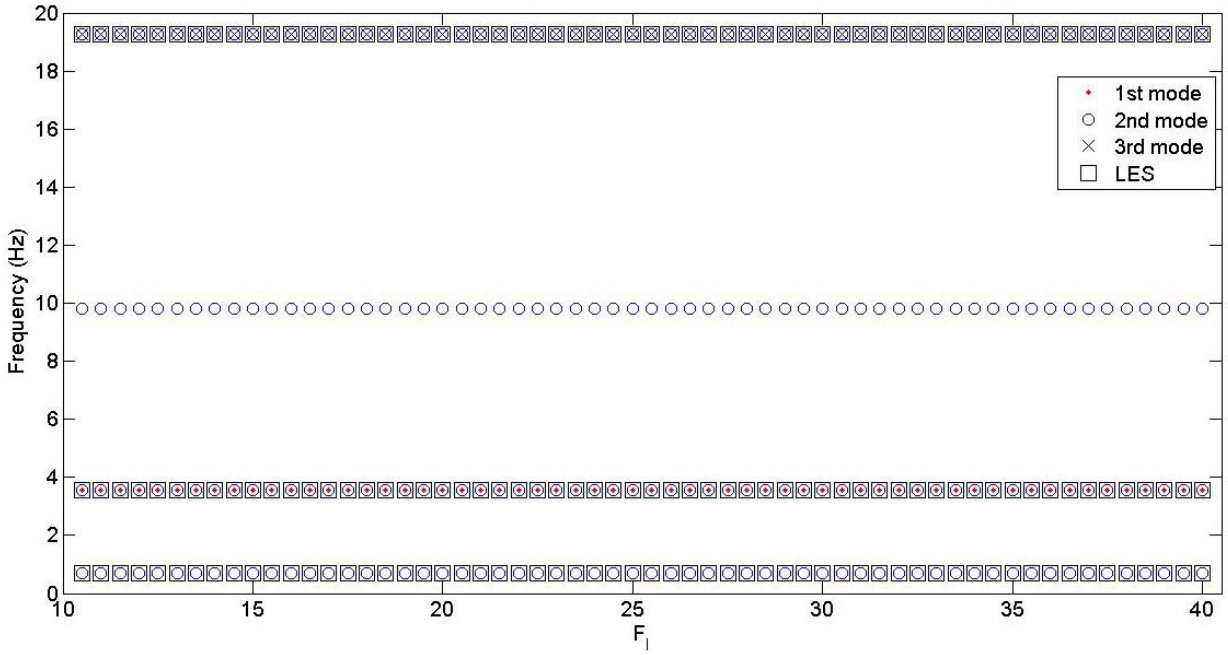

Figure 3.30: Dominant frequency as a function of F_I at $D_1 = 0.7$ for LES.

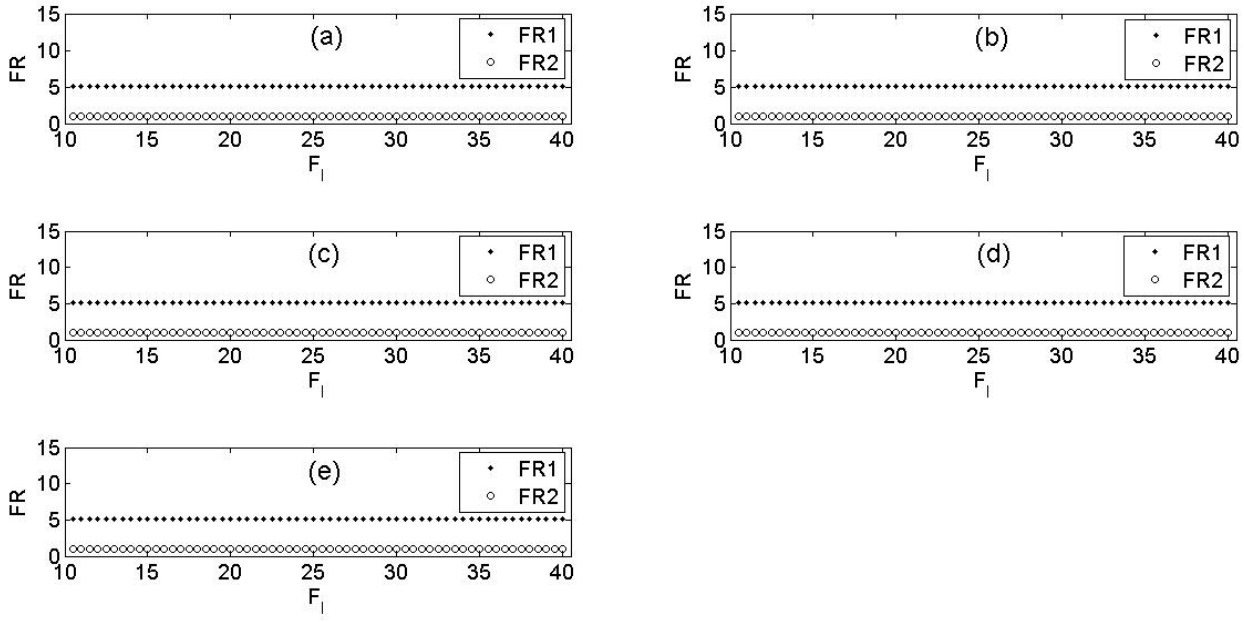

Figure 3.31: Frequency ratio as a function of F_I for LES: (a) $D_I = 0.3$; (b) $D_I = 0.4$; (c) $D_I = 0.5$; (d) $D_I = 0.6$ and (e) $D_I = 0.7$.

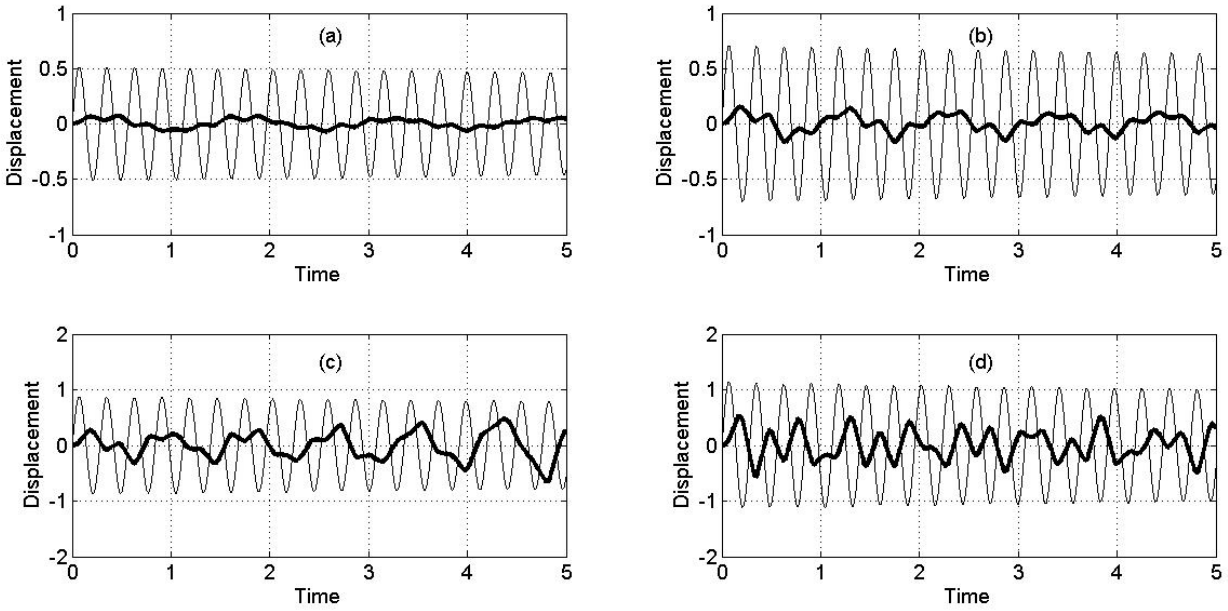

Figure 3.32: Time response for the 1st mode and NES when F_I applied at D_I = 0.3: (a) F_I = 10.5; (b) F_I = 14.5; (c) F_I = 18, and (d) F_I = 23.5; —— 1st mode, ▬▬ NES.

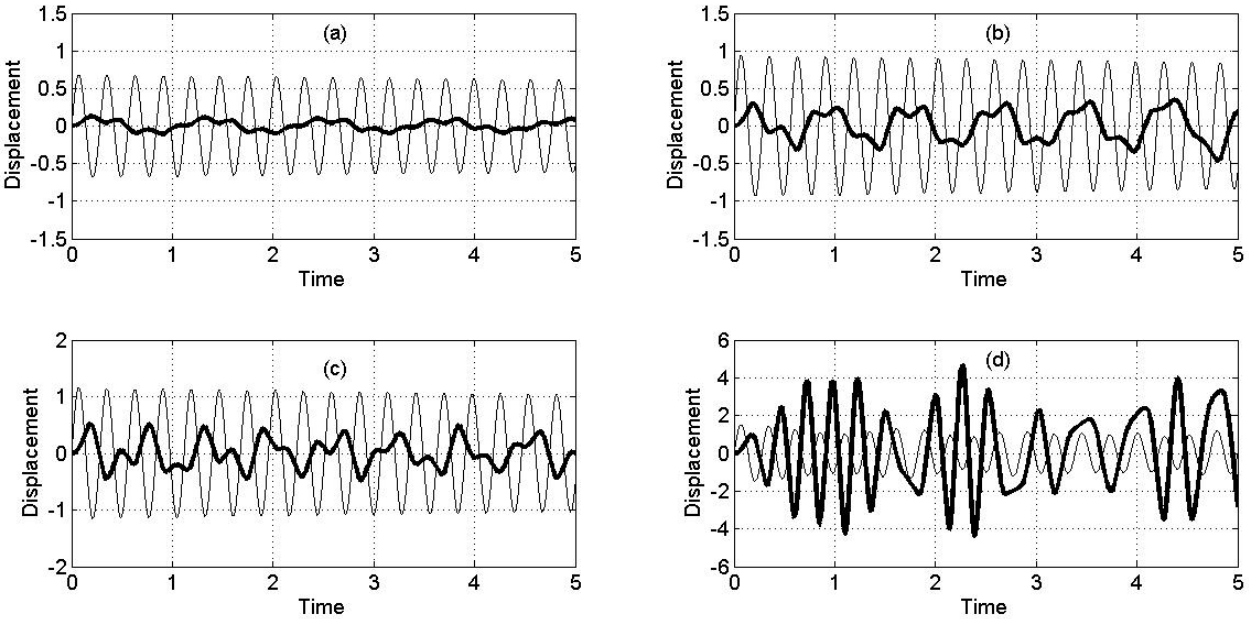

Figure 3.33: Time response for the 1st mode and NES when F_I applied at D_I = 0.4: (a) F_I = 10.5; (b) F_I = 14.5; (c) F_I = 18, and (d) F_I = 23.5; —— 1st mode, ▬▬ NES.

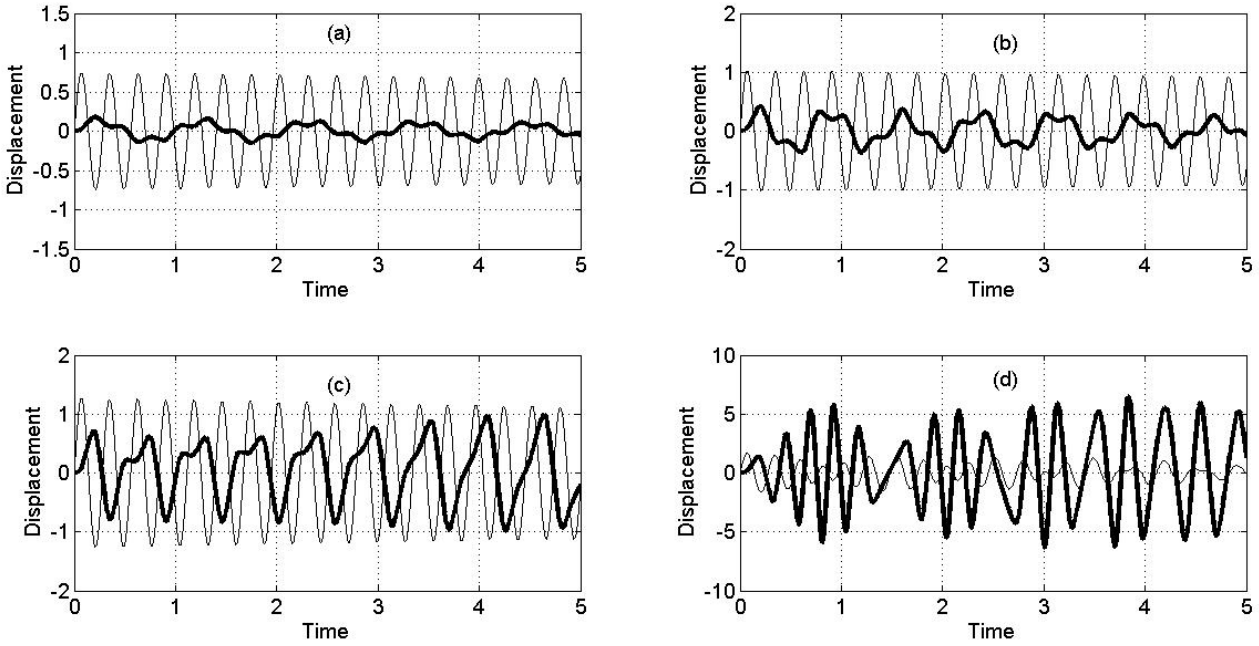

Figure 3.34: Time response for the 1st mode and NES when F_I applied at D_I = 0.5: (a) F_I = 10.5; (b) F_I = 14.5; (c) F_I = 18, and (d) F_I = 23.5; —— 1st mode, ▬▬ NES.

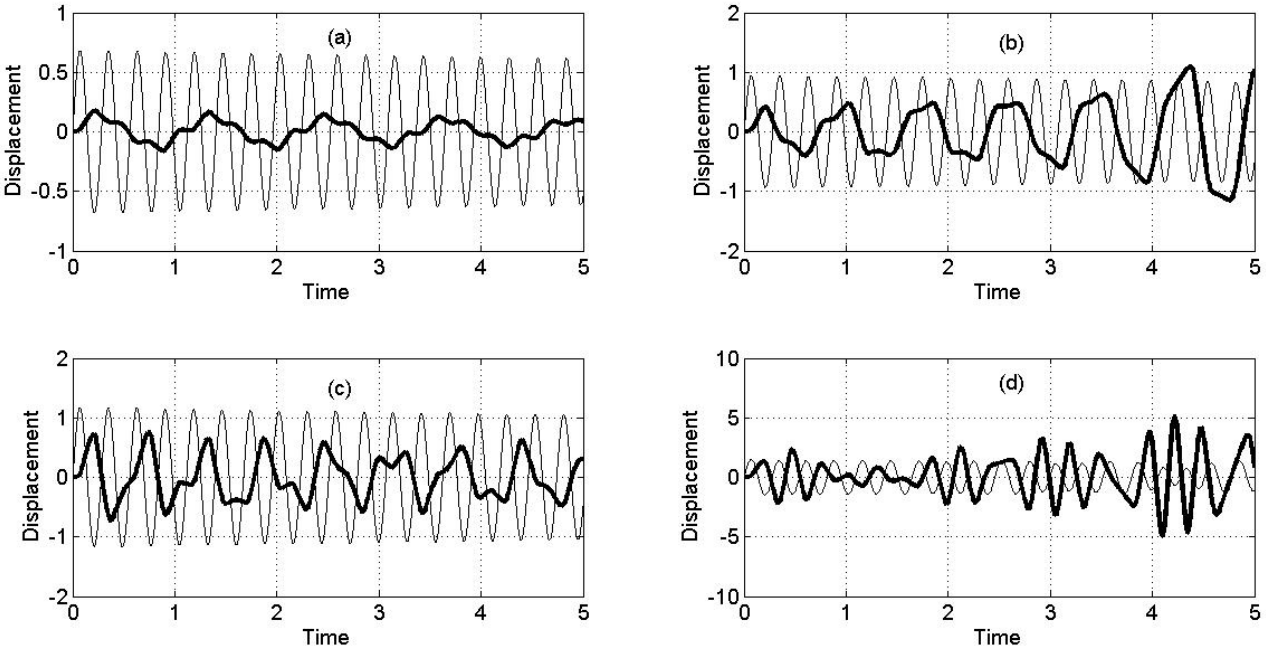

Figure 3.35: Time response for the 1st mode and NES when F_I applied at D_I = 0.6: (a) F_I = 10.5; (b) F_I = 14.5; (c) F_I = 18, and (d) F_I = 23.5; —— 1st mode, ▬▬ NES.

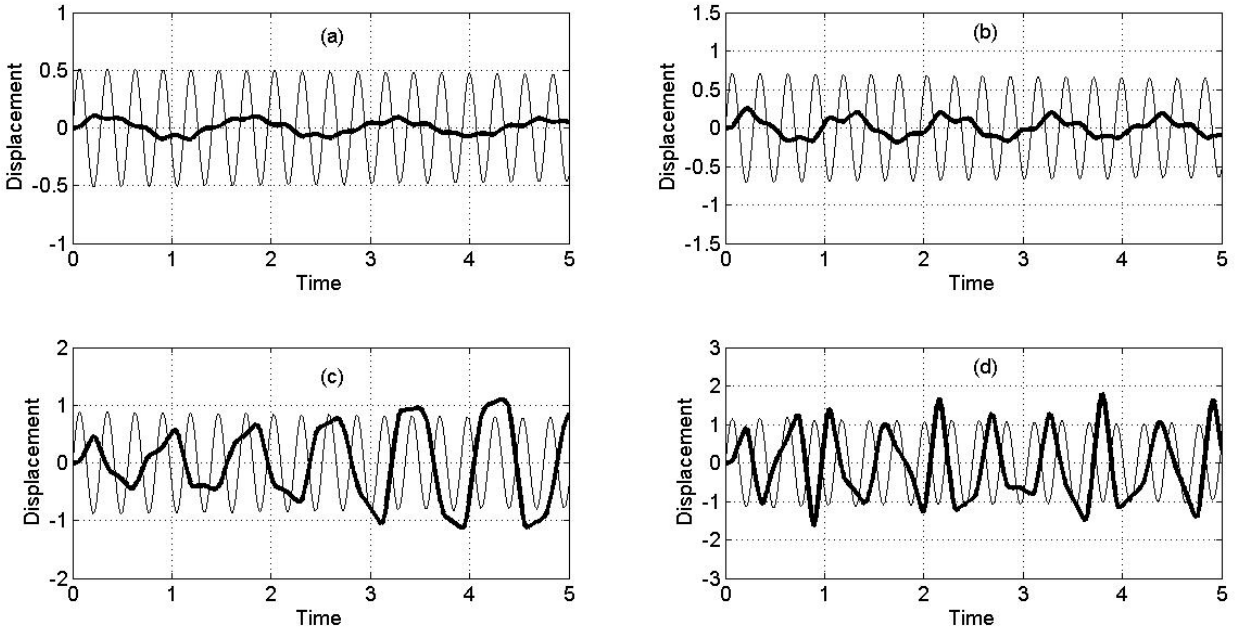

Figure 3.36: Time response for the 1st mode and NES when F_I applied at D_I = 0.7: (a) F_I = 10.5; (b) F_I = 14.5; (c) F_I = 18, and (d) F_I = 23.5; —— 1st mode, ▬▬ NES.

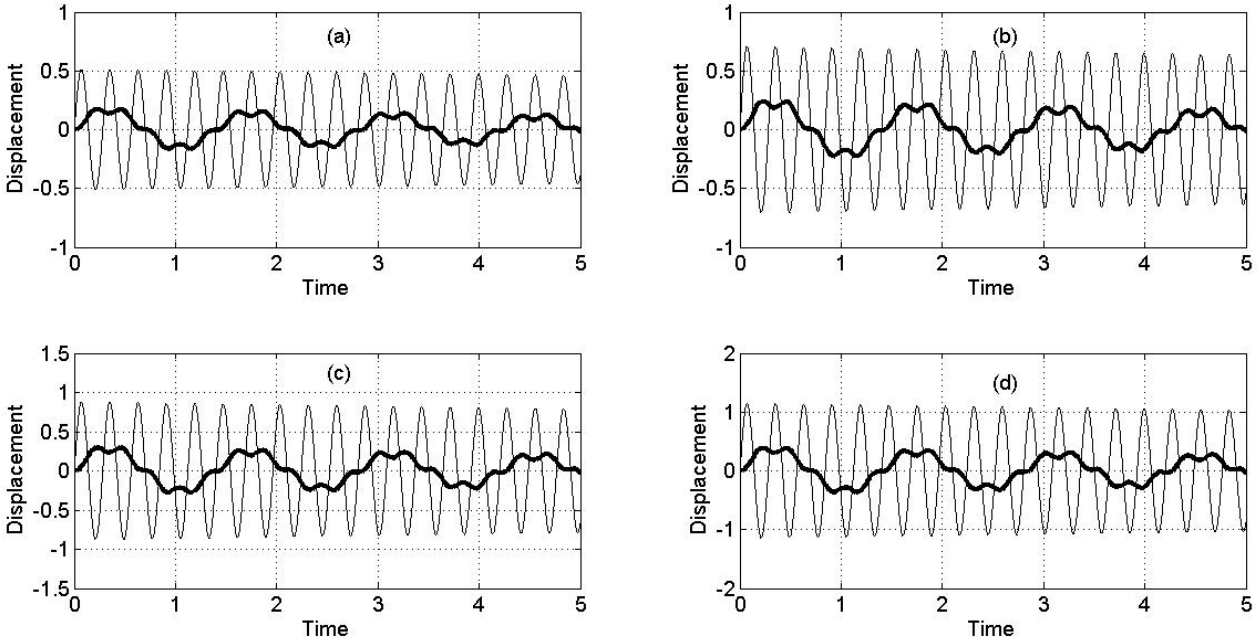

Figure 3.37: Time response for the 1st mode and LES when F_I applied at D_I = 0.3: (a) F_I = 10.5; (b) F_I = 14.5; (c) F_I = 18, and (d) F_I = 23.5; —— 1st mode, ▬▬ LES.

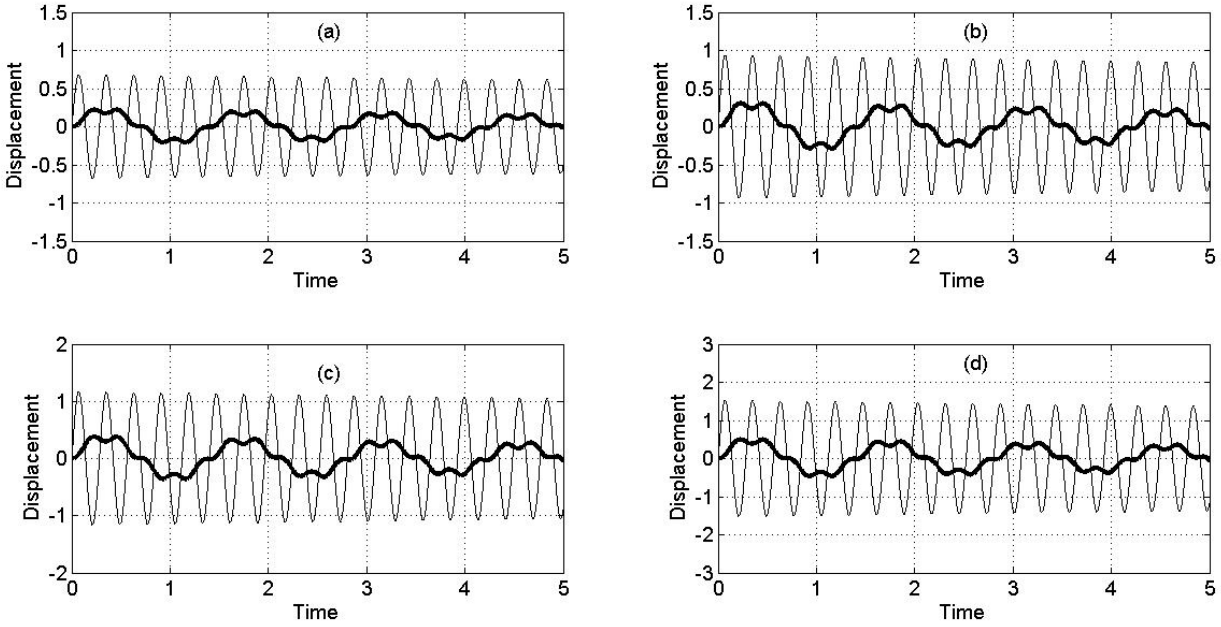

Figure 3.38: Time response for the 1st mode and LES when F_I applied at D_I = 0.4: (a) F_I = 10.5; (b) F_I = 14.5; (c) F_I = 18, and (d) F_I = 23.5; —— 1st mode, ▬▬ LES.

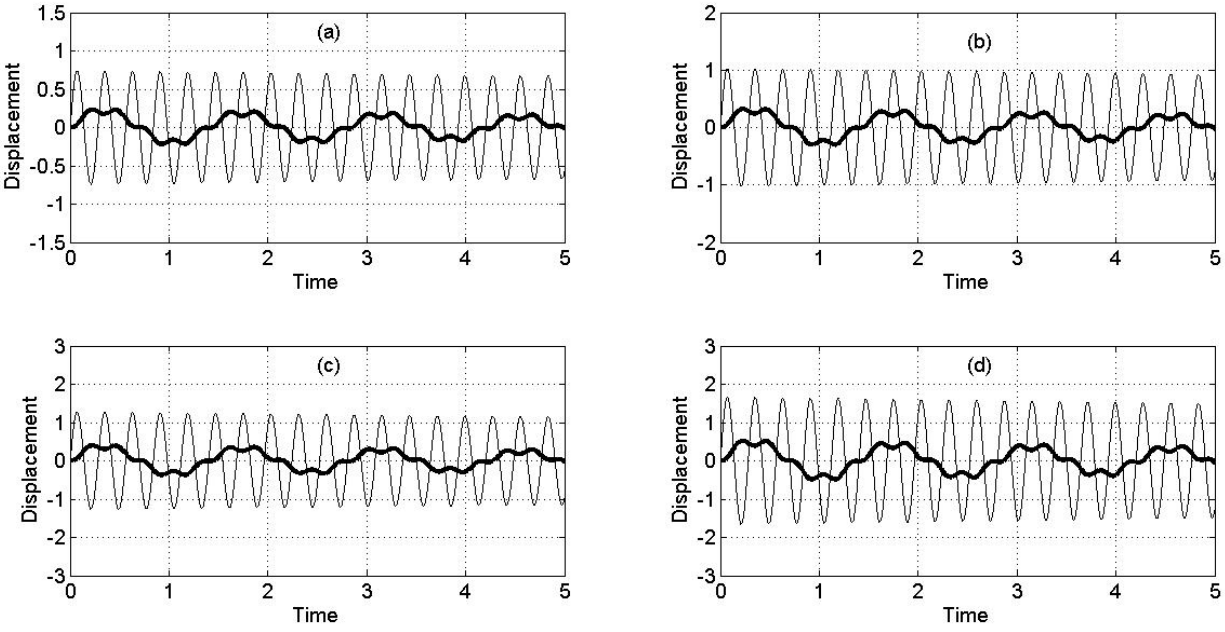

Figure 3.39: Time response for the 1st mode and LES when F_I applied at D_I = 0.5: (a) F_I = 10.5; (b) F_I = 14.5; (c) F_I = 18, and (d) F_I = 23.5; —— 1st mode, ▬▬ LES.

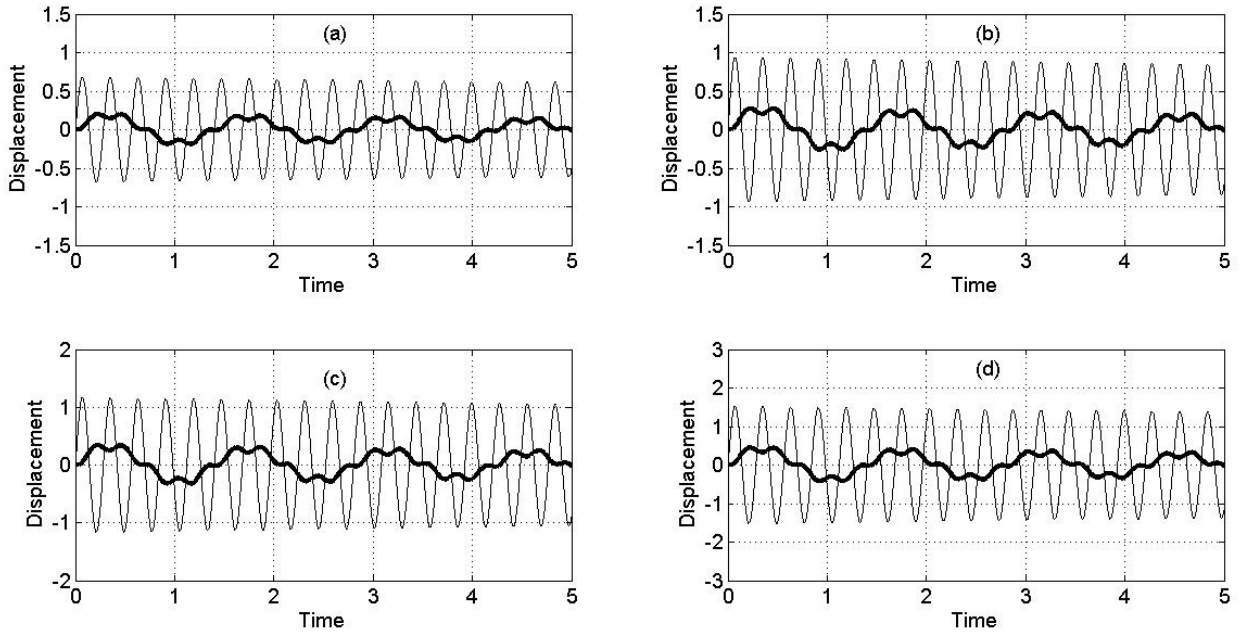

Figure 3.40: Time response for the 1st mode and LES when F_I applied at D_I = 0.6: (a) F_I = 10.5; (b) F_I = 14.5; (c) F_I = 18, and (d) F_I = 23.5; —— 1st mode, ▬▬ LES.

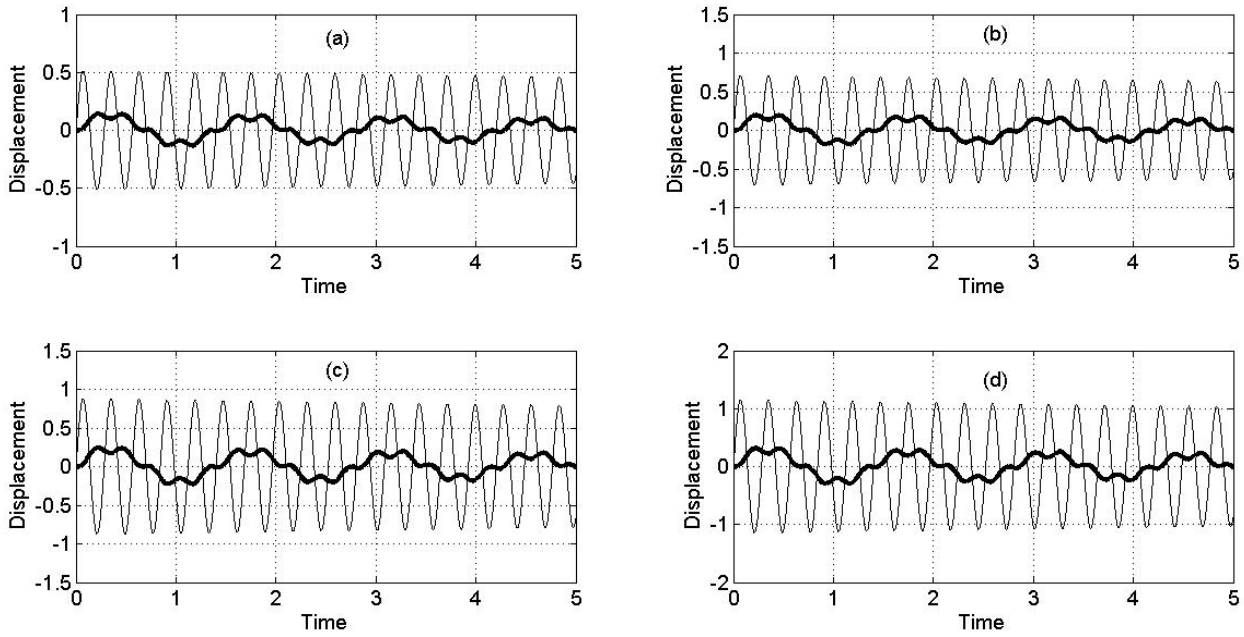

Figure 3.41: Time response for the 1st mode and LES when F_I applied at D_I = 0.7: (a) F_I = 10.5; (b) F_I = 14.5; (c) F_I = 18, and (d) F_I = 23.5; —— 1st mode, ▬▬ LES.

Chapter 4

Targeted Energy Transfer Under Periodic Excitation

In this chapter numerical analysis of the TET under periodic excitation will be given. In this work, a cosine function of dimensionless amplitude F_p and forcing frequency ω is used to simulate the periodic force applied to the beam at $X = D_1$. The dimensionless beam and ES equations introduced in equation (2.6), (2.8) and (2.9) will be simulated over a selected range of D_1 and ω. The simulated modal and ES responses will then be used to calculate the average energy dissipation by the ES, total energy in the beam and ES for each cycle.

With the harmonic forcing function, the dimensionless beam equation (2.6) becomes

$$W_{XXXX} + \alpha_1 W_{\tau\tau} + \alpha_2 W_{\tau} = F_{ES}(\tau)\delta(X - D) + F_p \cos\omega\tau\ \delta(X - D_1). \quad (4.1)$$

By separation of variables and orthogonality, the modal equation of motion is

$$g_{k,\tau\tau} + \frac{\alpha_2}{\alpha_1} g_{k,\tau} + \frac{\beta_k^4}{\alpha_1} g_k = f_{ES}(\tau) + f_P \cos\omega\tau \quad (4.2)$$

where $f_{ES}(\tau) = \dfrac{F_{ES}(\tau)\, a_k(D)}{\alpha_1}$ and $f_p = \dfrac{F_p\, a_k(D_1)}{\alpha_1}$.

The simulation is conducted based on the fixed $F_p = 15$ for $\omega = 0.5 \sim 21$ Hz, with 0.5 Hz increment, and D_1 = 0.3 ~ 0.7, with 0.1 increment. To ensure the steady state is reached, 400,000 data points are simulated and the last 200,000 data points are used to calculate the relevant energy terms. For the periodic forcing, the energy transfer is characterized on the cycle-to-cycle bases. Here, the energy terms introduced in section (2.5) are modified accordingly,

$$\overline{E}_{bn} = \left\langle \frac{1}{T_1}\int_{\tau}^{\tau+T_1} \left[T_n + P_n\right] d\tau \right\rangle,$$

$$\overline{ET}_{beam} = \sum_{n=1}^{N} \overline{E}_{bn},$$

$$\overline{ET}_{NES} = \left\langle \frac{1}{T_1}\int_{\tau}^{\tau+T_1} \left[\frac{1}{2} Y_{\tau}^2 + \frac{1}{4} b_3 (Y - W_D)^4 \right] d\tau \right\rangle,$$

and

$$\overline{ET}_{LES} = \left\langle \frac{1}{T_1}\int_{\tau}^{\tau+T_1}\left[\frac{1}{2}Y_{\tau}^2 + \frac{1}{2}b_2(Y-W_D)^2\right]d\tau \right\rangle$$

where, $T_1 = \dfrac{2\pi}{\omega}$ is the forcing period and $\langle\ \rangle$ denotes a temporal average overall the T_1-dimensionless time segments in the steady state period. The energy dissipation in ES is modified similarly,

$$\overline{E}_{NES,LES} = \left\langle \frac{1}{T_1}\int_{\tau}^{\tau+T_1} b_1\left(Y_{\tau} - W_{D,\tau}\right)^2 d\tau \right\rangle.$$

In addition, the energy ratio is defined to characterize the energy dissipation of the ES per total energy of the beam, $R_1 = \dfrac{\overline{E}_{NES,LES}}{\overline{ET}_{beam}}$.

The results of these energy quantities are given in Figures 4.1~4.5. As expected, the data indicate that most of the energy remains in the resonance mode of the beam when the forcing frequency lies in the neighborhood of the natural frequencies. Multi-modal vibration appears more prevalent when the forcing frequency lies in between the natural frequencies of the beam (Figures 4.1a~4.5a). But such a frequency range also defines a neighborhood where the ES can be less effective. In particular, R_1, which measures the ratio of the dissipated energy by ES and the total beam energy can drop significantly (Figures 4.1c~4.5c). (Note that the results shown in these figures are in logarithmic scale.) For example, R_1 drops significantly in the frequency neighborhoods around $f_{\mathrm{I}} = 7.5\,\mathrm{Hz}$ and $f_{\mathrm{II}} = 21\,\mathrm{Hz}$ at $D_1 = 0.3$. As D_1 increases, the drop around f_{I} begins to diminish, while the drop around f_{II} persists with $f_{\mathrm{II}} \cong 21$ Hz at $D_1 = 0.3$ and $f_{\mathrm{II}} \cong 15.5$ Hz at $D_1 = 0.7$.

The overall effectiveness of the ES appears to be minimal. For example, only $R_1 \cong e^{-5}$ is reached in all cases. However, the performance of the ES appears quite "uniform" in that R_1 in selected frequency range does not show large variation. The frequencies ranges are mostly found in the neighbourhood of the resonance frequency. The location of the applied periodic force D_1 can affect the location as well as the length of such frequency ranges. In particular, such frequency range is widened as the periodic force moves towards the center portion of the beam.

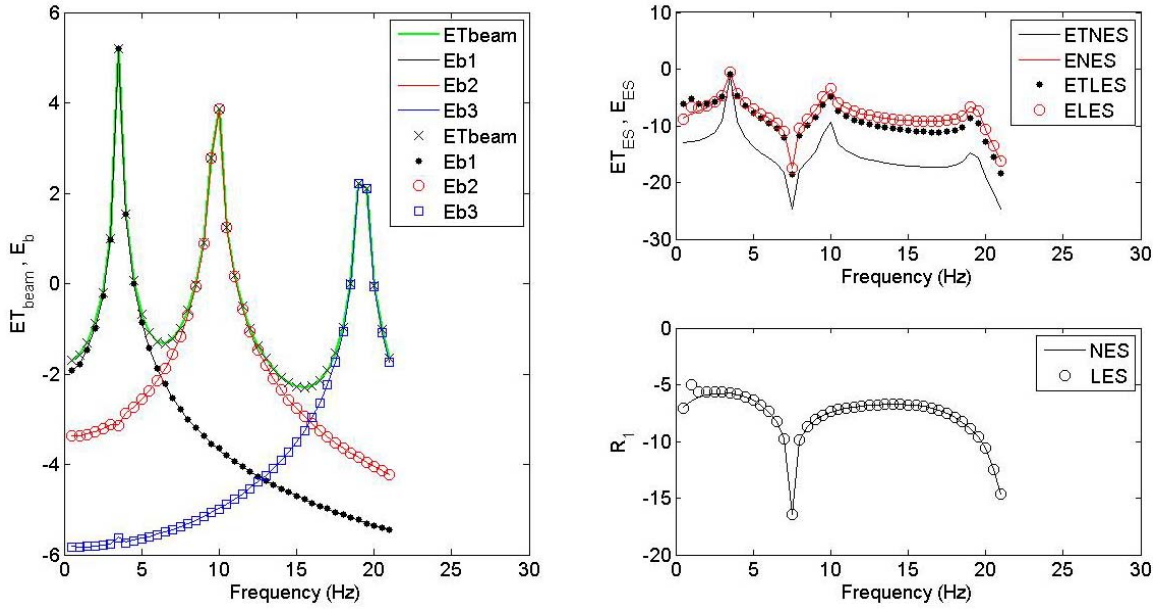

Figure 4.1: Energy characterization of the beam with the forcing frequency at $D_1 = 0.3$: (a) total energy in the beam and each vibration mode; (b) stored and dissipated energy of the ES and (c) the ratio of the energy dissipation by the ES and the total energy in the beam (solid lines refer to NES and symbols refer to LES).

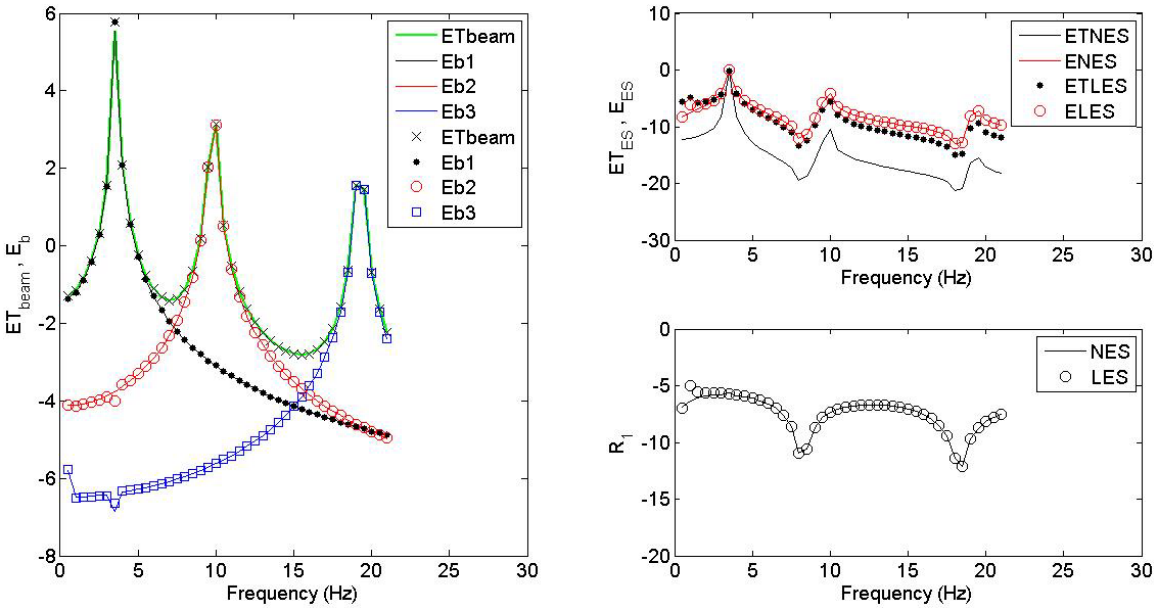

Figure 4.2: Energy characterization of the beam with the forcing frequency at $D_1 = 0.4$: (a) total energy in the beam and each vibration mode; (b) stored and dissipated energy of the ES and (c) the ratio of the energy dissipation by the ES and the total energy in the beam (solid lines refer to NES and symbols refer to LES).

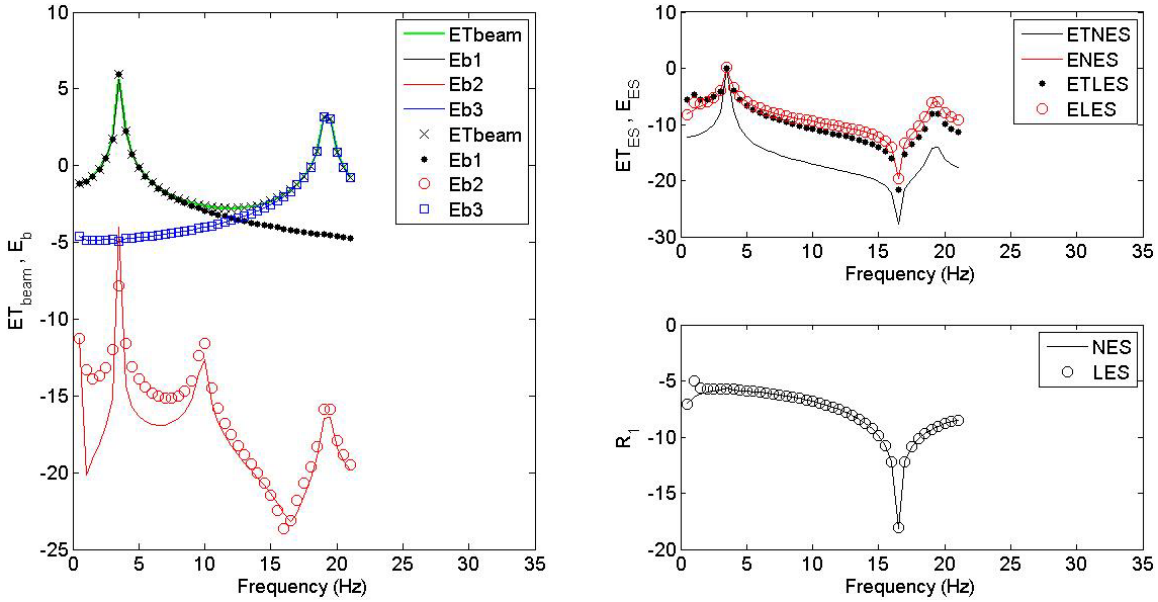

Figure 4.3: Energy characterization of the beam with the forcing frequency at $D_1 = 0.5$: (a) total energy in the beam and each vibration mode; (b) stored and dissipated energy of the ES and (c) the ratio of the energy dissipation by the ES and the total energy in the beam (solid lines refer to NES and symbols refer to LES).

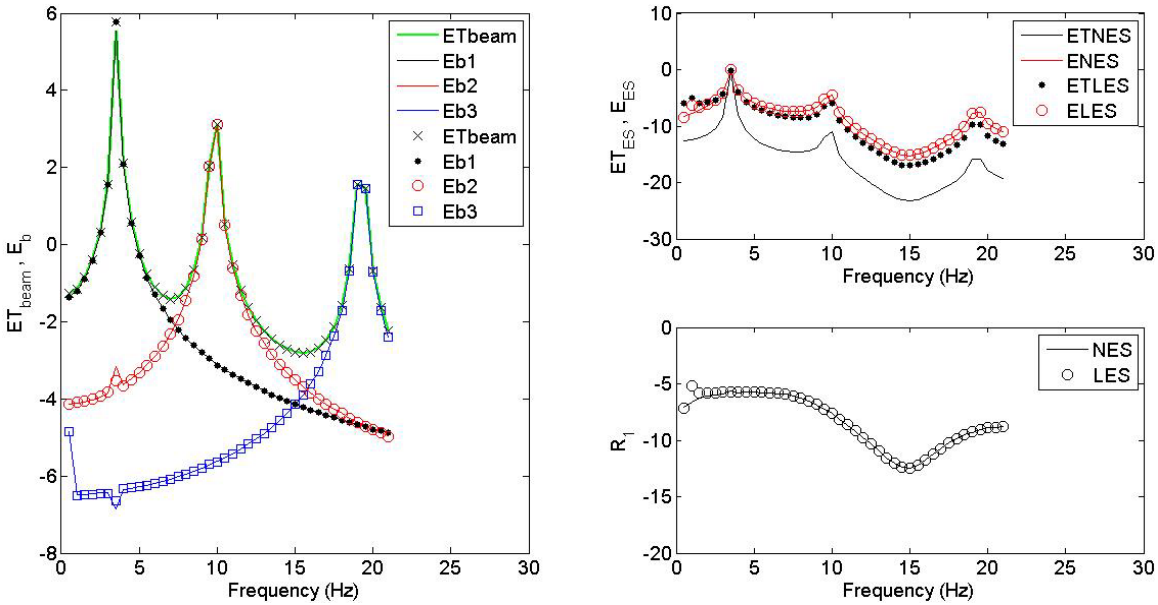

Figure 4.4: Energy characterization of the beam with the forcing frequency at $D_1 = 0.6$: (a) total energy in the beam and each vibration mode; (b) stored and dissipated energy of the ES and (c) the ratio of the energy dissipation by the ES and the total energy in the beam (solid lines refer to NES and symbols refer to LES).

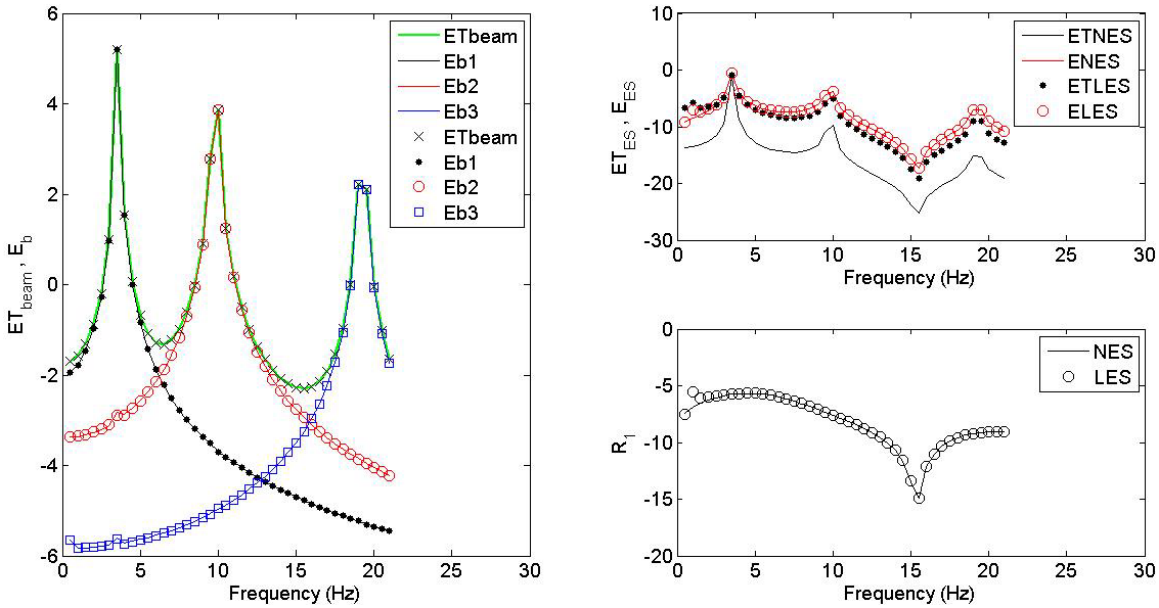

Figure 4.5: Energy characterization of the beam with the forcing frequency at $D_1 = 0.7$: (a) total energy in the beam and each vibration mode; (b) stored and dissipated energy of the ES and (c) the ratio of the energy dissipation by the ES and the total energy in the beam (solid lines refer to NES and symbols refer to LES).

Chapter 5

Discussions, Conclusion and Future Works

5.1. Discussions and Conclusion

Numerical results of the targeted energy transfer between the Euler-Bernoulli beam and ES are presented. Both NES and LES are considered for the beam under impact and periodic excitations. The investigation was focused on the effectiveness of the TET by varying the location of the excitation, the impact strength and the forcing amplitude and frequency of the periodic excitation. Other interesting and equally important parameters, including the ES location D, ES parameters, b_1 (dimensionless damping coefficient), b_2 (dimensionless linear stiffness coefficient), b_3 (dimensionless nonlinear stiffness coefficient), and the beam parameters, C_C (dimensionless damping coefficient), C_K (dimensionless stiffness coefficient), were held fixed and their effects were not examined. To determine the interesting parameter range is part of the challenge of the investigation. In this work, weak damping is considered. This is aimed at allowing the resonance modal interaction to be the primary contributor to the underlying energy transfer. While intuition would suggest more energy dissipation with a higher damping, it is plausible that the "signature" of the resonance mode vibration may become less obvious. Nevertheless, this, as well as other parameters, would be the part of the considerations intended for the future work.

The main observation of the numerical results is the predominant role of the first bending mode in the TET with the ES. This is consistently observed in the impact and periodic forcing excitations, and is independent of the location of the applied force. Given the particular geometrical fixed-fixed boundary condition used in the present study, and the fact that only one excitation force is applied, it is a reasonable outcome since the first bending mode is more likely excited than the higher order modes.

For the impact excitation, the effectiveness of the LES in TET as measured by the E_{LES} is independent of the impulsive force magnitude F_I. This result can be verified based on the linear system theory (Appendix C). But for NES, the results from E_{NES} indicated that a threshold F_I value exists, beyond which more efficient energy transfer can be achieved. The effectiveness of the TET appears to depend on the relative locations between the applied force and the ES

location: the farther away the applied force from the ES, the less effective is the NES. For example, the largest value of E_{NES} (>80%) is reached when the applied force is exactly located at the attachment site of the NES. The same F_I threshold discussed above also affects the time period for the energy dissipation, $\tau_{\%p}^{(NES)}$. In particular, $\tau_{\%p}^{(NES)}$ can drop significantly for larger F_I value. For the LES, $\tau_{\%p}^{(LES)}$ is again independent of F_I since E_{LES} is independent of F_I. Given any % p, the threshold value for the $\tau_{\%p}^{(NES,LES)}$varies with the location of the applied force: a much shorter time to achieve % p dissipation when the applied force is closer to the ES. Further understanding of $\tau_{\%p}^{(NES,LES)}$can be of practical interest for the design of ES since it reflects how efficient the ES can be for the TET.

In an attempt to understand the underlying modal interaction, the dominant Fourier modes in the vibrations of the beam and the ES are extracted directly from the PSD calculations. Since the dynamics of the LES is independent of F_I, the dominant Fourier modes change only for the NES case. Two specific frequency ratios, FR1 and FR2, are used to summarize the modal interaction between the first bending mode and the NES. An initial drop of these ratios can be observed for small F_I. Interestingly, an "asymptotic" FR1 ~ 3, FR2 ~ 1 are observed for large F_I. This implies the modal interaction between the beam and the NES remained unchanged when the impulsive force is large.

For the periodic excitation given by the harmonic function, three major observations were made. First, the ratio, R_1, which measures the energy dissipation relative to the amount of total energy in the beam, exhibits relatively small variation across a wide forcing frequency range. Secondly, there exist particular frequency windows where R_1 can drop significantly. It is found that both the width of these frequency windows as well as the location on the frequency axis vary with the forcing location. Once again, the variation appears to depend on the relative locations between the ES and the applied force: the closer the applied force is to the attachment site of the ES, the less pronounced the change is seen in the R_1 ratio. The last observation is that the poor performance of the ES when it comes to energy dissipation on the cycle-to-cycle basis. For example, for D = 0.4 and D_1 = 0.4, R_1 only reaches approximately ~ $e^{0.5}$.

5.2. Recommendations for Future Work

While the preliminary investigation has uncovered several interesting features in the TET between the Euler-Bernoulli beam and the ES, there is still a large parameter space to explore. In particular, the following future research works may be considered.

- Numerical simulations should be expanded with a broader consideration of other system parameters. In addition to those mentioned at the beginning of this chapter, the location of the ES attachment site, different material properties are also of importance when it comes to the design and vibration control of eliminating unwanted vibration. In addition, numerical analysis using more bending modes may be necessary when nonlinear effect of the beam vibration is considered.
- Analytical study of the underlying Hamiltonian system will add new insights to the underlying dynamics of TET between beam type structure and ES. The analysis can lead to the identification of specific periodic orbits of the NES, the so-called the nonlinear normal modes (NNM), and their coupling with the vibration of the beam. The understanding of the dynamics of the NNM allows a more detail examination of the so-called resonance capture in the TET process.
- It is of interest to further explore the dynamics of the NES in the chaotic regime. From the attachment site, NES is directly driven by the dynamics of the beam. For the Euler-Bernoulli beam, chaos is less likely since the beam is only capable of “simple” harmonic oscillation. Future work should include nonlinear elements in the primary structure so as to explore the effect of chaotic dynamics in the TET process. Given the sensitivity of the chaotic dynamics and the stability of the dynamic regime, it is plausible that more efficient and effective TET can be achieved.

Appendix A

A.1 Clamped-clamped boundary configuration for the slender beam

Table A.1: Weighted natural frequencies and mode shapes for clamped-clamped configuration of a slender beam [1].

Configuration	Mode shape	σ_n	Weighted natural frequencies, $\beta_n L$
Clamped-Clamped	$a_n(x) = (\cosh \beta_n x - \cos \beta_n x)$ $- \sigma_n (\sinh \beta_n x - \sin \beta_n x)$	0.9825 1.0008 0.9999 1.0000 0.9999 1 for $n > 5$	4.73004074 7.85320462 10.9956078 14.1371655 17.2787597 $\frac{(2n+1)\pi}{2}$ for $n > 5$

Appendix B

B.1 MATLAB codes

The following MATLAB codes were used to determine the response of the beam and energy sink as well as energy absorption and dissipation by the energy sink subjected to impact and harmonic excitation.

RESPONSE TO THE IMPACT EXCITATION

```
function [t,x]=beam(N,d,d1,Imp,J)

[m,b1,b2,b3,ad,ad1,coefC,coefK,coefF]=setparam(N,d,d1);
dt = 0.001;
npt = 200000;
tspan = (1:npt)*dt;
options = odeset('RelTol',1e-5,'AbsTol',1e-10);
if isempty(Imp)
   Imp=10.5:0.5:40;
   NImp=length(Imp);
   J=1:NImp;
else
   NImp=1;
end

for i=1:NImp
   % disp(['Impulse = ',num2str(I(J))]);
    X0=zeros(2*N+2,1);
    X0(2:2:2*N)=Imp(J(i))*ad1;
    [t,x]=ode45(@vf,tspan,X0,options,N,coefC,coefK,coefF,m,b1,b2,b3,ad);
    output=strcat('d0.4_d10.5_I',num2str(J(i)),'.mat');
    eval(['save ',output,' t x']);
end

% ------------------------------------------------------------------------

function g = vf(t,X,N,coefC,coefK,coefF,m,b1,b2,b3,ad)

g=zeros(2*N+2,1);
wd = sum(ad.*X(1:2:2*N-1));
wddot = sum(ad.*X(2:2:2*N));
FNES = b1*(X(2*N+2) - wddot) + b3*(X(2*N+1) - wd)^3; % for NES
%FNES = b1*(X(2*N+2) - wddot) + b2*(X(2*N+1) - wd); % for LES

g(1:2:2*N-1)=X(2:2:2*N);
g(2:2:2*N)= -coefC*X(2:2:2*N) - coefK.*X(1:2:2*N-1) + coefF*FNES;
g(2*N+1) = X(2*N+2);
g(2*N+2) = -FNES/m;

% ------------------------------------------------------------------------
```

```
function [m,b1,b2,b3,ad,ad1,coefC,coefK,coefF]=setparam(N,d,d1)

load betaL.mat;
BETA=betaL(1:N);

% ************************ parameters for beam
EI=1;
rho=2700;
A=1/2700;
L=1;
gamma=0.02;
an=inline('cosh(b*x)-cos(b*x) - sigma*(sinh(b*x)-sin(b*x))','b','sigma','x');
ad=zeros(N,1);
ad1=zeros(N,1);
for i=1:N
    ad(i,1)=an(BETA(i),sig(i),d);
    ad1(i,1)=an(BETA(i),sig(i),d1);
end
L2=1; % int an^2 dx ~ 1

% ************************ parameters for ES
m=0.05;
k=0.05;
c=5e-4;

T=1;
% ************************ dimensionless beam parameters
alpha1=(rho*A*L^4)/(EI*T^2);
alpha2=(gamma*L^4)/(EI*T);
coefC=alpha2/alpha1;
coefK=BETA(1:N).^4./alpha1;
coefF=(ad./L2)./alpha1;

% ************************ dimensionless ES parameters
b1=c*T/m;
b2=k*T^2/m;
b3=k*L^2*T^2/m;

showparam=0;
if showparam
   clc;
   disp('************************************************');
   disp('parameters used in the simulation:');
   disp(['b1 = ',num2str(b1)]);
   disp(['b2 = ',num2str(b2)]);
   disp(['b3 = ',num2str(b3)]);
   disp(['coefC = ',num2str(coefC)]);
   disp(['coefK = ',num2str(coefK')]);
   disp(['coefF = ',num2str(coefF')]);
   disp('************************************************');
end
```

ENERGY CALCULATION FOR IMPACT EXCITATION

```
function
[ETB,EBmode,ETNES,totalE,Eimpact,ENES,rEB,rEBmode,rETNES]=energy_imp(nfiles,N
,d,d1)
[m,b1,b2,b3,BETA,alpha1,ad,ad1,EI,L]=setparam(N,d,d1);
Imp=10.5:.5:40;
L2=1;rhoA=1;dt=0.001;

for J=1:nfiles
    disp(['processing file #: ',num2str(J)]);
    eval(['load ' strcat('d0.4_d10.5_I',num2str(J),'.mat')]);
    [npt,nvar]=size(x);
    N=nvar/2-1;
    dt=t(2)-t(1);

    % ************************* KE, PE for the beam
    KE=zeros(npt,1);
    PE=zeros(npt,1);
    for i=1:N
        KEi=x(:,2*i).^2*L2*alpha1*0.5;
        PEi=x(:,2*i-1).^2*BETA(i)^4*0.5;
        KE=KE+KEi;
        PE=PE+PEi;
        EBmode(:,i,J)=KEi+PEi;
    end
    ETB(:,J)=KE+PE;

    % ************************* KE, PE for the ES
    wd=zeros(npt,1);
    wddot=zeros(npt,1);
    for i=1:N
        wd=wd+ad(i)*x(:,2*i-1);
        wddot=wddot+ad(i)*x(:,2*i);
    end

    KENES=0.5*m*x(:,2*N+2).^2;
    PENES=0.25*b3*(x(:,2*N+1)-wd).^4;
    ETNES(:,J)=KENES+PENES;

    % ************************* Other Energy measures
    totalE(:,J)=ETB(:,J)+ETNES(:,J);
    for i=1:N
        rEB(:,J)=ETB(:,J)./totalE(:,J);            % totalE% in beam
        rEBmode(:,i,J)=EBmode(:,i,J)./totalE(:,J); % totalE% in mode
        rETNES(:,J)=ETNES(:,J)./totalE(:,J);       % totalE% in NES
    end

    X0=zeros(2*N+2,1);
    X0(2:2:2*N)=Imp(J)*ad1;
    Eimpact(J)=0.5*sum(X0(2:2:2*N).^2)*EI/L*alpha1;
    ENES(:,J)=cumsum((x(:,2*N+2)-wddot).^2*dt)*b1/Eimpact(J); %b1=0.8
end
```

```
 % ************************************************************

function [m,b1,b2,b3,BETA,alpha1,ad,ad1,EI,L]=setparam(N,d,d1)

load betaL.mat;
BETA=betaL(1:N);

% ************************* parameters for beam
EI=1;
rho=2700;
A=1/2700;
L=1;
gamma=0.02;
an=inline('cosh(b*x)-cos(b*x) - sigma*(sinh(b*x)-sin(b*x))','b','sigma','x');
ad=zeros(N,1);
ad1=zeros(N,1);
for i=1:N
    ad(i,1)=an(BETA(i),sig(i),d);
    ad1(i,1)=an(BETA(i),sig(i),d1);
end
L2=1; % int an^2 dx ~ 1

% ************************* parameters for ES
m=0.05;
k=0.05;
c=5e-4;

T=1;
% ************************* dimensionless beam parameters
alpha1=(rho*A*L^4)/(EI*T^2);  % .. unit length beam mass

% ************************* dimensionless ES parameters
b1=c*T/m;
b2=k*T^2/m;
b3=k*L^2*T^2/m;
```

RESPONSE TO THE PERIODIC EXCITATION

```
function [t,x]=beam_perd(N,d,d1,freq,J)

[m,b1,b2,b3,ad,coefC,coefK,coefF,coefP]=setparam(N,d,d1);
FP=15;
if nargin==3
   freq=0.5:0.5:21;
   Nfreq=length(freq);
   J=1:Nfreq;
else
   Nfreq=1;
end

dt = 0.001;
```

```
npt =400000;
tspan = (1:npt)*dt;
X0=zeros(2*N+2,1);
options=odeset('RelTol',1e-5,'AbsTol',1e-10);
for i=1:Nfreq
    omega=2*pi*freq(i);

[t,x]=ode45(@vf,tspan,X0,options,N,coefC,coefK,coefF,coefP,m,b1,b2,b3,ad,FP,o
mega);

output=strcat('d',num2str(d),'.d1',num2str(d1),'.freq',num2str(J(i)),'.mat');
    eval(['save ',output,' dt x']);
    X0=x(end,:)'; % passing the last x value as new init cond.
end

% ------------------------------------------------------------------------

function g = vf(t,X,N,coefC,coefK,coefF,coefP,m,b1,b2,b3,ad,FP,omega)

wd = sum(ad.*X(1:2:2*N-1));
wddot = sum(ad.*X(2:2:2*N));
FNES = b1*(X(2*N+2) - wddot) + b3*(X(2*N+1) - wd)^3;  %for NES
%FNES = b1*(X(2*N+2) - wddot)+b2*(X(2*N+1) - wd);  %for LES

g=zeros(2*N+2,1);
g(1:2:2*N-1)=X(2:2:2*N);
g(2:2:2*N)= -coefC*X(2:2:2*N)-coefK.*X(1:2:2*N-
1)+coefF*FNES+coefP*FP*cos(omega*t);
g(2*N+1) = X(2*N+2);
g(2*N+2) = -FNES/m;

% ------------------------------------------------------------------------

function [m,b1,b2,b3,ad,coefC,coefK,coefF,coefP]=setparam(N,d,d1)

load betaL.mat;
BETA=betaL(1:N);

% ************************* parameters for beam
EI=1;
rho=2700;
A=1/2700;
L=1;
gamma=0.02;
an=inline('cosh(b*x)-cos(b*x) - sigma*(sinh(b*x)-sin(b*x))','b','sigma','x');
ad=zeros(N,1);
ad1=zeros(N,1);
for i=1:N
    ad(i,1)=an(BETA(i),sig(i),d);
    ad1(i,1)=an(BETA(i),sig(i),d1);
end
L2=1; % int an^2 dx ~ 1

% ************************* parameters for ES
m=0.05;
```

```
k=0.05;
c=5e-4;

T=1;
% ************************* dimensionless beam parameters
alpha1=(rho*A*L^4)/(EI*T^2);
alpha2=(gamma*L^4)/(EI*T);
coefC=alpha2/alpha1;
coefK=BETA(1:N).^4./alpha1;
coefF=(ad./L2)./alpha1;
coefP=(ad1./L2)./alpha1;

% ************************* dimensionless ES parameters
b1=c*T/m;
b2=k*T^2/m;
b3=k*L^2*T^2/m;

showparam=0;
if showparam
   clc;
   disp('*************************************************');
   disp('parameters used in the simulation:');
   disp(['b1 = ',num2str(b1)]);
   disp(['b2 = ',num2str(b2)]);
   disp(['b3 = ',num2str(b3)]);
   disp(['coefC = ',num2str(coefC)]);
   disp(['coefK = ',num2str(coefK')]);
   disp(['coefF = ',num2str(coefF')]);
   disp('*************************************************');
end
```

ENERGY CALCULATION FOR PERIODIC EXCITATION

```
function [totalE,ETB,EBmode,ETNES,ENES,InputE] = energy_perd(N,d,d1,FP)

[m,b1,b2,b3,ad,ad1,alpha1,BETA]=setparam(N,d,d1);
L2=1;

freq=0.5:0.5:21;
Nfreq=length(freq);
for ifreq=1:Nfreq
    disp(['processing freq.#: ',num2str(ifreq)]);
    eval(['load ' strcat('d0.4.d10.5.freq',num2str(ifreq),'.mat')]);

    % define segmentation
    [npt,nvar]=size(x);
    perd=1/freq(ifreq); % freq in Hz
    npt1perd=perd/dt;
    NSEG=npt/npt1perd;
    id=[0 round((1:NSEG)*npt1perd)];
```

```
    for iseg=1:fix(NSEG)
        J=(1:fix(npt1perd))+id(iseg);
        nptJ=length(J);

        % ************************* KE, PE for the beam
        KEiseg=zeros(nptJ,1);
        PEiseg=zeros(nptJ,1);
        for i=1:N
            KEi=x(J,2*i).^2*L2*alpha1*0.5;
            PEi=x(J,2*i-1).^2*BETA(i)^4*0.5;
            KEiseg=KEiseg+KEi;
            PEiseg=PEiseg+PEi;
            EBmode(iseg,i,ifreq)=mean(KEi+PEi);
        end
        ETB(iseg,ifreq)=mean(KEiseg+PEiseg);

        % ************************* KE, PE for the ES
        wd=zeros(nptJ,1);
        wddot=zeros(nptJ,1);
        wddot1=zeros(nptJ,1);
        for i=1:N
            wd=wd+ad(i)*x(J,2*i-1);
            wddot=wddot+ad(i)*x(J,2*i);
            wddot1=wddot+ad1(i)*x(J,2*i);
        end
        KENES=0.5*m*x(J,2*N+2).^2;
        PENES=0.25*b3*(x(J,2*N+1)-wd).^4; %for NES
        %PENES=0.5*b2*(x(J,2*N+1)-wd).^2; % for LES
        ETNES(iseg,ifreq)=mean(KENES+PENES);
        totalE(iseg,ifreq)=ETB(iseg,ifreq)+ETNES(iseg,ifreq);

        % ************************* Other Energy measures
        rEB(iseg,ifreq)=ETB(iseg,ifreq)./totalE(iseg,ifreq);
        rEd(iseg,ifreq)=ETNES(iseg,ifreq)./totalE(iseg,ifreq);
        for i=1:N
            rEBmode(iseg,i,ifreq)=EBmode(iseg,i,ifreq)./totalE(iseg,ifreq);
        end

InputE(iseg,ifreq)=mean(cumsum(cos(2*pi*freq(ifreq)*J').*wddot1))*dt*FP;
        ENES(iseg,ifreq)=mean(cumsum((x(J,2*N+2)-wddot).^2))*dt*b1;
    end
end


function [m,b1,b2,b3,ad,ad1,alpha1,BETA]=setparam(N,d,d1)

load betaL.mat;
BETA=betaL(1:N);

% ************************* parameters for beam
EI=1;
rho=2700;
A=1/2700;
L=1;
```

```
gamma=0.02;
an=inline('cosh(b*x)-cos(b*x) - sigma*(sinh(b*x)-sin(b*x))','b','sigma','x');
ad=zeros(N,1);
ad1=zeros(N,1);
for i=1:N
    ad(i,1)=an(BETA(i),sig(i),d);
    ad1(i,1)=an(BETA(i),sig(i),d1);
end

% ************************* parameters for ES
m=0.05;
k=0.05;
c=5e-4;

T=1;
% ************************* dimensionless beam parameters
alpha1=(rho*A*L^4)/(EI*T^2);  % .. unit length beam mass

% ************************* dimensionless ES parameters
b1=c*T/m;
b2=k*T^2/m;
b3=k*L^2*T^2/m;
```

Appendix C

C.1 Energy dissipation by the LES due to impulsive force

It is possible to show the independence of the E_{LES} with the impulsive force F_I. First, let Y_l, l = 1, …, N be the solution of the differential equation

$$\varepsilon Y_{l,\tau\tau} + b_1 Y_{l,\tau} + b_3 Y_l - b_1 a_l(D) g_{l,\tau} - b_3 a_l(D) g_l = 0 \tag{1}$$

so that $Y = \sum_{l=1}^{N} Y_l$ satisfies the LES equation of motion $\varepsilon Y_{\tau\tau} + b_1(Y_\tau - W_{D,\tau}) + b_3(Y - W_D) = 0$ shown in (2.9). Now, recall the modal equation of motion of the beam (2.12) and substitute W_D, $W_{D,\tau}$ by their modal sum:

$$\begin{aligned} & g_{l,\tau\tau} + C_c g_{l,\tau} + C_k g_l = C_f F_{ES} = C_f \left[b_1(Y_\tau - W_{D,\tau}) + b_3(Y - W_D) \right] \\ & \quad = C_f b_1 \left[\sum_{l=1}^{N} Y_{l,\tau} - \sum_{l=1}^{N} a_l(D) g_{l,\tau} \right] + C_f b_3 \left[\sum_{l=1}^{N} Y_l - \sum_{l=1}^{N} a_l(D) g_\tau \right] \\ & \Rightarrow g_{l,\tau\tau} + \left[\left\{ C_c + C_f b_1 a_l(D) \right\} g_{l,\tau} + \sum_{m \pm l}^{N} C_f b_1 a_m(D) g_{m,\tau} - C_f b_1 \sum_{m=1}^{N} Y_{m,\tau} \right] + \\ & \qquad \left[\left\{ C_k + C_f b_3 a_l(D) \right\} g_l + C_f b_3 \sum_{m \pm l}^{N} a_m(D) g_m - C_f b_3 \sum_{m=1}^{N} Y_m \right] = 0 \end{aligned} \tag{2}$$

Let $\vec{Z} = (g_1, ..., g_n, Y_1, ..., Y_N)^T_{2N \times 1}$ and combine (1), (2) to write the equations of motion in the vector form

$$\underline{\underline{M}} \ddot{\vec{Z}} + \underline{\underline{C}} \dot{\vec{Z}} + \underline{\underline{K}} \vec{Z} = \vec{0}$$

where

$$\underline{\underline{M}} = \left[\begin{array}{c|c} \mathrm{I}_{N \times N} & 0 \\ \hline 0 & \mathrm{I}_{N \times N} . \varepsilon \end{array} \right],$$

$$\underline{\underline{C}} = \left[\begin{array}{cccc|c} C_c + C_f b_1 a_1(D) & C_f b_1 a_2(D) & \cdots & C_f b_1 a_N(D) & \\ C_f b_1 a_1(D) & C_c + C_f b_1 a_2(D) & \cdots & \vdots & 1_{N\times N}.(-C_f b_1) \\ \vdots & \vdots & \ddots & \vdots & \\ C_f b_1 a_1(D) & \cdots & \cdots & C_c + C_f b_1 a_N(D) & \end{array}\right.$$
$$\left.\begin{array}{cccc|c} -b_1 a_1(D) & 0 & \cdots & 0 & \\ 0 & -b_1 a_2(D) & \cdots & \vdots & \\ \vdots & \vdots & \ddots & \vdots & II_{N\times N}.b_1 \\ 0 & \cdots & 0 & -b_1 a_N(D) & \end{array}\right],$$

and

$$\underline{\underline{K}} = \left[\begin{array}{cccc|c} C_k + C_f b_3 a_1(D) & C_f b_3 a_2(D) & \cdots & C_f b_3 a_N(D) & \\ C_f b_3 a_1(D) & C_k + C_f b_3 a_2(D) & \cdots & \vdots & 1_{N\times N}.(-C_f b_3) \\ \vdots & \vdots & \ddots & \vdots & \\ C_f b_3 a_1(D) & \cdots & \cdots & C_k + C_f b_3 a_N(D) & \end{array}\right.$$
$$\left.\begin{array}{cccc|c} -b_3 a_1(D) & 0 & \cdots & 0 & \\ 0 & -b_3 a_2(D) & \cdots & \vdots & \\ \vdots & \vdots & \ddots & \vdots & II_{N\times N}.b_3 \\ 0 & \cdots & 0 & -b_3 a_N(D) & \end{array}\right],$$

and initial condition

$$\vec{Z}(0) = \vec{0}, \quad \dot{\vec{Z}}(0) = \begin{pmatrix} g_{1,\tau}(0^+) \\ \vdots \\ g_{N,\tau}(0^+) \\ 0 \\ \vdots \\ 0 \end{pmatrix}_{2N\times 1} = \begin{pmatrix} a_1(D) \\ \vdots \\ a_N(D) \\ 0 \\ \vdots \\ 0 \end{pmatrix} \frac{F_I}{\alpha_1}.$$

Note $1_{N\times N}$ from above is an $N \times N$ matrix with all its entries being 1.

To write the above in the first order form, introduce $\vec{U} = \begin{pmatrix} \vec{z}^T & \dot{\vec{z}}^T \end{pmatrix}^T$. Now the equation of motion can be written as $\dot{\vec{U}} = A\vec{U}$ where

$$\dot{\vec{U}} = \begin{pmatrix} \dot{\vec{Z}} \\ \ddot{\vec{Z}} \end{pmatrix} = A\vec{U} = \left[\begin{array}{c|c} 0_{N\times N} & \mathrm{II}_{N\times N} \\ \hline \underline{\underline{M}}^{-1}.\underline{\underline{K}} & \underline{\underline{M}}^{-1}.\underline{\underline{C}} \end{array}\right]\vec{U} \tag{3}$$

with the initial condition

$$\vec{U}(0)=\begin{pmatrix}\vec{Z}(0)\\ \dot{\vec{Z}}(0)\end{pmatrix}=\begin{pmatrix}0\\ \vdots\\ a_1(D)\\ \vdots\\ a_N(D)\\ \vdots\\ 0\end{pmatrix}\frac{F_I}{\alpha_1}=\vec{H}\frac{F_I}{\alpha_1}$$

By the linear system theory [17], the solution to (3) is given by

$$\vec{U}=e^{A\tau}\vec{U}(0)=\left(e^{A\tau}\vec{H}\right)\frac{F_I}{\alpha_1}$$

where e^A denotes the matrix exponential. Since $\dot{\vec{U}}=\left(\frac{Ae^{A\tau}\vec{H}}{\alpha_1}\right)F_I$, it is now clear that all the velocity components vary as linear functions of F_I. Following (2.32), E_{LES} is therefore independent of F_I, since the impact energy in the denominator also varies as a linear function of F_I.

References

1. Inman, D. J. (2001). *Engineering vibration* (2nd ed.). Upper Saddle River, N.J.: Prentice Hall.
2. Lee, Y.S., Vakakis, A.F., Bergman, L.A., McFarland, D.M. , Kerschen, G, Nucera, F., Tsakirtzis, S., Panagopoulos, P.N., Passive non-linear targeted energy transfer and its applications to vibration absorption, Part K: Journal of Multi-body Dynamics, 2008, 222.2, 77-134. Print.
3. Kerschen,G., Kowtko, J. J.,Mcfarland, M., Bergman, L.A., Vakakis, A.F., Theoretical and experimental study of multimodal targeted energy transfer in a system of coupled oscillators, Nonlinear Dyn., 2007, 4, 285–309.
4. Vakakis, A. F. (2009). *Nonlinear targeted energy transfer in mechanical and structural systems I*. Dordrecht: Springer.
5. Nayfeh, A.H., Mook, D.T., *Nonlinear Oscillations*, John Wiley & Sons, New York, 1995.
6. Shaw, S.W., Pierre, C., Normal modes of vibration for nonlinear vibratory systems, J. Sound Vib. 164, 85–124, 1993.
7. Vakakis, A., Manevitch, L., Gendelman, O., and Bergman, L. Dynamics of linear discrete systems connected to local, essentially non-linear attachments. J. Sound Vibr., 2003, 264, 559–577.
8. Gendelman, O., Manevitch, L., Vakakis, A., and M'Closkey, R. Energy pumping in coupled mechanical oscillators, part I: dynamics of the underlying Hamiltonian systems. Trans. ASME, J. Appl. Mech., 2001, 68, 34–41.
9. Lee, Y., Kerschen, G., Vakakis, A., Panagopoulos, P., Bergman, L., and McFarland, D. M. Complicated dynamics of a linear oscillator with a light, essentially nonlinear attachment. Phys. D, 2005, 204(1–2), 41–69.
10. Malatkar, P., Nayfeh, A.H., On the transfer of energy between widely spaced modes in structures, Nonl. Dyn. 2003, 31, 225–242.
11. Gendelman, O., Gorlov, D., Manevitch, L., and Musienko, A. Dynamics of coupled linear and essentially nonlinear oscillators with substantially different masses. J. Sound Vibr., 2005, 286, 1–19.

12. Gendelman O.V., Lamarque C.H., Dynamics of linear oscillator coupled to strongly nonlinear attachment with multiple states of equilibrium. Chaos, Solitons and Fractals, 2005, 24, 501–509
13. Gendelman, O.V., Sapsis T., Vakakis A.F., Bergman, L.A., Enhanced passive targeted energy transfer in strongly nonlinear mechanical oscillators, J. Sound and Vib. 2011, 330, 1–8.
14. Kerschen, G., Lee, Y., Vakakis, A., McFarland, D. M., and Bergman, L. Irreversible passive energy transfer in coupled oscillators with essential nonlinearity. SIAM J. Appl. Math., 2006, 66(2), 648–679.
15. Georgiadis, F., Vakakis, A., McFarland, D. M., and Bergman, L. Shock isolation through passive energy pumping caused by nonsmooth nonlinearities. Int. J. Bifurcation Chaos, 2005, 15(6), 1989–2001.
16. Rao, S. S., & Yap, F. F. (2005). *Mechanical vibrations* (SI ed., [4th ed.). Singapore: Pearson Prentice Hall.
17. Chen, C., & Chen, C. (2012). *Linear system theory and design* (5th ed.). New York: Holt, Rinehart, and Winston.
18. MathWorks, I. (1996). *MATLAB: the language of technical computing.* (Version 5. ed.). Natick, MA: MathWorks.